FROM ADAPTATION AND ACCLIMATION TO ENGINEERING: INVESTIGATING HOW PHOTORESPIRATORY MECHANISMS CONTROL PHOTOSYNTHETIC CARBON FIXATION

By

Luke Michael Gregory

A DISSERTATION

Submitted to
Michigan State University
in partial fulfillment of the requirements
for the degree of

Plant Biology – Doctor of Philosophy
Molecular Plant Sciences – Dual Major

2024

ABSTRACT

Anthropogenic activities are rapidly changing the composition and thermal conditions of the global atmosphere, leading to fundamental trade-offs in photosynthetic carbon metabolism. Unique challenges of photosynthetic carbon fixation under future climate conditions – mainly elevated temperatures – include increased rates of photorespiration, which limit C_3 photosynthetic performance. Photorespiration initiates when oxygen binds to rubisco, the enzyme responsible for carbon fixation, instead of carbon dioxide. The resulting oxygenation reaction produces 2-phosphoglycolate, an intermediate that inhibits carbon assimilation and allocation. To reduce the inhibition of carbon metabolism, photorespiration detoxifies and recycles 2-phosphoglycolate through a set of reactions that salvage most of the initial carbon fixed by rubisco. While the rate of photorespiratory influx is set by rubisco, downstream photorespiratory enzymes must process the subsequent photorespiratory intermediates that are produced. If photorespiratory influx outpaces downstream metabolic capacity, a reduction of photosynthetic net carbon fixation is anticipated due to insufficient conversion rate and accumulation of various biologically active intermediates. Managing these photorespiratory intermediates is important to maintain plant vigor, especially in dynamic environments where photorespiratory influx is unpredictable. Currently, it is unclear whether photorespiratory biochemistry, downstream of rubisco, adjusts to handle a greater carbon influx through photorespiration.

The work in this dissertation looks past rubisco, which has been a prominent focus in engineering efforts, to explore downstream photorespiratory enzymes that directly manage carbon flux through photorespiration. I first investigate the hallmarks of a temperature-tolerant photorespiratory pathway in *Rhazya stricta*, a C_3 shrub native to the hot-arid regions in the Middle East. I found that *R. stricta* supports higher rates of photorespiration under elevated temperatures and that these higher rates of photorespiration correlate with increased activity of key photorespiratory enzymes; phosphoglycolate phosphatase and catalase, compared to *Nicotiana tabacum*. I then studied the acclimation potential of photorespiratory capacity in *Betula papyrifera*, with particular interest in whether enzyme activities acclimate to changes in photorespiratory influx. I found no plasticity in photorespiratory capacity when *B. papyrifera* was exposed

to six different CO_2 concentrations and temperatures scenarios, and that a fixed capacity is maintained under each growth condition. The fixed capacity is likely due to the existence of safety factors in the pathway that manages unpredictable photorespiratory influx in dynamic environments. Finally, I explored whether replacing native catalase in *Arabidopsis thaliana* with a foreign catalase isoform conferred any benefit to photorespiratory carbon recycling efficiency. To explore this question, we generated three transgenic independent expression lines of *Heliobacter pylori* catalase in *A. thaliana cat2*-KO to determine their *in vivo* and *in vitro* function. I found that two out of the three transgenic lines have similar amounts of CO_2 loss from photorespiration compared to wildtype line and were able to rescue the *cat2*-KO growth phenotype, while having less catalase activity than wildtype.

The findings from this dissertation contribute to the long-range goal of engineer photorespiration to improve photosynthetic carbon fixation under future climate conditions in C_3 crop systems.

This dissertation is dedicated to my mother, Mary C. Gregory†.
Thank you for imparting your work ethic onto me, teaching
me the value of perseverance, and for exemplifying a
selflessness towards others.

ACKNOWLEDGEMENTS

I am grateful for the invaluable support and encouragement I have received throughout my dissertation work and my development into an early career scientist at Michigan State University. This would not have been possible without the guidance of numerous mentors, my committee, the camaraderie of my peers, and the broader plant science community that has surrounded me for the past five years.

First and foremost, I would like to thank my Ph.D. supervisor, Berkley Walker, who has challenged me to become a better scientist. Whether it was help with a technical writing, imparting extensive knowledge of plant physiology, research freedom, or professional mentorship all have contributed to the scientist I am today.

I am indebted to the past and present members of the Walker lab for their impactful interactions and mentorship, which significantly contributed to my growth as a scientist. In particular, I would like to thank Ludmila Roze, Mauri Tejera-Nieves, Deserah (Dez) Strand, Xinyu Fu, and Kaila Smith for teaching me their expertise and for their entertainment over the years. Additionally, I would like to thank Ludmila Roze and Xinyu Fu for considering my contributions to their projects worthy of authorship.

Lastly, I extend gratitude to my family, with special acknowledgements to my brother Jacob Gregory and fiancée Kathryn (KT) Skolnick, for their unwavering support and encouragement throughout my graduate studies.

TABLE OF CONTENTS

CHAPTER 1: Introduction

Adapted from:

Gregory, L.M., Roze, L.V. & Walker, B.J. (2023) Increased activity of core photorespiratory enzymes and CO_2 transfer conductances are associated with higher and more optimal photosynthetic rates under elevated temperatures in the extremophile *Rhazya stricta*. Plant, Cell & Environment, 46, 3704–3720.

Gregory, L.M., Scott, K.F., Sharpe, L.A., Roze, L.V., Schmiege, S.C., Way D.A., & Walker, B.J. Rubisco activity and activation state dictate photorespiratory plasticity in *Betula papyrifera* acclimated to future climate conditions. (Submitted to *Scientific Reports*)

Leaf-level gas-exchange in C_3 land plants

Leaf-level gas exchange describes the movement of gases, primarily CO_2, and H_2O, into and out of the leaves through the pore in the substomatal cavity. H_2O vaporizes from liquid to gas and transpires from the leaf to the atmosphere (i.e., evapotranspiration), while CO_2 travels in the opposite direction and serves as an inorganic carbon source for metabolism (Evans *et al.*, 2009; Kaldenhoff, 2012). In C_3 species, which will be a focus in this dissertation, CO_2 movement is directly dependent on gaseous/liquid diffusion from the atmosphere (C_a) to the intercellular air space of the leaf (C_i) and continues its diffusion path into the chloroplast (C_c). Notability the atmospheric CO_2 is not in perfect equilibrium with the CO_2 in the chloroplast (i.e., $C_a > C_c$), as each portion of the diffusion pathway imposes a resistance to CO_2 diffusion (Evans *et al.*, 2009; Evans *et al.*, 1996; Farquhar *et al.*, 1982).

The first is a resistance barrier, known as stomatal conductance (g_{sw}), constrains CO_2 and H_2O exchange with the atmosphere and the intercellular airspace through the stomatal pore (Farquhar *et al.*, 1982). The second resistance barrier to CO_2 diffusion, known as mesophyll conductance (g_m), constrains only the transfer of CO_2 from the intercellular airspace to the carboxylation site in the chloroplast. This mesophyll space is made up of the diffusion path from the intercellular air space through the cell wall, the cytosol, the double membrane of the chloroplast and travels through the aqueous phase of the stroma (Evans, 2021). The CO_2 that makes it to the chloroplast can be incorporated into the plant by a complex series of enzymatically regulated chemical reactions, known as the Calvin-Benson Cycle (or C_3 cycle), that is initiated by ribulose-1,5,-bisphosphate carboxylase/oxygenase (rubisco).

Rubisco: the coordinator of carbon flux

The fixation of CO_2 through rubisco carboxylation (v_c) initiates net carbon fixation (A) through the Calvin-Benson cycle, while the fixation of O_2 through rubisco oxygenation (v_o) initiates photorespiration. Rubisco was discovered to have dual substrate affinity for CO_2 and O_2 (Bowes *et al.*, 1971). Similar to CO_2, O_2 can diffuse readily into the leaf and to the chloroplast through similar processes. This is mainly a problem for C_3 plants as they have not evolved the mechanisms to concentrate CO_2 around rubisco to prevent O_2 addition (like C_4 or CAM plants). Subsequently, CO_2 and

O_2 were found to behave as competitive inhibitors towards each other (Badger *et al.*, 1974; Bowes *et al.*, 1972; Laing, 1974; Peisker, 1974). Although the kinetic partitioning between CO_2 and O_2 addition favors rubisco carboxylation (rubisco specificity; $S_{c/o}$), rubisco oxygenation reactions frequently occur (Tcherkez, 2016; Tcherkez *et al.*, 2006).

The carboxylation of RuBP, yields two molecules of 3-phosphoglycerate (3-PGA) that are further metabolized by the Calvin-Benson Cycle. However, when rubisco catalyzes the oxygenation of RuBP, one molecule of 3-PGA, and one molecule of 2-phosphoglycolate (2-PG) are produced. While 3-PGA can be metabolized by Calvin-Benson cycle, 2-PG is an inhibitory intermediate of the Calvin-Benson cycle enzymes must be detoxified (Anderson, 1971; Flügel *et al.*, 2017; Kelly *et al.*, 1976; Kelly *et al.*, 1977).

The photorespiratory pathway

To reduce the inhibition of the Calvin-Benson Cycle enzymes, a process known as photorespiration detoxifies and recycles 2-PG through a set of reactions that salvage most of the carbon initially present in 2-PG (see Figure 1.1 for review on photorespiratory pathway).

Although the photorespiratory pathway represents a metabolic repair system to convert 2-PG back to 3-PGA and is a particular solution that has evolved to handle rubisco oxygenation, it lowers the efficiency of photosynthesis by reducing *A* (Bauwe *et al.*, 2012). Rates of *A* can be accurately modeled based on the reaction kinetics of rubisco for either CO_2 or O_2 by the following equation:

$$A = v_c - 0.5v_o - R_L \quad (1)$$

Where, v_c and v_o denote rubisco carboxylation and oxygenation rates, and R_L represents respiration in the light (Walker *et al.*, 2016). The loss of photorespiratory carbon (0.5) is generally assumed to occur through the decarboxylation of glycine to serine in the mitochondrion by glycine decarboxylase complex (GDC) (Abadie *et al.*, 2016; Somerville, 2001; Somerville *et al.*, 1980). However, there has been evidence suggesting additional CO_2 is released from non-enzymatic decarboxylation (NED) that occurs with hydrogen peroxide (H_2O_2) and photorespiratory intermediates, glyoxylate and hydroxypyruvate (Bao *et al.*, 2021). Additional CO_2 from NED combined with CO_2 loss from GDC would further reduce *A* by increasing the stoichiometric loss of CO_2 per

oxygenation (i.e., raising 0.5). Altogether, the cost of photorespiration on *A* depends on the rate of v_o. While early estimates of photorespiratory CO_2 loss reduce *A* by ~25% under laboratory conditions (25◦C & 350 ppm), the CO_2 loss under dynamic conditions can vary with growth conditions or fluctuating environmental pressures (Sharkey, 1988; Walker *et al.*, 2016).

The influence of abiotic factors in the context of future climate conditions

Anthropogenic activities are rapidly changing the composition and thermal conditions of the global atmosphere, leading to fundamental trade-offs in photosynthetic carbon metabolism. Burning fossil fuels has and continues to liberate enormous quantities of CO_2 and other greenhouse gases into the atmosphere, which has increased global temperatures due to their role in radiative heat transfer (Wei *et al.*, 2018). The most recent Intergovernmental Panel on Climate Change (IPCC) report indicates that global surface temperatures have increased faster in the last 50 years due to anthropogenic greenhouse gas release than in any other 50-year period in the previous 2000 years (Lee *et al.*, 2023).

The enrichment of atmospheric CO_2 concentrations and warming of the atmosphere exert opposite effects on rates of rubisco v_c and v_o. Considering just an increase in CO_2 concentration, rubisco catalyzes more carboxylation reactions due to the heightened partial pressure of chloroplastic CO_2 surrounding the enzyme (Drake *et al.*, 1997). However, as climates warm, temperature-dependent shifts in rubisco specificity ($S_{c/o}$) and gas solubility cause greater rates of rubisco oxygenation than at lower temperatures. The temperature response of $S_{c/o}$ decreases with temperature because the Michaelis-Menten constant (K_m) for CO_2 increases. This increase in K_m decreases the CO_2 affinity of rubisco and therefore reduces the $S_{c/o}$ (Hall *et al.*, 1983; Hermida-Carrera *et al.*, 2016; Jordan *et al.*, 1984). The temperature response of the relative concentration of CO_2/O_2 decreases with temperature, limiting the CO_2 partial pressure at rubisco. Therefore, elevated temperatures will cause rubisco to catalyze more oxygenation reactions with RuBP, producing larger amounts of 2-PG.

Photorespiratory capacity and the influence of enzymatic bottlenecks

While rubisco sets the rate of 2-phosphoglycolate (2-PG) production through v_o (photorespiratory influx), the enzymes downstream of rubisco must process the subsequent photorespiratory intermediates that are produced. Some of these reactions process biologically inert photorespiratory intermediates, like glycine, but others degrade biologically active intermediates, such as 2-phosphoglycolate (2-PG), glycolate, and H_2O_2. If there is mismatch between photorespiratory influx and the capacities of downstream photorespiratory reactions, photorespiratory intermediates will accumulate due to insufficient conversion rates. This capacity of photorespiration is set by the maximal reaction velocity (V_{max}) for each enzyme downstream of rubisco. Mismanagement of photorespiratory capacity to the rates of photorespiratory influx could appear as enzymatic bottlenecks, where rate of the reaction is significantly limited by the activity of the enzyme. Managing these intermediates is important to maintain plant vigor, especially in changing environments where photorespiratory influx is unpredictable. Currently, it is unclear if photorespiratory biochemistry downstream of rubisco adjusts to handle a greater carbon influx through photorespiration.

Overall goal of the research

The long-range goal is to engineer photorespiration to improve net carbon fixation under future climate conditions in C_3 crops. The objective of this dissertation contributes to this long-range goal through the identification of key photorespiratory mechanisms that maintain *A* in adapted (chapter 2), acclimated (chapter 3), and engineered (chapter 4) plant systems. This research looks past rubisco, which has been a prominent focus in engineering efforts, to explore downstream photorespiratory enzymes that directly manage carbon flux through photorespiration. My central hypothesis throughout this dissertation is that photorespiratory capacity limits *A* when photorespiratory influx outpaces downstream photorespiratory capacity. The insufficient conversion rate and therefore accumulation of various biologically active photorespiratory intermediates, such as 2-phosphoglycolate or H_2O_2, could led to a reduction of *A* due to inhibitory effects on the Calvin-Benson Cycle, increase photorespiratory CO_2 release, or have broader consequences related to plant signaling. The rationale underlying the dissertation research is that, once key enzymatic steps or

bottlenecks are identified, we can increase photorespiratory capacity through engineering or breeding efforts to maintain photosynthetic performance when v_o is unpredictable in fluctuating environmental conditions. In the absence of such knowledge, improvements to C_3 crop productivity under future climate conditions – mainly elevated temperatures - will be limited.

Figures

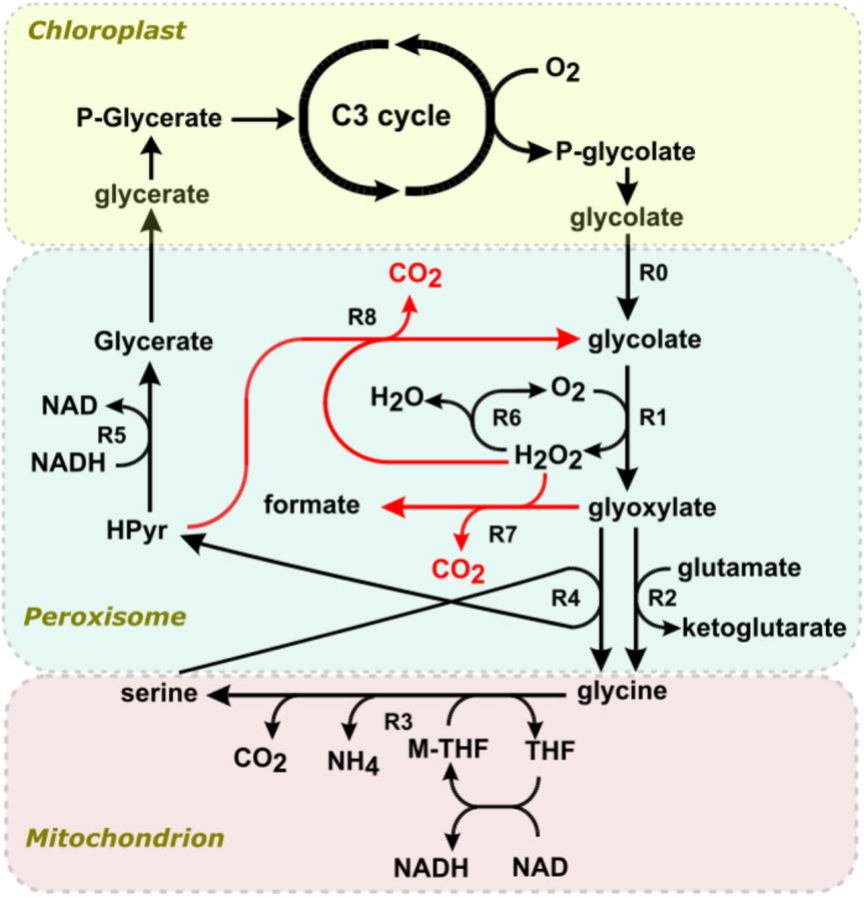

Figure 1.1. Photorespiratory Pathway. Following the oxygenation of RuBP by rubisco in the chloroplast and the formation of phosphoglycolate (2-PG), phosphoglycolate phosphatase (PGP) converts 2-PG into glycolate. Glycolate in transported to the peroxisome where glycolate oxidase (GO) catalyzes the conversion of glycolate in the presence of O_2 to glyoxylate and hydrogen peroxide (H_2O_2). H_2O_2 is decomposed in the peroxisome into H_2O and O_2 by catalase (CAT), while glyoxylate is animated with glutamate or alanine to produce glycine via aminotransferase (GGAT or AGAT). Glycine in transported into the mitochondrion and decarboxylated to produce serine by glycine decarboxylate complex and serine hydromethyltransferase. Serine is transported back to the peroxisome and converted to hydroxypyruvate by serine glyoxylate aminotransferase (SGAT). hydroxypyruvate is reduced by hydroxypyruvate reductase (HPR) to form glycerate. Glycerate is transported back to the chloroplast and catalyzed by glycerate kinase (GLYK) to 3-PGA, which re-enter the C_3 cycle. Image reproduced from: Catalase protects against nonenzymatic decarboxylations during photorespiration in *Arabidopsis thaliana*, Bao *et al.*, Plant Direct Volume 5 Issue 12. Copyright (c) [2021] authors hold copyright and have given permission to reproduce.

LITERATURE CITED

Abadie, C., Boex-Fontvieille, E. R., Carroll, A. J., & Tcherkez, G. (2016). In vivo stoichiometry of photorespiratory metabolism. *Nature Plants, 2*(2), 1-4.

Anderson, L. E. (1971). Chloroplast and cytoplasmic enzymes II. Pea leaf triose phosphate isomerases. *Biochimica et Biophysica Acta (BBA) - Enzymology, 235*(1), 237-244. doi:https://doi.org/10.1016/0005-2744(71)90051-9

Badger, M. R., & Andrews, T. J. (1974). Effects of CO2, O2 and temperature on a high-affinity form of ribulose diphosphate carboxylase-oxygenase from spinach. *Biochemical and Biophysical Research Communications, 60*(1), 204-210. doi:https://doi.org/10.1016/0006-291X(74)90192-2

Bao, H., Morency, M., Rianti, W., Saeheng, S., Roje, S., Weber, A. P. M., & Walker, B. J. (2021). Catalase protects against nonenzymatic decarboxylations during photorespiration in Arabidopsis thaliana. *Plant Direct, 5*(12), e366. doi:https://doi.org/10.1002/pld3.366

Bauwe, H., Hagemann, M., Kern, R., & Timm, S. (2012). Photorespiration has a dual origin and manifold links to central metabolism. *Current Opinion in Plant Biology, 15*(3), 269-275. doi:10.1016/j.pbi.2012.01.008

Bowes, G., & Ogren, W. L. (1972). Oxygen inhibition and other properties of soybean ribulose 1,5-diphosphate carboxylase. *J Biol Chem, 247*(7), 2171-2176.

Bowes, G., Ogren, W. L., & Hageman, R. H. (1971). Phosphoglycolate production catalyzed by ribulose diphosphate carboxylase. *Biochemical and Biophysical Research Communications, 45*(3), 716-722. doi:https://doi.org/10.1016/0006-291X(71)90475-X

Drake, B. G., Gonzàlez-Meler, M. A., & Long, S. P. (1997). More efficient plants: a consequence of rising atmospheric CO2? *Annual Review of Plant Biology, 48*(1), 609-639.

Evans, J. R. (2021). Mesophyll conductance: walls, membranes and spatial complexity. *New Phytologist, 229*(4), 1864-1876. doi:https://doi.org/10.1111/nph.16968

Evans, J. R., Kaldenhoff, R., Genty, B., & Terashima, I. (2009). Resistances along the CO2 diffusion pathway inside leaves. *Journal of Experimental Botany, 60*(8), 2235-2248. doi:10.1093/jxb/erp117

Evans, J. R., & Von Caemmerer, S. (1996). Carbon Dioxide Diffusion inside Leaves. *Plant Physiol, 110*(2), 339-346. doi:10.1104/pp.110.2.339

Farquhar, G. D., & Sharkey, T. D. (1982). Stomatal Conductance and Photosynthesis. *Annual Review of Plant Physiology, 33*(1), 317-345. doi:10.1146/annurev.pp.33.060182.001533

Flügel, F., Timm, S., Arrivault, S., Florian, A., Stitt, M., Fernie, A. R., & Bauwe, H. (2017). The Photorespiratory Metabolite 2-Phosphoglycolate Regulates Photosynthesis and Starch Accumulation in Arabidopsis. *The Plant Cell, 29*(10), 2537-2551. doi:10.1105/tpc.17.00256

Hall, N. P., & Keys, A. J. (1983). Temperature dependence of the enzymic carboxylation and oxygenation of ribulose 1, 5-bisphosphate in relation to effects of temperature on photosynthesis. *Plant Physiology, 72*(4), 945-948.

Hermida-Carrera, C., Kapralov, M. V., & Galmés, J. (2016). Rubisco Catalytic Properties and Temperature Response in Crops. *Plant Physiology, 171*(4), 2549-2561. doi:10.1104/pp.16.01846

Jordan, D. B., & Ogren, W. L. (1984). The CO2/O2 specificity of ribulose 1,5-bisphosphate carboxylase/oxygenase. *Planta, 161*(4), 308-313. doi:10.1007/BF00398720

Kaldenhoff, R. (2012). Mechanisms underlying CO2 diffusion in leaves. *Curr Opin Plant Biol, 15*(3), 276-281. doi:10.1016/j.pbi.2012.01.011

Kelly, G. J., & Latzko, E. (1976). Inhibition of spinach-leaf phosphofructokinase by 2-phosphoglycollate. *FEBS Letters, 68*(1), 55-58. doi:https://doi.org/10.1016/0014-5793(76)80403-6

Kelly, G. J., & Latzko, E. (1977). Chloroplast Phosphofructokinase: II. Partial Purification, Kinetic and Regulatory Properties. *Plant Physiology, 60*(2), 295-299. doi:10.1104/pp.60.2.295

Laing, W. A. (1974). Regulation of Soybean Net Photosynthetic CO(2) Fixation by the Interaction of CO(2), O(2), and Ribulose 1,5-Diphosphate Carboxylase. *Plant Physiology, 54*(5), 678-685. doi:10.1104/pp.54.5.678

Lee, H., Calvin, K., Dasgupta, D., Krinner, G., Mukherji, A., Thorne, P., . . . Barrett, K. (2023). Climate change 2023: synthesis report. Contribution of working groups I, II and III to the sixth assessment report of the intergovernmental panel on climate change. 35-115.

Peisker, M. (1974). model describing the influence of oxygen on photosynthetic carboxylation. *Photosynthetica*.

Sharkey, T. D. (1988). Estimating the rate of photorespiration in leaves. *Physiologia Plantarum, 73*(1), 147-152. doi:https://doi.org/10.1111/j.1399-3054.1988.tb09205.x

Somerville, C. R. (2001). An early Arabidopsis demonstration. Resolving a few issues concerning photorespiration. *Plant Physiology, 125*(1), 20-24.

Somerville, C. R., & Ogren, W. L. (1980). Photorespiration mutants of Arabidopsis thaliana deficient in serine-glyoxylate aminotransferase activity. *Proceedings of the National Academy of Sciences, 77*(5), 2684-2687.

Tcherkez, G. (2016). The mechanism of Rubisco-catalysed oxygenation. *Plant, Cell & Environment, 39*(5), 983-997. doi:https://doi.org/10.1111/pce.12629

Tcherkez, G. G., Farquhar, G. D., & Andrews, T. J. (2006). Despite slow catalysis and confused substrate specificity, all ribulose bisphosphate carboxylases may be nearly perfectly optimized. *Proceedings of the National Academy of Sciences, 103*(19), 7246-7251. Retrieved from https://www.ncbi.nlm.nih.gov/pmc/articles/PMC1464328/pdf/zpq7246.pdf

Walker, B. J., VanLoocke, A., Bernacchi, C. J., & Ort, D. R. (2016). The Costs of Photorespiration to Food Production Now and in the Future. *Annual Review of Plant Biology, 67*(1), 107-129. doi:10.1146/annurev-arplant-043015-111709

Wei, P. S., Hsieh, Y. C., Chiu, H. H., Yen, D. L., Lee, C., Tsai, Y. C., & Ting, T. C. (2018). Absorption coefficient of carbon dioxide across atmospheric troposphere layer. *Heliyon, 4*(10), e00785. doi:10.1016/j.heliyon.2018.e00785

CHAPTER 2: Increased activity of core photorespiratory enzymes and CO_2 transfer conductances are associated with higher and more optimal photosynthetic rates under elevated temperatures in the extremophile *Rhazya stricta*

This research was adapted from:

Gregory, L.M., Roze, L.V. & Walker, B.J. (2023) Increased activity of core photorespiratory enzymes and CO_2 transfer conductances are associated with higher and more optimal photosynthetic rates under elevated temperatures in the extremophile *Rhazya stricta*. Plant, Cell & Environment, 46, 3704–3720.

Abstract

Unique challenges of photosynthetic carbon fixation at elevated temperatures include increased photorespiration and optimizing intrinsic water use efficiency (*WUE*). To determine how plants can adapt to facilitate high rates of photorespiration at elevated temperatures while also maintaining water-use efficiency, we performed in-depth gas exchange and biochemical assays of the C_3 extremophile, *Rhazya stricta*. These results demonstrate that *R. stricta* supports higher rates of photorespiration under elevated temperatures and that these higher rates of photorespiration correlate with increased activity of key photorespiratory enzymes; phosphoglycolate phosphatase and catalase. The increased photorespiratory enzyme activities may increase the overall capacity of photorespiration by reducing enzymatic bottlenecks and allowing minimal inhibitor accumulation under high photorespiratory rates. Additionally, we found the CO_2 transfer conductances (stomatal and mesophyll) are re-allocated to increase the water-use efficiency in *R. stricta* but not necessarily the photosynthetic response to temperature. These results suggest important adaptive strategies in *R. stricta* that maintain photosynthetic rates under elevated temperatures with optimal water loss. The strategies found in *R. stricta* may inform breeding and engineering efforts in other C_3 species to improve photosynthetic efficiency at high temperatures.

Keywords: Photorespiration, *Rhazya stricta*, phosphoglycolate phosphatase, catalase, water-use efficiency, CO_2 transfer conductance

Introduction

Global warming has increased the frequency of high temperature events that place physiological constraints on C_3 photosynthetic performance. This warming is happening rapidly; the most recent IPCC report estimates global surface temperatures will increase by 1.4°C – 4.8°C in the next century, meaning that future plants will experience higher temperatures than they have experienced in at least the last 100,000 years (Pörtner *et al.*, 2022). Increasing global surface temperatures will raise air temperature and alter atmospheric vapor pressure deficit (VPD), which directly influences various physiological processes in plants (Moore *et al.*, 2021). These physiological processes include enzymatic temperature response, leaf energy balance, stomatal behavior, cell membrane properties, and changes in photosynthetic performance (Larkindale *et al.*, 2004; Marcum, 1998; Moore *et al.*, 2021; Prasertthai *et al.*, 2022; Urban *et al.*, 2017a; Urban *et al.*, 2017b). While all these physiological processes are important, photosynthetic performance under future climates is of particular interest due to its participation in the global carbon cycle and recent efforts to improve its efficiency (De Souza *et al.*, 2022; Kromdijk *et al.*, 2016; South *et al.*, 2018). Photorespiration and intrinsic water use efficiency (*WUE*) will disproportionately affect C_3 species as temperatures increase since they lack the carbon concentrating mechanism of C_4 or CAM species. Understanding how C_3 species will manage higher photorespiratory fluxes and optimize *WUE* at elevated temperatures will help us resolve temperature-dependent mechanisms and likely advance breeding and engineering strategies in C_3 species.

Increased photorespiration limits C_3 photosynthetic performance at elevated temperatures. The photorespiration pathway begins when O_2 binds to ribulose-1,5-bisphosphate carboxylase/oxygenase (rubisco) instead of CO_2. The resulting oxygenation of ribulose-1,5-bisphosphate (RuBP) produces 3-phosphoglycerate (3-PGA), a C_3 cycle intermediate, and 2-phosphoglycolate (2-PG), an intermediate that inhibits the C_3 cycle enzymes triose phosphate isomerase and sedoheptulose-1,7-bisphosphatase (Anderson, 1971; Flügel *et al.*, 2017). To reduce the inhibition of the C_3 cycle enzymes, photorespiration detoxifies and recycles 2-PG back into 3-PGA through a set of reactions that occur in the chloroplast, peroxisome, mitochondrion, and cytosol

(see Figure 1.1 in Chapter 1). Although the photorespiratory pathway is an effective solution to handle RuBP oxygenation, it lowers the efficiency of photosynthesis by reducing net carbon fixation by releasing CO_2 (Bauwe *et al.*, 2012). Relative rates of RuBP oxygenation increase with temperature due to decreases in rubisco specificity and decreased solubility of CO_2 relative to O_2 (Hall *et al.*, 1983; Hermida-Carrera *et al.*, 2016; Jordan *et al.*, 1984). Therefore, under elevated temperature, greater oxygenation rates will increase rates of 2-PG production that need to be detoxified and recycled by the photorespiratory pathway. While rubisco kinetics and gas solubilities determine the rate at which 2-PG is initially produced following rubisco oxygenation, the temperature response of downstream photorespiration and the effects on subsequent CO_2 loss is unclear. Loss of CO_2 occurs through the decarboxylation of glycine in the mitochondrion; however, there is evidence for additional release of CO_2 from non-enzymatic decarboxylation reactions that occur within the peroxisome, especially under elevated temperatures (Abadie *et al.*, 2016; Bao *et al.*, 2021; Somerville, 2001; Somerville *et al.*, 1980; Walker *et al.*, 2013). The CO_2 released from nonenzymatic decarboxylation reactions combined with CO_2 loss from GDC would reduce net carbon fixation.

Another challenge of maintaining C_3 photosynthetic performance at elevated temperatures is preserving plant water. The driving force of water vapor loss or transpiration from the plant to the atmosphere is VPD. VPD, which is the difference in water vapor partial pressure between the intercellular airspace of the leaf and the atmosphere, responds to air temperature. As temperatures rise, VPD increases curvilinearly and drives greater transpiration rates (Lawrence, 2005). The greater rates of transpiration alter CO_2 and H_2O exchange between plants and the atmosphere and cause a greater water loss per carbon assimilated (or reduction in *WUE*) because CO_2 and H_2O exchange through the same stomatal pore (Rawson *et al.*, 1977). While the stomatal conductance (g_{sw}) constrains CO_2 and H_2O exchange with the atmosphere and the intercellular airspace, mesophyll conductance (g_m) constrains only the transfer of CO_2 from the intercellular airspace to the site of carboxylation without a corresponding loss of H_2O. Given the ability of g_m to facilitate CO_2 transfer without accompanying H_2O loss, it is unclear to what degree plants adapted to high temperatures have exploited this property to limit water loss while maximizing CO_2 availability. The reduction of CO_2

availability through regulated decreases in g_{sw} is large enough to decrease photosynthetic performance in C_3 plants, which lack a carbon concentrating mechanism.

Does C_3 photosynthetic performance always decrease with increasing temperatures, or have some C_3 species adapted to facilitate high rates of photorespiration while maintaining photosynthesis and *WUE* at elevated temperatures? To explore this question, we investigated how *Rhazya stricta*, a C_3 desert extremophile, has adapted to maintain photosynthetic performance at elevated temperatures. *R. stricta* is ideal for studying heat adaptation as it is native to hot-arid environments. Past work suggests that *R. stricta* has distinct physiological adaptations to extreme temperatures (Lawson et al., 2014; Yates et al., 2014). For example, leaf temperature during *in situ* diurnal measurements of *R. stricta* climbed from 26°C to 43°C with an accompanying increase in photorespiration (Lawson *et al.*, 2014). During this increase in temperature, the relative water content in the leaf was stable, suggesting there was no water stress.

In this paper, we determine how *R. stricta* facilitates high rates of photorespiration while maintaining photosynthesis and *WUE* at elevated temperatures. Here, we hypothesize that *R. stricta* maintains photorespiratory capacity at elevated temperatures through increased activity of key photorespiratory enzymes. We additionally hypothesize that *R. stricta* optimizes *WUE* by favoring g_m relative to g_{sw} under elevated temperatures. To test these hypotheses, we compared various physiological and biochemical parameters in two species, *Nicotiana tabacum*, a thermotolerant C_3 species, and *R. stricta*, an extremophilic C_3 species. The results from these measurements indicate that *R. stricta* maintains higher rates of photorespiration than *N. tabacum* under moderate and elevated temperatures and that these higher rates of photorespiration correlate with increased activity of key photorespiratory enzymes; phosphoglycolate phosphatase and catalase. Additionally, the g_{sw} and g_m appear to be optimized for water-use efficiency but not necessarily photosynthetic carbon gain to temperature in *R. stricta*. These results suggest important adaptive strategies in *R. stricta* that maintain photosynthetic rates under elevated temperatures with optimal water loss.

Material and Methods

Plant Material and Growth Conditions

R. stricta seeds were wild-collected for this study and are available through the Millennial Seed Bank coordinated by the Royal Botanical Gardens, Kew Serial number 220547. Prior to planting, *R. stricta* seeds were surface-sterilized inside a Laminar hood with 100% ethanol for five minutes followed by a seven-minute soak in 25% bleach solution. Seeds were then washed and vortexed three times in deionized water. After sterilization, seeds germinated in a petri dish filled with deionized water for two-weeks. During the two weeks, water was changed as needed to remove yellow exudate to avoid possible allelopathic inhibition of germination. Seeds were transferred when roots emerged and were 1 cm in length to 11.36 L pots containing half Sure-Mix potting soil (Michigan Grower Products, Inc., Galesburg, MI) and half sand mixture. *R. stricta* were grown for an additional eight weeks until leaves were large enough for gas exchange measurements. *N. tabacum* were sown and grown in 0.7 L pots containing Sure-Mix potting soil (Michigan Grower Products, Inc., Galesburg, MI) for 4-6 weeks until leaves were large enough for gas exchange measurements. Both *R. stricta* and *N. tabacum* plants were grown in a greenhouse with an average day/night temperature of 34/27◦C and a 16/8 photoperiod of supplemental light (150 µmol m^{-2} s^{-1}). Plants were watered as needed with ½-strength Hoagland's solution.

Estimating C_i^* and R_L using the common intersection method

Gas exchange was measured on the youngest, fully expanded leaves of *R. stricta* and *N. tabacum* using a LI-6800 (LI-COR Biosciences, USA) using a 9 cm^2 chamber with 50:50 blue:red LEDs to better replicate the blue to red ratio of the solar spectrum at the earth's surface. To shift between temperatures ranging from 20◦C to 40◦C, the LI-6800 was placed inside a climate-controlled chamber (Percival Scientific, USA). The apparent CO_2 compensation point uncorrected for g_m (C_i^*) and rates of CO_2 release from non-photorespiratory processes in the light (R_L) were measured using the common intersection method (Laisk, 1977; Walker *et al.*, 2016a). During the measurement, steady-state *A* was measured at 3, 5, 7, 9, 11, 40 pascal (Pa) CO_2 under various light intensities (250, 165, 120, 80, 50 µmol PAR m^{-2} s^{-1}), with a flow rate of 500 µmol s^{-1}. Linear fits of the CO_2 response curves were made for each light intensity. A

linear regression of the slope-intercept from these linear fits was used to estimate C_i^* and R_L.

Measuring g_m with gas exchange and ^{13}C isotope discrimination

g_m was measured using *in vivo* gas exchange combined with on-line measurements of the carbon isotope discrimination method with a system as described previously (Fu *et al.*, 2023)(See Appendix 1). Briefly, gas exchange was performed as above using an LI-6800 with 9 cm^2 chamber with 50:50 blue:red LEDs. To measure carbon isotope discrimination, the LI-6800 was coupled to a tunable infrared laser differential absorption spectrometer (TILDAS-CS, Aerodyne Research, USA). The CO_2 in the leaf chamber, flow rate, and irradiance were set to 40 Pa CO_2, 300 µmol s^{-1}, 1750 µmol PAR m^{-2} s^{-1}, respectively. Measurements were made under 2% O_2 to minimize uncertainties about precise photorespiratory fractionation (*f*) values and since g_m has not been shown to be oxygen dependent (further validated below). To measure under 2% O_2, N_2 and O_2 were mixed by mass-flow controllers (Alicat Scientific, Inc., USA). For calibrating the $\delta^{13}C$ values, a reference line was supplied with isotopically characterized CO_2 ($\delta^{13}C$ vs. VPDB: -4.6 ± 0.3 ‰, (Airgas Specialty Gases, USA)). Leaves were measured after reaching steady-state assimilation rate (*A*) at each temperature starting at 20°C and increasing to 40°C, by 5°C steps. g_m was calculated from carbon isotope equations presented previously (Ubierna *et al.*, 2018) that build upon foundation work in isotope-ration mass spectroscopy-based approaches in isotope discrimination (Evans *et al.*, 1986; Farquhar *et al.*, 1982; Farquhar *et al.*, 2012) and the recent advances in online methods using tunable diode lasers (Barbour *et al.*, 2007; Tazoe *et al.*, 2011; von Caemmerer *et al.*, 2015).

Measuring the temperature response for photorespiratory discrimination and fractionation

Photorespiratory discrimination (Δ_f) and the $^{12}C/^{13}C$ fractionation during photorespiration (*f*) for *R. stricta* and *N. tabacum* were resolved using the *in vivo* gas exchange combined with on-line measurements of the carbon isotope discrimination (described above). Leaves were measured at 25°C and 35°C, both at 2% and 21% oxygen. g_m was determined at 2% oxygen where photorespiratory release of CO_2 was minimized assuming f = 11.8‰ (with the corresponding rubisco ^{13}C fractionation; 30‰)

(Tcherkez, 2006; Ubierna *et al.*, 2018). We then assumed the g_m measurements at 2% oxygen were the same as the g_m at 21% oxygen to solve for Δ_{gm} at both measuring temperatures. g_m was also determined assuming f = 11.8‰ for both oxygen concentrations for each temperature. We could calculate Δ_f using:

$$\Delta_f = \Delta_i - \Delta_o - \Delta_{g_m} - \Delta_e \quad (1)$$

Then, with Δ_f, derive f by:

$$f = \frac{1 - t}{1 + t}\frac{\alpha_e}{\alpha_f}\Delta_f \frac{C_a}{A} \quad (2)$$

(Evans *et al.*, 2013; Ubierna *et al.*, 2018)

Calculating Γ^*

Γ^* in *R. stricta* and *N. tabacum* was calculated using C_i^*, R_L and g_m. Γ^* was determined according to

$$\Gamma^* = C_i^* + \frac{R_L}{g_m} \quad (3)$$

(Von Caemmerer, 2000). To account for internal dependency on solved parameters, g_m and Γ^* were re-solved iteratively using previous g_m, and Γ^* values; iterations continued until there was no change in re-solved g_m, and Γ^*.

Estimating rates of v_c and v_o

v_c and v_o for *R. stricta* and *N. tabacum* were estimated according to

$$v_c = \frac{A + R_L}{1 - \Gamma^*/C_c} \quad (4)$$

$$v_o = \frac{v_c - A - R_L}{0.5} \quad (5)$$

(Walker *et al.*, 2020). Where, the partial pressure of CO_2 at the site of rubisco catalysis (C_c) was determined by

$$C_c = C_i - \frac{A}{g_m} \quad (6)$$

Finding saturating light intensity and maximum quantum yield

Gas exchange was measured on the youngest, fully expanded leaves of *R. stricta* and *N. tabacum* using a LI-6800 (LI-COR Biosciences, USA) using a 6 cm^2 chamber with 50:50 blue:red LEDs. During the measurement, steady-state A was

measured at 40 Pa CO_2 under monotonically decreasing light intensities (2000, 1500, 1000, 750, 500, 350, 250, 150, 75, 50, 45, 40, 35, 30, 25, 20, 15, 10, 5 µmol PAR m^{-2} s^{-1}) with a flow rate of 500 µmol s^{-1}. The leaf absorptivity in *R. stricta* and *N. tabacum* leaves was measured using a SpectroClip-JAZ-TR integrating sphere (Ocean Optics inc., USA) and used to calculate absorbed quanta. To find maximum quantum yield of CO_2 fixed per photon absorbed, the relationship of assimilation to absorbed quanta was then fit to a linear regression at low light intensity.

Measuring $v_{c,max}$ and J_{max} with the Dynamic Assimilation Technique

Gas exchange was measured on the youngest, fully-expanded leaves of *R. stricta* and *N. tabacum* using a LI-6800 (LI-COR Biosciences, USA) with a 6 cm^2 chamber with 50:50 blue:red LEDs. To shift between temperatures ranging from 20°C to 40°C, the LI-6800 was located inside of a climate-controlled chamber (Percival Scientific, USA). Range matching and dynamic calculations were preformed according to manufacturer's instructions. CO_2 response curves for fitting maximum rate of rubisco carboxylation ($v_{c,max}$) and maximum rate of electron transport (J_{max}) were measured under saturating light (1750 µmol PAR m^{-2} s^{-1}) from 150 Pa CO_2 to 5 Pa CO_2 with a flow rate of 200 µmol s^{-1}. Leaves stabilized at 150 Pa CO_2 at the measuring temperature for 30-40 minutes before decreasing CO_2 concentrations monotonically. This method was utilized to reduce the oscillations that occur under triose-phosphate utilization limitation (McClain *et al.*, 2023); however, this parameter could still not properly be fitted. $v_{c,max}$ and J_{max} were estimated using an R-based *ACi* fitting tool (Gregory *et al.*, 2021) (see https://github.com/poales/msuRACiFit to access Rscript with user-friendly interface)(See Appendix 2).

We used the Dynamic Assimilation Technique rather than using a steady-state method to generate the CO_2 response curves. Response curves that utilize continuous ramping of CO_2 aren't new, as the Dynamic Assimilation Technique is based on the previously established RACiR method (Stinziano *et al.*, 2017). The difference between the two is that the Dynamic Assimilation Technique does not require an empty chamber correction, which saves time during the measurement (Saathoff *et al.*, 2021). The speed in which the CO_2 response curves can be obtained (i.e., 5-7 minutes) compared to the traditional (i.e., 40-45 minutes) was especially important for measuring each genotype

under a range of temperatures where we wanted to limit the plant's exposure to each condition.

Calculating Lg_{tc}, Lg_m and WUE

Using the CO_2 response curves from above, Lg_{tc} and Lg_m were calculated at ambient CO_2 concentration (40-42 Pa CO_2). Lg_{tc} was calculated according to

$$L_{g_{tc}} = \frac{A_{sl} - A_n}{A_{sl}} \quad (7)$$

(Warren, 2004). Where A_n is the A that occurs at C_a 40-42 Pa CO_2 and A_{sl} (assuming no stomatal resistance) is the A that occurs when C_i 40-42 Pa CO_2. Lg_{tc} was calculated according to

$$L_{g_m} = \frac{A_{ml} - A_n}{A_{ml}} \quad (8)$$

where A_{ml} (assuming stomatal but no mesophyll resistance) is the A that occurs when $C_c = C_i$ when C_a is 40-42 Pa CO_2. *WUE* was calculated from gas exchange measurements at 40 Pa CO_2 according to

$$WUE = \frac{A}{g_{sw}} \quad (9)$$

(Vialet-Chabrand *et al.*, 2016).

Preparing crude protein extract for protein quantification and enzymatic assays

Crude protein extracts were prepared from the youngest, fully expanded leaves of *R. stricta* and *N. tabacum*. Leaf punches were obtained from *R. stricta* and *N. tabacum* using a cork borer (8.15 mm and 17 mm), immediately frozen in liquid N_2, and stored at -80°C. Leaf material was homogenize on ice with 1 mL of the Extraction buffer (50 mM EPPS buffer, pH 8.0, containing 1 mM EDTA, 10 mM DTT, 0.1% Triton X-100 [v/v], 0.5% polyvinylpyrrolidone, and 10 uL 1X SigmaFAST Protease Inhibitor Cocktail, EDTA Free (Sigma, St. Louis, MO, USA)), using a 2 mL glass-to-glass homogenizer (Kontes Glass Co., Vineland, NJ, USA). The homogenate was transferred into a 1.5 mL plastic Eppendorf tube and clarified by centrifugation for 10 min at 13,500 g and 4°C (Eppendorf Centrifuge 5424R). The supernatant, containing the clarified crude protein extract, was used for protein quantification and enzyme assays.

Protein quantification

Soluble protein content was determined in crude protein extract (Bio-Rad Protein Assay; BIO-RAD, USA) according to the manufacturer instructions using a SpectraMax M2 Microplate Reader (Molecular Devices, San Jose, CA, USA).

Enzymatic Assays

All enzyme activities were measured by *spectrophotometric* assays with the use of SpectraMax M2 Plate reader and SoftMax Pro7 software (Molecular Devices, San Jose, CA, USA). PGP, GO, GGAT, AGAT, SGAT, HPR, and GLYK assays were performed in a 200 µL total reaction mix using polystyrene or acrylic UV transparent 96-well microplates (Corning, Kennebunk, ME, USA), while the CAT assay was performed in 1 mL reaction mix using a quartz cuvette. The pH of reactions was selected based on the organellar pH where the reaction occurs (Heinze *et al.*, 2002; Kendziorek *et al.*, 2008; Liu *et al.*, 2008; Shen *et al.*, 2013). All enzyme assays were performed across two temperatures (25°C and 35°C) with three technical replicates. There were 4 – 5 independent biological replicates measured using leaf tissue from different plants.

Phosphoglycolate phosphatase (PGP) activity

PGP activity was determined in *R. stricta* and *N. tabacum* colormetrically by the production of inorganic phosphate with the following modifications (Pai *et al.*, 1990; Schwarte *et al.*, 2007). 194 µL of reaction buffer (50 mM HEPES buffer, pH 7.5, 1 mM EDTA, and 10 mM $MgCl_2$) were combined with 4 µL of crude protein extract and 2 µL 200 mM 2-PG was added to initiate the reaction. The addition of the substrate was performed using a 96-well microplate replicator (Boekel, Feasterville-Trevose, PA, USA). After 5 min the reaction was terminated by addition 32 µL of Pi reagent (2.5 N H_2SO_4, 0.2 mM antimony potassium tartrate, 4.9 mM ammonium molybdate, and 30 mM ascorbic acid). The plate was covered with parafilm, and the spectrophotometric readings were taken after 45 min at 880 µm using SpectraMax M2. To adjust for Pi that was produced independently from the PGP reaction, a control, containing reaction buffer and crude protein extract, was incubated for 5 min, then the reagent was added followed by 2-PG. A standard curve for Pi was constructed in the range 0.05 – 0.35 ug Pi per well using KH_2PO_4. PGP specific activity was expressed in µmoles of 2-phosphoglycolate m^{-2} s^{-1}.

Glycolate oxidase (GO) activity

The activity of GO was determined in *R. stricta* and *N. tabacum* by formation of glyoxylate phenylhydrazone (Baker *et al.*, 1966; Zelitch *et al.*, 2008) with the following modifications. The reaction mix contained 20 µL 0.5 mM K-phosphate buffer, pH 8.1, 10 µL of 110 mM phenylhydrazine, 10 µL 1.3 mM riboflavin, 3 µL crude protein extract, 152 µL sterile nQ water and 5 µL of 100 mM glycolic acid. The reaction was initiated with glycolic acid after the mix was pre-incubated for 5 min without the substrate. The addition of the substrate was performed with the use of a 96-well microplate replicator (Boekel, Feasterville-Trevose, PA, USA). Control contained 5 µL water instead of the substrate. The increase in OD at 324 um was measured in an acrylic UV transparent plate (Corning, Kennebunk, ME, USA) for 5 min every 10 sec. GO specific activity was calculated using the molar extinction coefficient of the glyoxylate-phenylhydrazone complex (17 mM^{-1} cm^{-1}) and expressed as µmol glyoxylate m^{-2} s^{-1}.

Catalase (CAT) activity

The activity of CAT was determined in *R. stricta* and *N. tabacum* by the decomposition of H_2O_2 (Aebi, 1983; Zelitch, 1989) with the following modifications. Small molecules from crude protein extract from both species were excluded using a Spin-X UF 500 10 K MWCO (Corning/Sigma-Aldrich, Inc. St. Louis, MO, USA) protein concentrator cartridges to removes low molecular weight compounds, including specialized metabolites, which extensively absorb at 240 nm and interfere with the catalase assay. In brief, 300 µL crude protein extract and 200 µL extraction buffer with no PVDP were applied to the concentrator cartridge and centrifuged for 25 min, 15,000 rcf, 4◦C. After centrifugation, an additional 200 µL of extraction buffer with no PVDP was added following another centrifugation under the same parameters. The extract from the concentrator cartridge was adjusted to 300 µL with extraction buffer with no PVDP before enzymatic assay so that catalase was not concentrated during this step. Since the concentrator membrane removes molecules up to 10 kDa and the molecular weight of catalase is ~60 kDa, catalase was not lost during this step and was not likely diluted or concentrated on a volume (or by extension, an area) basis. It is possible that soluble proteins lower than 10 kDa passed through the concentrator, resulting in an increase in

catalase activities expressed on a protein basis. This protein loss was ~10% of the total soluble protein as determined by a Bradford assay.

The reaction mix containing 965.5 µL 50 mM K-phosphate buffer, pH 8.1, and 15 µL extract, was incubated for 1.5 min to determine the rate of background change in optical density. The reaction was initiated with 33.5 µL 30 mM H_2O_2 and the decline in optical density at 240 nm was observed for 1.5 min with 10 sec intervals using spectrophotometer SpectraMax M2. The initial rate of reaction was determined during first 30 sec and the specific activity was expressed as µmoles H_2O_2 m^{-2} s^{-1} using molar extinction coefficient for H_2O_2 at 240 nm 43.6 $M^{-1}cm^{-1}$.

Glutamate glyoxylate aminotransferase (GGAT), alanine glyoxylate aminotransferase (AGAT), and serine glyoxylate aminotransferase (SGAT) activities

The activity of GGAT, AGAT, and SGAT were determined spectrophotometrically as described previously(Liepman *et al.*, 2001, 2003). Recombinant N-terminal 6xHis tagged HPR1 from *A. thaliana* was used as a coupling enzyme in the assay for SGAT. HPR1 was produced in *E. coli* LMG194 using a plasmid pBADAtHPR1 (obtained from S. Timm, University of Rostok, Germany), and the expression and purification of the enzyme were performed essentially as described previously (Liu *et al.*, 2020). The specific activity of GGAT, AGAT, and SGAT were expressed in µmoles of (Glutamate, Alanine, Serine) m^{-2} s^{-1}.

Hydroxypyruvate reductase (HPR) activity

The activity of HPR was determined in *R. stricta* and *N. tabacum* by the oxidation of NADH (Tolbert *et al.*, 1970) with the following modifications. The reaction was initiated by adding 4 µL of 25 Na beta-hydroxypyruvate to the reaction mix, containing 192 µL of reaction buffer (100 mM K-phosphate buffer, pH 8.1, 0.15 mM NADH) and 4 µL crude extract. The addition of the substrate was performed with the use of a 96-well microplate replicator. The decrease in absorbance at 340 nm was monitored continuously for 5 min. To determine the rate of background utilization of NADH, the controls contained 4 µL H_2O instead of the substrate. The specific activity of HPR was expressed in µmoles of hydroxypyruvate m^{-2} s^{-1}.

Glycerate kinase (GLYK) activity

The activity of GLYK was determined by linking formation of 3-phosphoglycerate to NADH oxidation using a set of coupling enzymes identical to the set of coupling enzymes used for measuring rubisco activity (Walker *et al.*, 2016b). 192 µL reaction buffer (containing 50 mM HEPES, pH 7.8, 10 mM $MgCl_2$, 60 mM KCl, 1 mM ATP, 0.2 mM NADH) (Kleczkowski and Randall, 1988) were combined with 4 µL crude protein extract, 4 µL coupling enzymes (22.5 U ml^{-1} 3-phosphoglycerate kinase, 250 U mL^{-1} carbonic anhydrase, 12.5 U mL^{-1} creatine phosphokinase, 20 U mL^{-1} glyceraldehyde-3-phosphate dehydrogenase, 20 U mL^{-1} glycerol-3-phosphate dehydrogenase, 56 U mL^{-1} triose-phosphate isomerase), and the reaction was initiated by addition of 2 µL of 500 mM D-glycerate (5 mM final) (all from Sigma-Aldrich, Inc., St. Louis, MO, United States); the substrate was added with the use of a 96-well microplate replicator. The decrease in optical density at 340 nm was monitored for 10 min. The initial rate of reaction was used to express the specific activity as µmoles glycerate m^{-2} s^{-1}.

Data Processing and Statistical Analyses

Gas exchange, stable carbon isotope, and biochemical data were visualized and analyzed using custom scripts in R (R Core Team, 2021; RStudio Team, 2021). Student's t-test and repeated measures Two-way ANOVA were used to measure significance ($P < 0.05$). All ANOVA tests were followed with a Tukey's post-hoc test. Additionally, all gas-exchange data followed the reporting format and recommendations defined in (Ely *et al.*, 2021).

Results

R. stricta performs higher photorespiration than *N. tabacum* under elevated temperatures

To assess the ability of *R. stricta* and *N. tabacum* to fix carbon under ambient photorespiratory conditions, the temperature response of v_o, v_o/v_c, A and $A + R_L$ were measured under ambient O_2 conditions (21%) at low (250 µmol PAR m^{-2} s^{-1}) and high light (1750 µmol PAR m^{-2} s^{-1}) intensities (Figure 2.1 and Figure 2.2). v_o in *R. stricta* was significantly greater than *N. tabacum* at 25°C, 30°C, 35°C, and 40°C under low light and greater at 25°C, 30°C, and 40°C at high light (Figure 2.1A & C). At the growth temperature (~30°C), v_o in *R. stricta* was 48% (low light) and 60% (high light) greater than *N. tabacum.* The relative rate of rubisco oxygenation (v_o/v_c) in *R. stricta* was significantly greater than *N. tabacum* at 25°C and 40°C under low light and greater at 25°C, 30°C, and 40°C under high light (Figure 2.1B & D). The increased v_o and v_o/v_c in *R. stricta* indicate that rubisco catalyzes oxygenation reactions more frequently than *N. tabacum* and therefore, experiences a greater photorespiratory pressure under most temperatures. *R. stricta* had similar rates of *A* to *N. tabacum* at 20°C, 25°C, 35°C, and 40°C; but a greater rate at 30°C under low light (Figure 2.2A). Under high light, *R. stricta* had similar rates of *A* as compared to *N. tabacum* at 20°C, 35°C, and 40°C; but a greater rate at 25°C and 30°C (Figure 2.2C). At the growth temperature, *A* in *R. stricta* was 20% (low light) and 16% (high light) larger than *N. tabacum.* R_L, which is needed to determine gross assimilation, was greater in *R. stricta* than *N. tabacum* at 20°C, 25°C, 30°C, 35°C, and 40°C (Figure 2.6A). Gross assimilation was higher in *R. stricta* than *N. tabacum* at 25°C, 30°C, and 35°C under low light (Figure 2.2B). Under high light, gross assimilation in *R. stricta* was similar to *N. tabacum* at 20°C, 35°C, and 40°C; but a greater at 25°C and 30°C (Figure 2.2D). These results indicate that the photosynthetic rate in *R. stricta* did not decrease despite high rates of photorespiration.

To understand *R. stricta* and *N. tabacum* abilities to fix carbon under minimal photorespiratory conditions, the temperature response of v_o, v_o/v_c, A, and $A + R_L$ were measured under low O_2 conditions and high light (2% 1750 PAR; Figure 2.7). In contrast to the ambient O_2 conditions, v_o in *R. stricta* was similar to *N. tabacum* at 25°C and 40°C, but less than *N. tabacum* at 25°C, 30°C and 35°C (Figure 2.7A). As expected, the rates

of v_o in both species were reduced to a fraction of the 21% values under 2% O_2. v_o/v_c in *R. stricta* was similar to *N. tabacum* at 20°C, 25°C, 30°C, and 35°C, but greater than *N. tabacum* at 40°C (Figure 2.7B). Under this minimal photorespiration, *R. stricta* had lower rates of A and $A + R_L$ than *N. tabacum* at 20°C, 25°C, 30°C, 35°C, and 40°C (Figure 2.7C and D). The results indicate under minimal photorespiratory conditions, *R. stricta* ability to fix carbon is reduced compared to *N. tabacum*.

Photosynthetic biochemical limitations of *R. stricta* and *N. tabacum*

To understand the biochemical limitations on photosynthesis, the temperature response of the J_{max} and the $v_{c,max}$ were estimated in *R. stricta* and *N. tabacum*. J_{max} in *R. stricta* was similar to *N. tabacum* at 20°C, but greater than *N. tabacum* at 25°C, 30°C, 35°C, and 40°C (Figure 2.3A). In contrast to J_{max}, $v_{c,max}$ did not have a consistent trend in *R. stricta*. $v_{c,max}$ in *R. stricta* was similar to *N. tabacum* at 20°C, greater than *N. tabacum* at 25°C, 30°C, and 40°C, but less than *N. tabacum* at 35°C.

To find the saturating light intensity and to understand photosynthetic capacity in *R. stricta* and *N. tabacum*, a light response curve was measured at 25°C (Figure 2.8). Maximum quantum yield of CO_2 fixed per photon absorbed (Φ_{CO2}) was significantly greater in *R. stricta* (0.060 ± 0.0047) than *N. tabacum* (0.046 ± 0.0017) at 25°C.

Quantifying the photorespiratory CO_2 compensation point (Γ^*) under ambient O_2 conditions links rubisco kinetics with the stoichiometry of CO_2 release per rubisco oxygenation from photorespiration (Walker *et al.*, 2016a). Additionally, the temperature response of Γ^* provides a key parameter needed to calculate v_o, v_c, and g_m. Γ^* in *R. stricta* was greater than *N. tabacum* at 30°C and 40°C, but similar to *N. tabacum* at 20°C, 25°C, and 35°C (Figure 2.6B).

To understand whether differences in Γ^* are related to a variable or constant α between *R. stricta* and *N. tabacum*, we measured photorespiratory discrimination (Δ_f) and the $^{12}C/^{13}C$ fractionation during photorespiration (f). Interestingly, there was no significant difference between the species for either parameter at 25°C or 35°C (Figure 2.9). To understand whether oxygen sensitivity in g_m lead to misinterpretation in Δ_f and f calculation, we measured at 2% and 21% oxygen at two key temperatures (25°C and 35°C) and determined no oxygen sensitivity to g_m using different assumptions for photorespiratory fractionation (Figure 2.10).

Rhazya stricta partitions CO_2 transfer conductances for increased water use efficiency

The temperature response of stomatal conductance and mesophyll conductance to CO_2 (g_{tc} and g_m) were measured to determine the CO_2 diffusion differences between *R. stricta* and *N. tabacum* (Figure 2.4A and C). g_{tc} was lower in *R. stricta* than *N. tabacum* at all temperatures. g_m in *R. stricta* was similar to *N. tabacum* at 20°C, 25°C, and 30°C, but greater at 35°C and 40°C. The results indicate that there is a tradeoff in the diffusive barriers in *R. stricta* from stomatal to mesophyll conductance. The temperature response of the photosynthetic limitation imposed by stomatal conductance and mesophyll conductance to CO_2 (Lg_{tc} and Lg_m) were calculated to determine how much g_{tc} and g_m limit photosynthetic rate (Figure 2.4 B and D). Lg_{tc} in *R. stricta* was greater than *N. tabacum* at 35°C, but similar to *N. tabacum* at the other temperatures. Lg_m in *R. stricta* was greater than *N. tabacum* at 25°C and 30°C, but similar to *N. tabacum* at the rest of the temperatures. Overall, g_{tc} and g_m did not impose a significant limitation of photosynthetic rate as Lg_{tc} and Lg_m did not have consistent trends across temperature for *R. stricta* or *N. tabacum*.

The temperature response of water use efficiency (*WUE*) was calculated to determine how the CO_2 transfer conductances constrained water use in *R. stricta* and *N. tabacum* (Figure 2.11). *WUE* in *R. stricta* was greater compared to *N. tabacum* at 20°C, 25°C, 30°C, 35°C, and 40°C. The temperature response of WUE results indicate that *R. stricta* fixes carbon at a lower cost of water than *N. tabacum* on a stoichiometric basis.

Photorespiratory enzyme activity in _R. stricta_ compared to _N. tabacum_

We measured photorespiratory enzyme activities to determine which photorespiratory enzymes have higher activities and temperature responses in *R. stricta* as compared to *N. tabacum* (Figure 2.5 and Table 1.2). These enzymatic activities were measured in leaves in *R. stricta* and *N. tabacum* at 25°C and 35°C using crude protein extracts. The photorespiratory enzymes assayed PGP, GO, CAT, GGAT, AGAT, SGAT, HPR, and GLYK. *R. stricta* had greater PGP and CAT activities than *N. tabacum* at 25°C and 35°C. *R. stricta* had greater AGAT and SGAT activities than *N. tabacum* at 25°C. *R. stricta* had similar GO, GGAT, HPR, and GK activities to *N. tabacum* at 25°C and 35°C.

The temperature response ratio of the enzyme activities was calculated by dividing the activity per mg protein at 35°C by the activity per mg protein at 25°C for each enzyme to establish if there are greater enzyme activities (relative to 25°C) at the elevated temperature in *R. stricta* and *N. tabacum* (Figure 2.12). PGP had a greater relative increase in activity with temperature in *R. stricta* as compared to *N. tabacum*; however, GO, CAT, GGAT, AGAT, SGAT, HPR, and GLYK had similar temperature response ratios.

Discussion

Hallmarks of a temperature-tolerant photorespiratory pathway

These results demonstrate that *R. stricta* maintains higher rates of photorespiration under moderate and elevated temperatures and that these higher rates of activity correlate with increased activity of key photorespiratory enzymes. The higher rates of photorespiration are evident in the temperature response of v_o and v_o/v_c, which were greater in *R. stricta* than in *N. tabacum* at moderate (25°C and 30°C) and elevated (35°C and 40°C) temperatures (Figure 2.1). Higher rates of photorespiration in *R. stricta* were accompanied by increased activities of specific photorespiratory enzymes. In *R. stricta*, PGP and CAT activities were greater than *N. tabacum* at 25°C and 35°C (Figure 2.5A & C). These higher photorespiratory enzyme activities in *R. stricta* compared to *N. tabacum* support the hypothesis that *R. stricta* has adapted to high photorespiratory pressure at moderate and elevated temperature by increased activity of these key enzymes. Additionally, the temperature response ratio of PGP activity in *R. stricta* was larger compared to *N. tabacum* (1.55 compared to 1.07; Figure 2.12). The larger temperature response of PGP indicates a larger V_{max} in the *R. stricta* at elevated temperatures than *N. tabacum*. The larger temperature response of PGP at elevated temperatures could not be explained by gene expression differences between the species as these assays were conducted *in vitro*. However, the increase could result from a more thermostable isoform of PGP in *R. stricta* than *N. tabacum*.

Increased activity of PGP may allow photorespiration to maintain low concentrations of 2-PG, an inhibitor of C_3 cycle enzymes, that accumulates under moderate and elevated temperatures. Past work supports the hypothesis that efficient degradation of 2-PG by PGP is critical for maintaining high rates of photosynthesis under higher photorespiratory conditions. For example, *Arabidopsis* overexpressing PGP maintain higher photosynthetic rates after short-term and long-term exposure to elevated temperatures as compared to wild-type and maintain a lower steady-state pool of 2-PG (Flügel *et al.*, 2017; Timm *et al.*, 2019). Therefore, minimizing the inhibition of photosynthesis by 2-PG appears to be a key feature for increasing the temperature resiliency of photorespiration in engineered and adapted plants.

CAT may also play a role in maintaining photosynthesis under higher photorespiratory pressure by detoxifying H_2O_2. Photorespiration is a large source of H_2O_2 in the light. H_2O_2 functions as a signaling molecule in both stress and developmental processes, where concentrations of H_2O_2 are likely under homeostatic regulation by foliar-expressed CAT in the peroxisome (Dat *et al.*, 2003; Queval *et al.*, 2008; Queval *et al.*, 2007). CAT-deficient *N. tabacum* has high concentrations of H_2O_2 that leads to cell death when plants were exposed to high photorespiratory pressure (Dat *et al.*, 2003). Other work with CAT-deficient plants indicate the enzyme is an important mediator of cellular toxicity during environmental stress (Willekens *et al.*, 1997). Additionally, there is evidence that H_2O_2 can react with glyoxylate and/or hydroxypyruvate resulting in non-enzymatic decarboxylation and release additional CO_2 from photorespiration (Cousins *et al.*, 2008; Grodzinski, 1978; Halliwell *et al.*, 1974; Keech *et al.*, 2012; Zelitch, 1992). For example, in a mutant with reduced foliar-expressed CAT, photosynthetic rates are reduced due to an increase in the stoichiometry release of CO_2 per oxygenation, most likely from the non-enzymatic decarboxylation with hydroxypyruvate and H_2O_2 (Bao *et al.*, 2021). This work supports the hypothesis that sufficient CAT activity plays a critical role preventing elevated H_2O_2 signaling and possibly the additional loss of CO_2 from photorespiration and is an adaptive strategy in *R. stricta* to moderate and elevated temperatures. Interestingly, we found no evidence that *N. tabacum* actually had an increase in CO_2 release per rubisco oxygenation as would be expected from excess non-enzymatic decarboxylations (discussed below). This finding indicates that the role of CAT in H_2O_2 signaling may be more important than any potential CO_2 loss from non-enzymatic decarboxylations.

Interestingly, when photorespiration was reduced under low O_2 conditions, both A and $A + R_L$ were lower in *R. stricta* compared to *N. tabacum* but were similar or slightly higher when measured under ambient O_2 conditions (Figure 2.7 & Figure 2.2). The higher rates of A and $A + R_L$ in *N. tabacum* supports that the photorespiratory pathway in *R. stricta* reduces the inhibition of photosynthesis under photorespiratory conditions more efficiently than *N. tabacum*. In other words, A in *N. tabacum* is more sensitive to photorespiratory intermediates, despite having only half the rates of v_o. The increase in A and $A + R_L$ under photorespiratory conditions in *R. stricta* is therefore likely due to the

greater activity of PGP and CAT in *R. stricta*, rather than an improved ability to fix carbon. These results also indicate that photosynthesis in *R. stricta* is adapted to environments with high photorespiratory pressure.

Managing CO_2 transfer conductance for improved water use efficiency

Our results demonstrate that *R. stricta* has a higher g_m that is compensated by a lower g_{tc}, resulting in a similar overall CO_2 transfer conductance limitation to photosynthesis. *R. stricta* exhibits a lower g_{tc} than *N. tabacum* across the entire temperature gradient (Figure 2.5A). However, this conductance difference between *R. stricta* and *N. tabacum* does not impose a larger CO_2 limitation on photosynthetic rate (Figure 2.5B). *R. stricta* has a greater g_m than *N. tabacum* at elevated temperatures (Figure 2.5C). This difference in g_m at elevated temperatures does not reduce the CO_2 limitation on photosynthetic rate (Figure 2.5D). So why does this re-partitioning strategy exist in *R. stricta* if it does not support an increase in net CO_2 assimilation? *R. stricta* appears to have re-partitioned the CO_2 transfer conductance at high temperatures from the stomata, which loses water, to the mesophyll, which does not.

The implications of this re-partitioning of conductances result in *R. stricta* having an increase in *WUE*. Although the lower g_{tc} indicates that the initial CO_2 delivery into the leaf was more restricted in *R. stricta* than *N. tabacum*, it also means that water has a more restricted path leaving the leaf. The lower g_{tc} in *R. stricta* resulted in a greater *WUE* than *N. tabacum* (Figure 2.11). The greater *WUE* indicates a lower cost of water loss per carbon assimilated, which is an important water-saving strategy. This water-saving strategy in *R. stricta* is consistent with other stomatal conductance measurements in other C_3 desert species, but the higher g_m has not yet been described to our knowledge (Driscoll *et al.*, 2021; Driscoll *et al.*, 2020; Kannenberg *et al.*, 2021; Ogle *et al.*, 2012).

Other adaptive strategies of photosynthesis appear similar between species

Biochemical limitations of photosynthesis reveal key similarities and differences between *R. stricta* and *N. tabacum*. In *R. stricta*, the J_{max} was greater than *N. tabacum* at 25°C, 30°C, 35°C, and 40°C (Figure 2.3A). These higher rates of J_{max} in *R. stricta* are consistent with a higher photorespiratory capacity in *R. stricta*, since photorespiration

dissipates more excitation energy from the electron transport chain than *N. tabacum* which would increase maximal rates of electron flux (Kozaki *et al.*, 1996).

In contrast to J_{max}, differences in $v_{c,max}$ were inconsistent between *R. stricta* and *N. tabacum*. In *R. stricta*, the $v_{c,max}$ was similar to N. tabacum at 20°C, and greater than *N. tabacum* at 25°C, 30°C, and 40°C (Figure 2.3A). Interestingly, $v_{c,max}$ in *R. stricta* was less than *N. tabacum* at 35°C. Generally, ignoring the 35°C data, there was a greater $v_{c,max}$ in *R. stricta* as temperature increased. Moreover, while we measured an increase in $v_{c,max}$ associated with temperature, others measure a $v_{c,max}$ independent of temperature in *in situ* studies of *R. stricta* (Lawson et al., 2014). Lawson *et al.,* point to a potential thermostable rubisco activase as a potential strategy *R. stricta* uses to maintain rubisco catalytic capacity and activity at elevated temperatures. Potentially, this thermotolerant rubisco activase could be the reason we see higher $v_{c,max}$ in *R. stricta* compared to *N. tabacum* at 25°C, 30°C, and 40°C. However, we did not measure rubisco activity or activation state in this study.

Carbon assimilation is in part determined by the CO_2 released from R_L. Minimizing R_L could be a strategy used by *R. stricta* to maintain a higher assimilation rate at elevated temperatures. Interestingly, R_L was greater in *R. stricta* compared to *N. tabacum* at each temperature (Figure 2.6A). The higher R_L meant that *R. stricta* is respiring more non-photorespiratory CO_2 than *N. tabacum* in the light. When considering rates of carbon assimilation, *R. stricta* had higher *A* than *N. tabacum* at 30°C under low light and at 25°C and 30°C under high light. In contrast, when the CO_2 loss from R_L is added back, *R. stricta* maintained higher $A + R_L$ than *N. tabacum* at 25°C, 30°C, and 35°C under low light, and at 25°C and 30°C under high light, meaning that *R. stricta* fixed more carbon at these temperatures (Figure 2.2). Therefore, the greater rates of R_L in *R. stricta* reduce the amount of carbon fixed and does not explain why *R. stricta* can maintain higher *A* at growth temperatures (~30°C) under low or high light intensity than *N. tabacum.* This result demonstrates that minimizing R_L does not appear to be a strategy that *R. stricta* uses to perform photosynthesis at higher rates compared to *N. tabacum* from a carbon budget perspective, but perhaps the elevated R_L contributes some yet-undescribed metabolic role in the elevated temperature tolerance.

Photosynthetic performance can also be characterized by Γ^* which links the specificity of rubisco for CO_2 over O_2 ($S_{c/o}$) to the stoichiometry of CO_2 release from rubisco oxygenation from photorespiration (α). A change in Γ^* may indicate differences in $S_{c/o}$ or α and may be an adaptive strategy in *R. stricta* to maintain photosynthetic performance. Interestingly, Γ^* was greater at 30°C and 40°C in *R. stricta* compared to *N. tabacum*, but similar at 20°C, 25°C, and 35°C. When considering changes in $S_{c/o}$, past work suggest that $S_{c/o}$ varies little within higher plants (Flamholz *et al.*, 2019) but *R. stricta* was not included in this analysis, therefore not ruling out that it has adapted an improved $S_{c/o}$. Since the temperature response of Γ^* does not show any decrease in *R. stricta* as compared to *N. tabacum,* we do not see any evidence for adaptive changes in $S_{c/o}$ as a strategy that *R. stricta* uses to perform photosynthesis.

When considering α, previous work has resolved α to be 0.5 moles of CO_2 loss per rubisco oxygenation. The CO_2 loss is primarily attributed to the decarboxylation of glycine from the mitochondrion; however, if additional CO_2 is lost from NED in the peroxisome, the additional moles of CO_2 loss would be captured in this term. Determining α *in vivo* is difficult since it is integral to many of the simplifications and assumptions needed to interpret any gas exchange data in C_3 plants. For example, taken at face value, the Γ^* data would suggest that α actually increases in *R. stricta* as compared to *N. tabacum* which, if true, would mean that *R. stricta* has a less efficient photorespiratory pathway from a carbon balance perspective assuming a similar $S_{c/o}$. However, determining Γ^* requires assumptions of α to calculate Γ^* in the first place (i.e., g_m) clouding this interpretation. As an independent indicator to support the use of a constant α in all our calculations, we surmised that additional CO_2 release would carry a different isotopic fractionation since it would arise from a different reaction (not glycine decarboxylase). This is supported by past work indicating that the transgenic rice with reduced glycine decarboxylase activity (and more alternative decarboxylation reactions with a higher α) have greatly decreased f values from 16.2‰ to ~3.3‰ (Giuliani *et al.*, 2019).

To determine if there was a decreased (or even different) f value consistent with a change in α, we measured Δ_f and f in *R. stricta* and *N. tabacum*. Interestingly, there was no significant difference between the species for either parameter at 25°C or 35°C

(Figure 2.9). Therefore, we do not see any evidence for differences in the reactions contributing to α between *R. stricta* and *N. tabacum*. Interestingly, there was an increase in R_L in *R. stricta* relative to *N. tabacum* but this can't be a reflection of a different α since this rate was not sensitive to different rates of photorespiration as indicated by the common intercept of the CO_2 response curves measured under different illumination during the common-intersection measurements. This approach cannot preclude a small rate of non-enzymatic decarboxylations or a reaction that has the same fractionation as glycine decarboxylation, but for the purposes of this study, we assume that $\alpha = 0.5$ for all the gas-exchange calculations. This assumption also suggests that the protection against these reactions by increased catalase expression may be accompanied by a self-regulating mechanism to down-regulate rubisco activity when catalase activity is too low to prevent them from happening, explaining why higher activities of catalase are important in *R. stricta*, but non-enzymatic decarboxylations do not appear to occur at high rates in *N. tabacum*.

Although *R. stricta* and *N. tabacum* share the same photosynthetic pathway (C_3 cycle), differences in Φ_{CO2} reveal changes in photosynthetic capacity (Figure 2.8). At 25°C, *R. stricta* had a significantly greater Φ_{CO2} (0.060 ± 0.0047) than *N. tabacum* (0.046 ± 0.0017). The question arises: What occurs between light absorption by the antennae and the carboxylation of CO_2 by rubisco that allows *R. stricta* to maximize the number of CO_2 fixed per photon absorbed? Perhaps non-photochemical quenching and/or photosynthetic control through cytochrome b_6f is less, leading to a higher light use efficiency of photosystem II and higher electron transfer rates per photon absorbed (Eberhard *et al.*, 2008). However, at low light absorption, we do not expect substantial non-photochemical quenching to occur in either species (Strand *et al.*, 2023). To understand the differences in coupling between the light absorption and Φ_{CO2}, we would need more characterizations of the upstream light reactions in both species.

Concluding Remarks

These results suggest important adaptive strategies used by *R. stricta* to maintain photosynthetic rates under moderate and elevated temperatures. To maintain high rates of photorespiration under most temperatures with minimal inhibitor accumulation, *R. stricta* increases photorespiratory capacity by reducing enzymatic

bottlenecks. A second adaptive strategy in *R. stricta* to elevated temperatures is to increase water-use efficiency by lowering g_{tc} and increasing g_m. These strategies found in *R. stricta* may inform breeding and engineering efforts in other C_3 species to improve photosynthetic efficiency at elevated temperature.

Acknowledgement

We would like to thank Dr. Salman Gulzar for help with *R. stric*ta cultivation and ecophysiology. We additionally thank Audrey Johnson for the valuable work and discussion during the cultivation process of *R. stricta*. We thank Deserah Strand for helpful discussion regarding Φ_{CO2} and potential adaptations in the light reaction pathway. We also thank Jim Klug and Cody Keilen (MSU Growth Chamber Facility) for overall greenhouse maintenance and pest management during plant cultivation. Finally, we would like to thank Hilary Stewart Williams for help setting up the tunable diode laser measurement system, including the software and hardware.

Figures

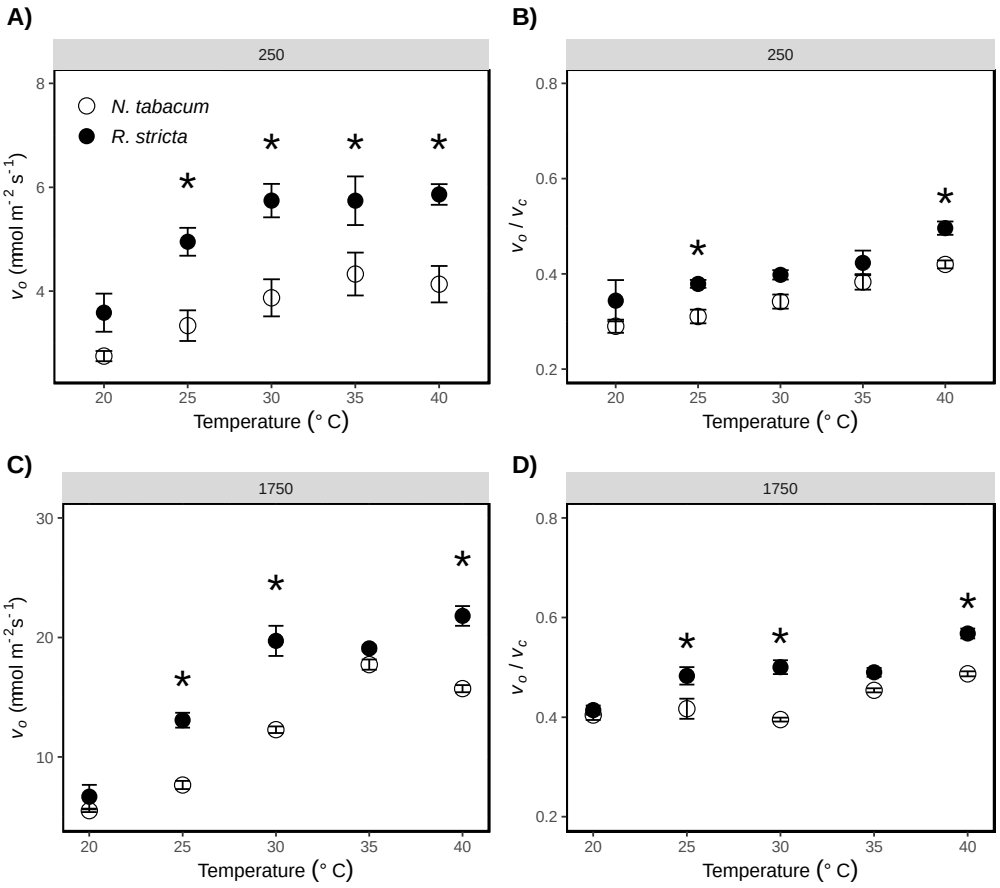

Figure 2.1. The temperature response of rubisco oxygenation rate in *Nicotiana tabacum* and *Rhazya stricta*. The temperature response of the oxygenation rate (v_o, A & C) and rubisco oxygenation per carboxylation (v_o/v_c, B & D) in *R. stricta* (closed symbols) and *N. tabacum* (open symbols). v_o and v_o/v_c were calculated from steady-state gas exchange measured under 40 Pa CO_2 and 250 or 1750 µmol PAR m^{-2} s^{-}

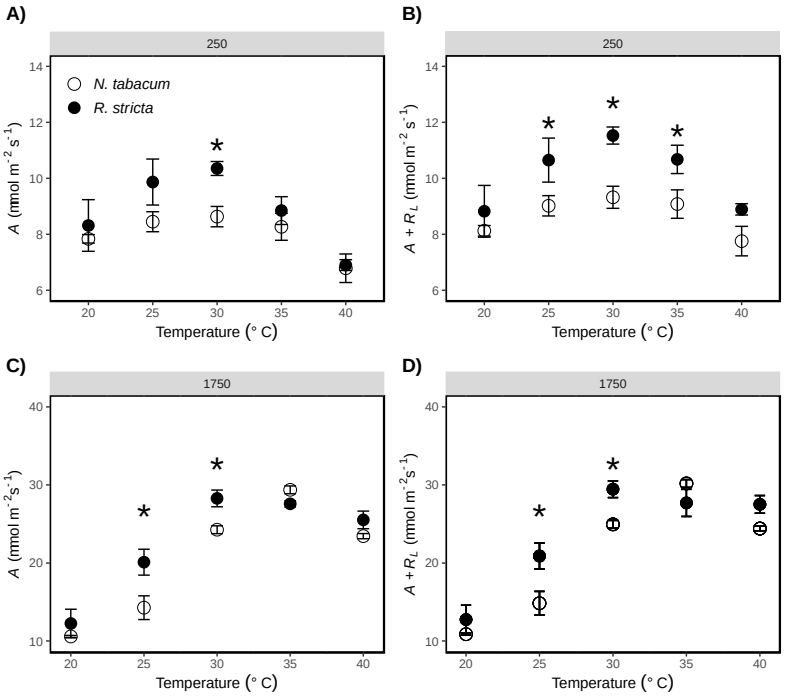

Figure 2.2. The temperature response of net and gross assimilation rates in *Nicotiana tabacum* and *Rhazya stricta*. The temperature response of net assimilation rate (*A*, A & C) and gross assimilation rate ($A + R_L$; B & D) in *R. stricta* (closed symbols) and *N. tabacum* (open symbols). *A* and $A + R_L$ were measured from steady-state gas exchange at 40 Pa CO_2 and 250 or 1750 µmol PAR m^{-2} s^{-1}. Shown are the means of 4 biological replicates with ± SE bars. Significant difference between species is indicated by an asterisk as determined by Two-way ANOVA with $P < 0.05$.

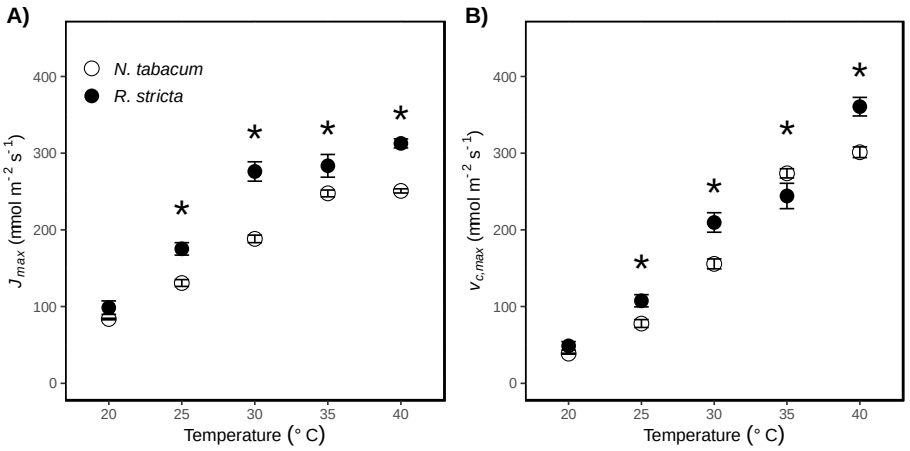

Figure 2.3. The temperature response of J_{max} and $v_{c,max}$ in *Nicotiana tabacum* and *Rhazya stricta*. The temperature response of the maximum rate of electron transport (J_{max}, A) and rubisco maximum carboxylation rates ($v_{c,max}$, B) in *R. stricta* (closed symbols) and *N. tabacum* (open symbols). J_{max} and $v_{c,max}$ were estimated from gas exchange measurements at 40-42 Pa CO_2 and 1750 µmol PAR m^{-2} s^{-1}. Shown are the means of 4 biological replicates with ± SE bars. Significant difference between species is indicated by an asterisk as determined by Two-way ANOVA with $P < 0.05$.

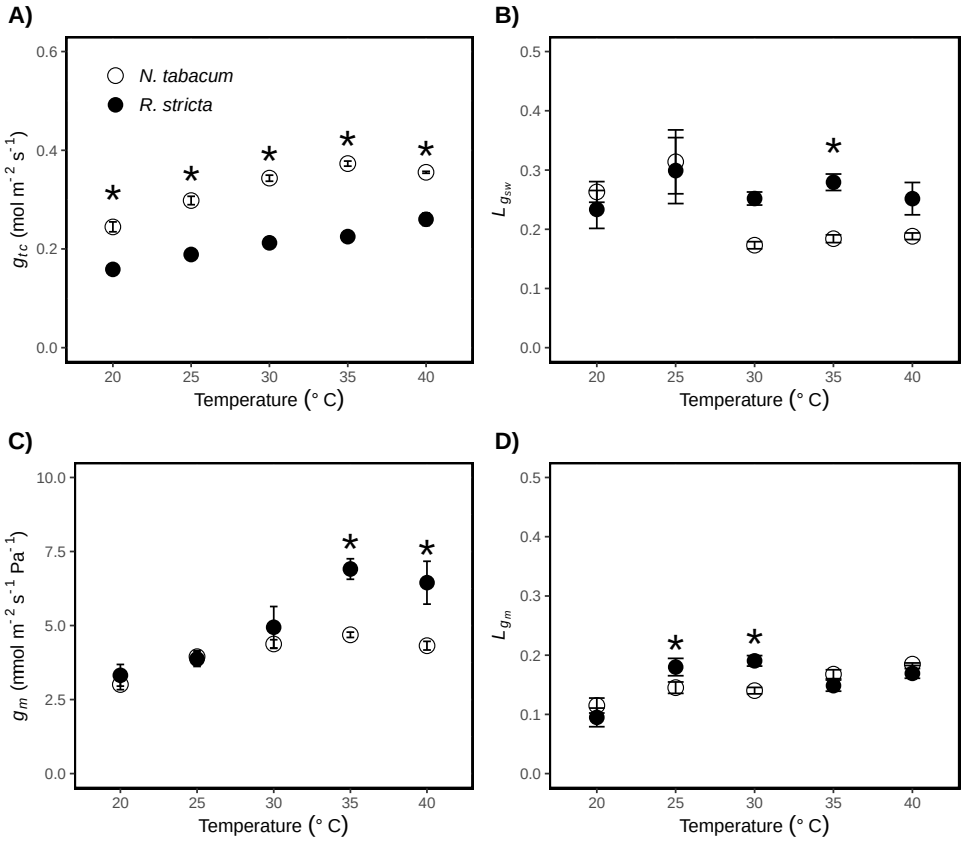

Figure 2.4. Temperature response of stomatal and mesophyll conductance and their limitations imposed on photosynthetic rate in *Nicotiana tabacum* and *Rhazya stricta*. The temperature response of stomatal conductance to CO_2 (g_{tc}, A), and mesophyll conductance to CO_2 (g_m, C) as well as the limitation imposed by both conductances (Lg_{tc} and Lg_m, B and D) *in R. stricta* (closed symbols) and *N. tabacum* (open symbols) . g_{tc} and g_m were measured from steady state gas exchange and on-line measurements of carbon isotope discrimination at 40 Pa CO_2 and 1750 µmol PAR m^{-2} s^{-1} (panels A & C). Lg_{tc} and Lg_m were estimated from gas exchange measurements at 40-42 Pa CO_2 and 1750 µmol PAR m^{-2} s^{-1}. Shown are the means of 4-5 biological replicates with ± SE bars. Significant difference between species is indicated by an asterisk as determined by Two-way ANOVA with $P < 0.05$.

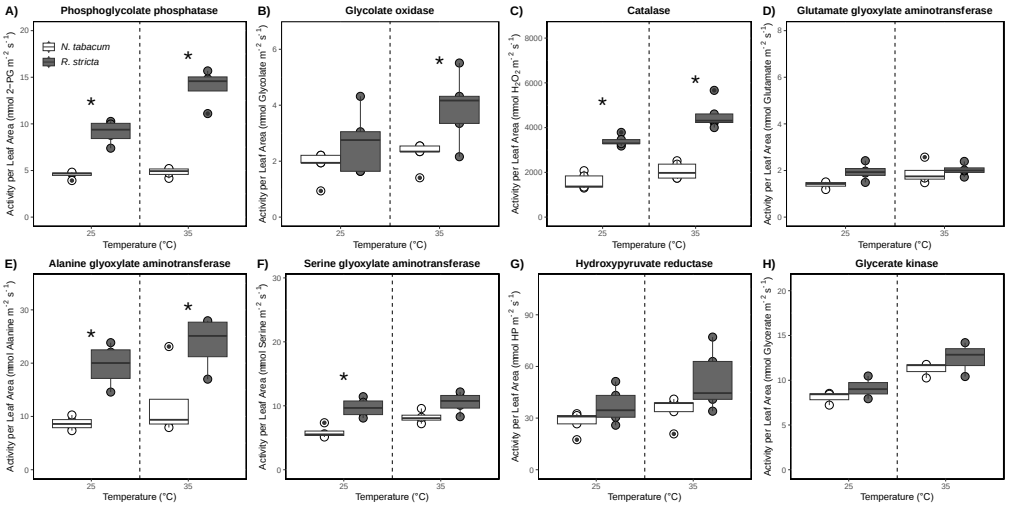

Figure 2.5. Photorespiratory enzymatic activities in *Nicotiana tabacum* and *Rhazya stricta* at 25°C and 35°C. Specific activities per m^2 leaf area were measured in *R. stricta* (black boxplot) and *N. tabacum* (white boxplot) using crude protein extracts for the enzymes phosphoglycolate phosphatase, glycolate oxidase, catalase, glutamate glyoxylate aminotransferase, alanine glyoxylate aminotransferase, serine glyoxylate aminotransferase, hydroxypyruvate reductase, and glycerate kinase. Shown are boxplots as well as points indicating the biological replicates. Significant difference between species is indicated by an asterisk as determined by Student's t-test with $P < 0.05$.

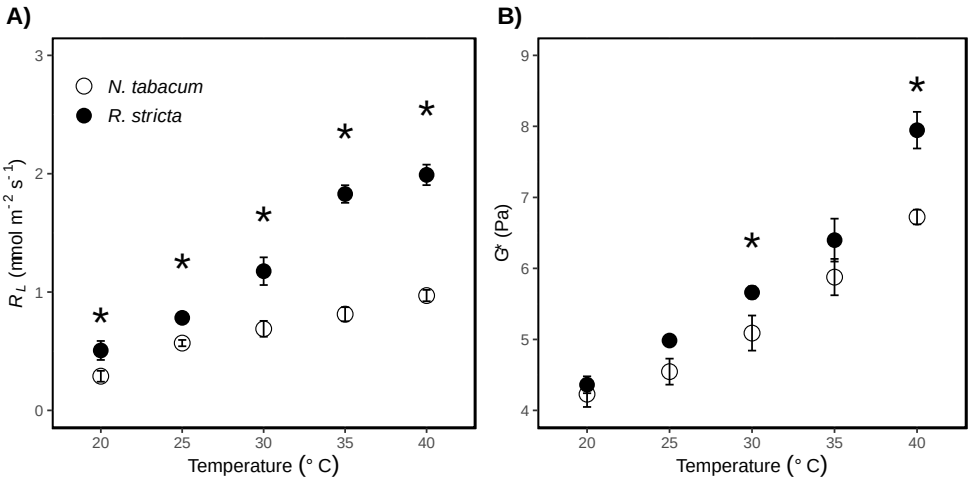

Figure 2.6. The temperature response of R_L and Γ^* in *Nicotiana tabacum* and *Rhazya stricta*. The temperature response of respiration in the light (R_L, A) and photorespiratory CO_2 compensation point (Γ^*, B) in *R. stricta* (closed symbols) and *N. tabacum* (open symbols). R_L and Γ^* were measured and calculated from steady-state gas exchange at 30, 50, 70, 90, 110 Pa CO_2 and 50, 80, 120, 165, 250 µmol PAR m^{-2} s^{-1}. Shown are the means of 4 biological replicates with ± SE bars. Significant difference between species is indicated by an asterisk as determined by Two-way ANOVA with $P < 0.05$.

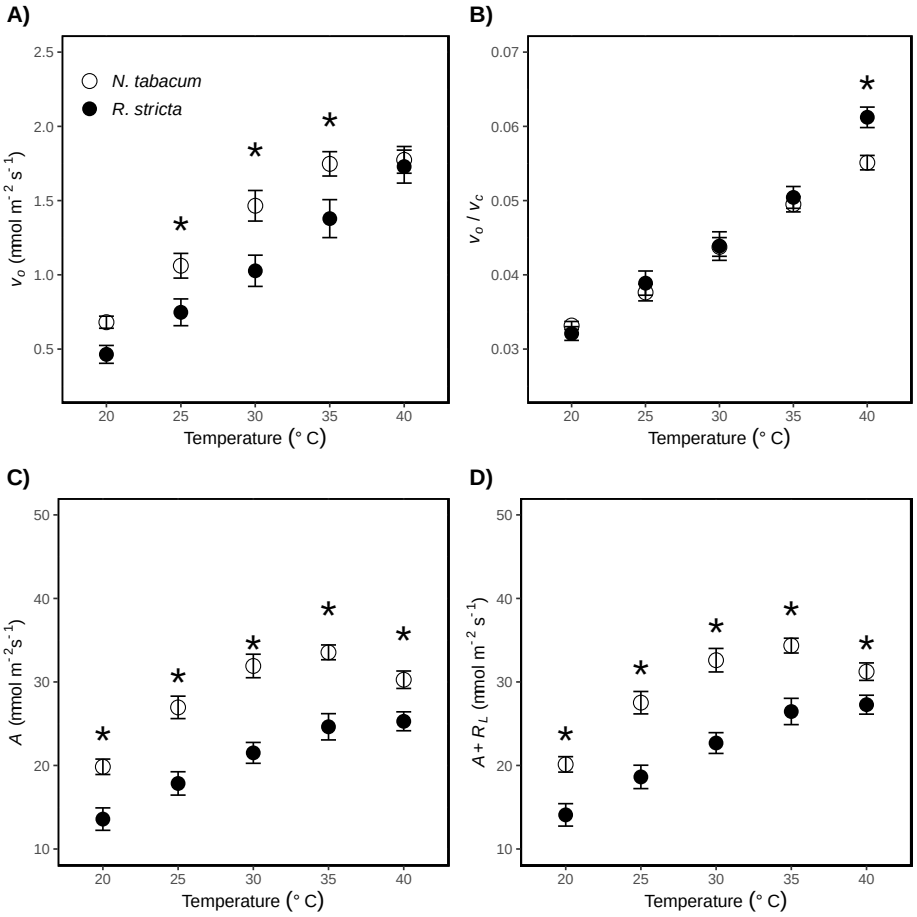

Figure 2.7. The temperature response of rubisco oxygenation rates and net and gross assimilation rates in *Nicotiana tabacum* and *Rhazya stricta* under low oxygen conditions. The temperature response of the oxygenation rate (v_o, A), rubisco oxygenation per carboxylation rate (v_o/v_c, B), net assimilation rate (A, C) and gross assimilation rate ($A + R_L$, D) in *R. stricta* (closed symbols) and *N. tabacum* (open symbols). v_o and v_o/v_c were calculated from steady-state gas exchange measurements at 40 Pa CO_2, 1750 µmol PAR m^{-2} s^{-1}, and 2% oxygen. A and $A + R_L$ were measured during steady state gas exchange and on-line measurements of carbon isotope discrimination at 40 Pa CO_2 and 1750 µmol PAR m^{-2} s^{-1}. Shown are the means of 5 biological replicates with ± SE bars. Significant difference between species is indicated by an asterisk as determined by Two-way ANOVA with $P < 0.05$.

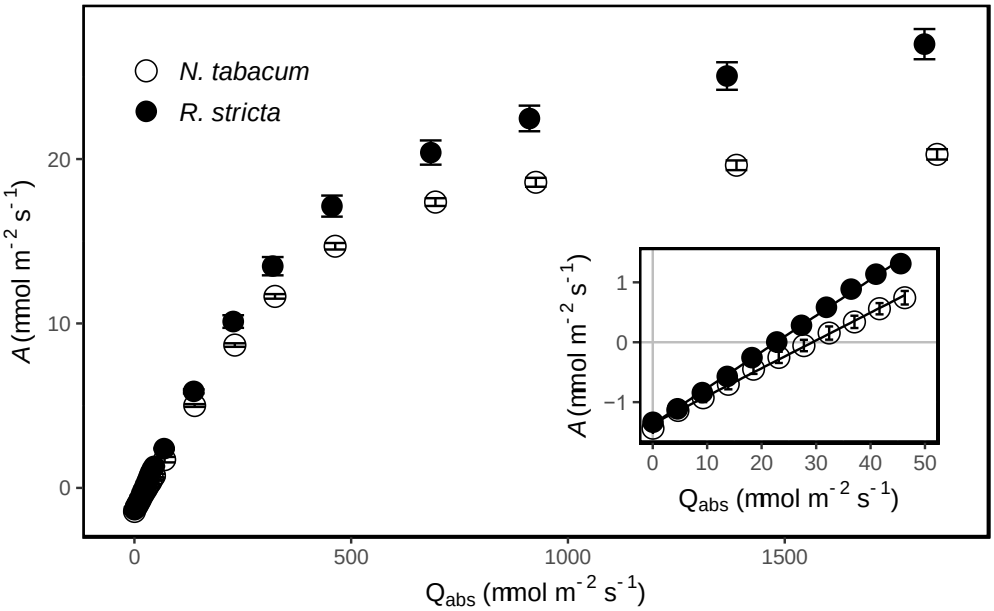

Figure 2.8. The light response curve of *Nicotiana tabacum and Rhazya stricta*. The light response of *R. stricta* (closed symbols) and *N. tabacum* (open symbols) was measured from steady-state gas exchange at 40 Pa CO_2 at 25◦C. Shown are the means of 3 biological replicates with ± SE bars. Maximum quantum yield (Φ_{CO2}) was estimated from a linear regression at low light intensity. Significant difference of Φ_{CO2} was determined between species as determined by Student's t-test with $P < 0.05$.

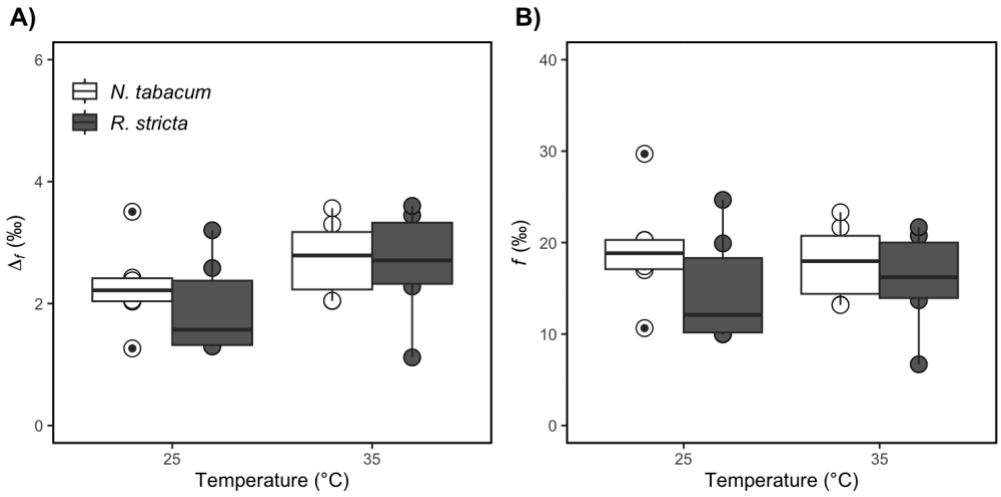

Figure 2.9. Temperature difference of *discrimination associated with photorespiration* and *the $^{12}C/^{13}C$ fractionation during photorespiration* in *Nicotiana tabacum and Rhazya stricta* at 25°C and 35°C. The temperature difference of Δ_f and *f* of *R. stricta* (closed symbols) and *N. tabacum* (open symbols) were measured under 21% oxygen and 40 Pa CO_2 at 1750 µmol PAR m^{-2} s^{-1}. Shown are boxplots as well as points indicating the biological replicates (n = 6). Significant difference between species is indicated by an asterisk as determined by Two-way ANOVA with $P < 0.05$.

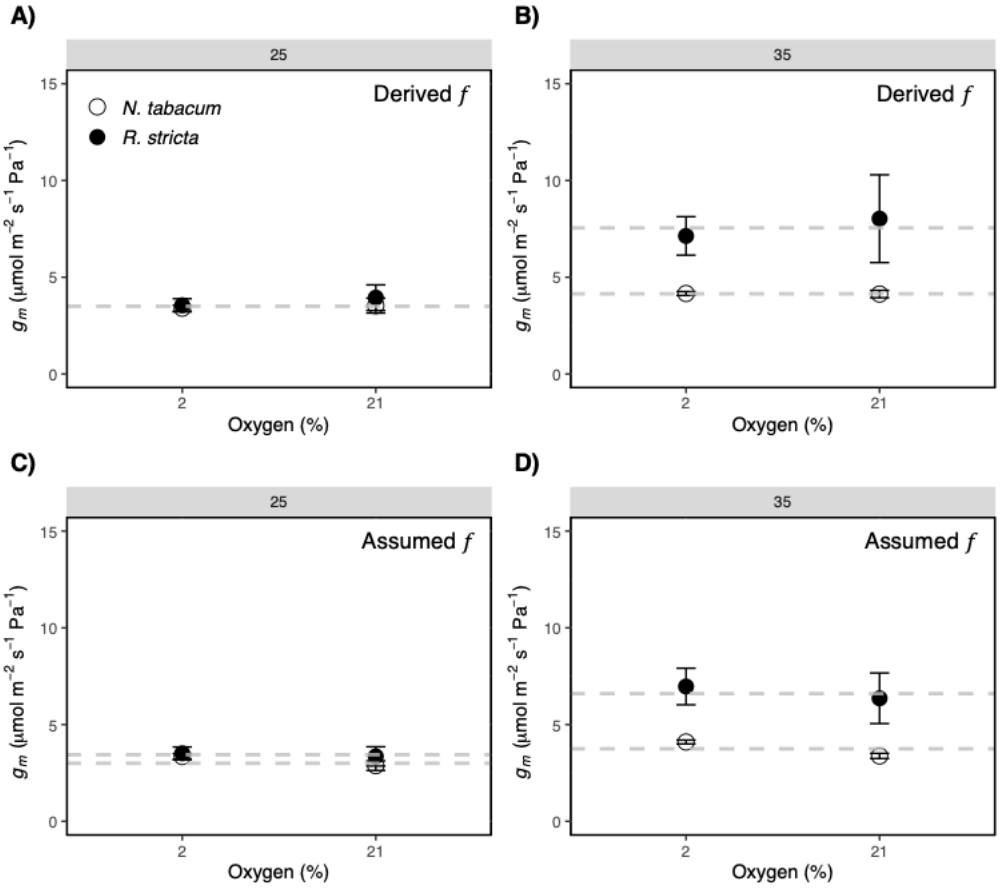

Figure 2.10. Oxygen independence of mesophyll conductance at 25°C and 35°C. The oxygen response of g_m of *R. stricta* (closed symbols) and *N. tabacum* (open symbols) was measured from steady state gas exchange and on-line measurements of carbon isotope discrimination at 40 Pa CO_2 and 1750 µmol PAR m^{-2} s^{-1} and resolved with the derived *f* (Figure 2.9B) and assumed *f* (11.8) values.

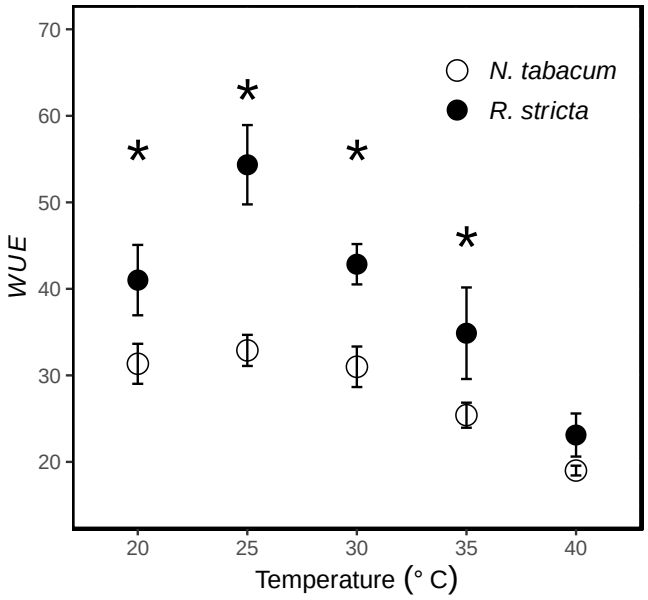

Figure 2.11. Temperature response of Intrinsic Water Use Efficiency in *Nicotiana tabacum* and *Rhazya stricta*. The temperature response of intrinsic water use efficiency (*WUE*) in *R. stricta* (closed symbols) and *N. tabacum* (open symbols). *WUE* was calculated from steady-state gas exchange measured at 40 Pa CO_2 and 250 µmol PAR m^{-2} s^{-1}. Shown are the means of 4 biological replicates with ± SE bars. Significant difference between species is indicated by an asterisk as determined by Two-way ANOVA with $P < 0.05$.

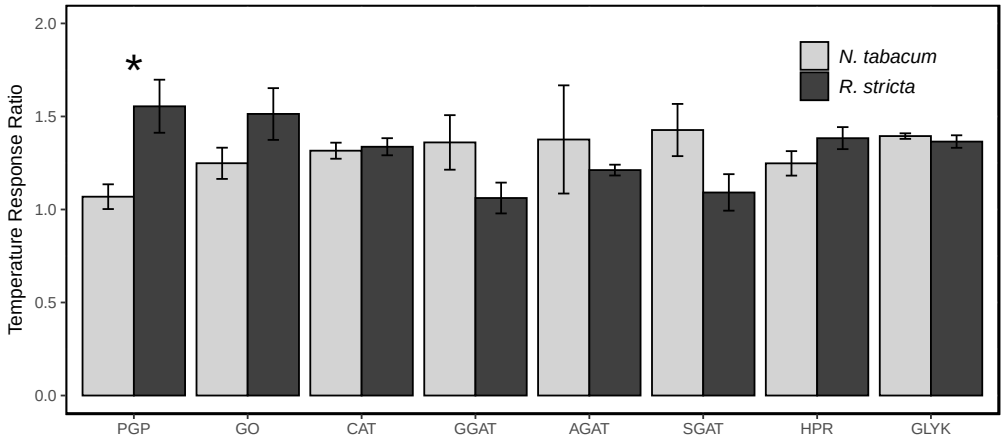

Figure 2.12. The temperature response ratio of the photorespiratory enzyme activities in *Nicotiana tabacum and Rhazya stricta*. The temperature response ratio of the activity per mg protein were calculated by dividing the activity at 35◦C by the activity at 25◦C for each enzyme in *R. stricta* (black bar) and *N. tabacum* (grey bar). Shown are the means of 3-5 biological replicates with ± SE bars. Significant difference between species is indicated by an asterisk as determined by Student's t-test with $P < 0.05$.

Tables

Table 1.1. Parameter definitions.

Parameter	***Biological Description***	***Unit***
A	Net CO_2 assimilation rate	μmol m^{-2} s^{-1}
C_a	The CO_2 partial pressure in the ambient air	Pa
C_i	The CO_2 partial pressure in the intercellular airspace of the leaf	Pa
C_i^*	The CO_2 partial pressure in the intercellular airspace of the leaf at the photorespiratory compensation point	Pa
C_c	The CO_2 partial pressure in the chloroplast	Pa
g_{sw}	Stomatal conductance to H_2O in air	mol m^{-2} s^{-1}
g_{tc}	Stomatal conductance to CO2 in air	mol m^{-2} s^{-1}
g_m	Mesophyll conductance to CO_2	μmol m^{-2} s^{-1} Pa^{-1}
J_{max}	Maximum rate of electron transport	μmol m^{-2} s^{-1}
Lg_{tc}	Limitation imposed by stomatal conductance on net CO_2 assimilation rate	%
Lg_m	Limitation imposed by mesophyll conductance on net CO_2 assimilation rate	%
$S_{c/o}$	specificity of rubisco for CO_2 relative to O_2	unitless
R_L	Non-photorespiratory CO_2 release in the light	μmol m^{-2} s^{-1}
v_c	The velocity of rubisco carboxylation	μmol m^{-2} s^{-1}
$v_{c,max}$	The maximum velocity of rubisco carboxylation	μmol m^{-2} s^{-1}
v_o	The velocity of rubisco oxygenation	μmol m^{-2} s^{-1}
v_o/v_c	The velocity of rubisco oxygenation per carboxylation	unitless
Γ^*	The CO_2 partial pressure in the chloroplast at the photorespiratory compensation point	Pa
α	Stoichiometric release of CO_2 per oxygenation reaction	mol mol^{-1}
Δ_f	Discrimination associated with photorespiration	‰
f	$^{12}C/^{13}C$ fractionation during photorespiration	‰
Φ_{CO2}	Maximum quantum yield of CO_2 fixed per photon absorbed	unitless

Table 1.2. Photorespiratory enzyme activities in *Nicotiana tabacum and Rhazya stricta* at 25°C and 35°C under protein and leaf area normalization. Specific activities per mg protein and per m^2 leaf area were measured in *R. stricta* and *N. tabacum* using crude protein extracts for the enzymes phosphoglycolate phosphatase (PGP), glycolate oxidase (GO), catalase (CAT), glutamate glyoxylate aminotransferase (GGAT), alanine glyoxylate aminotransferase (AGAT), serine glyoxylate aminotransferase (SGAT), hydroxypyruvate reductase (HPR), and glycerate kinase (GLYK). Shown are the means of 3-5 biological replicates with ± SD.

Species	Temperature (°C)	Enzyme	Protein (specific activity/mg)	Leaf Area (specific activity/m2)
N. tabacum	25	PGP	0.068 ± 0.003	4.525 ± 0.405
N. tabacum	35	PGP	0.072 ± 0.004	4.810 ± 0.482
R. stricta	25	PGP	0.122 ± 0.009	9.104 ± 1.312
R. stricta	35	PGP	0.188 ± 0.013	13.987 ± 2.002
N. tabacum	25	GO	0.028 ± 0.004	1.847 ± 0.526
N. tabacum	35	GO	0.033 ± 0.003	2.236 ± 0.475
R. stricta	25	GO	0.036 ± 0.007	2.680 ± 1.118
R. stricta	35	GO	0.052 ± 0.007	3.901 ± 1.242
N. tabacum	25	CAT	24.755 ± 2.689	1656.984 ± 360.000
N. tabacum	35	CAT	30.904 ± 2.389	2068.561 ± 357.603
R. stricta	25	CAT	45.684 ± 1.431	3400.906 ± 238.259
R. stricta	35	CAT	61.291 ± 3.922	4562.746 ± 652.885
N. tabacum	25	GGAT	0.021 ± 0.001	1.385 ± 0.146
N. tabacum	35	GGAT	0.028 ± 0.004	1.886 ± 0.477
R. stricta	25	GGAT	0.026 ± 0.003	1.943 ± 0.382
R. stricta	35	GGAT	0.027 ± 0.002	2.027 ± 0.276
N. tabacum	25	AGAT	0.13 ± 0.010	8.708 ± 1.275
N. tabacum	35	AGAT	0.186 ± 0.053	12.447 ± 7.162
R. stricta	25	AGAT	0.264 ± 0.028	19.621 ± 4.156
R. stricta	35	AGAT	0.32 ± 0.035	23.795 ± 5.143
N. tabacum	25	SGAT	0.088 ± 0.007	5.884 ± 0.998
N. tabacum	35	SGAT	0.123 ± 0.007	8.230 ± 0.991
R. stricta	25	SGAT	0.13 ± 0.010	9.712 ± 1.534
R. stricta	35	SGAT	0.141 ± 0.011	10.498 ± 1.701
N. tabacum	25	HPR	0.416 ± 0.041	27.813 ± 6.205
N. tabacum	35	HPR	0.518 ± 0.055	34.644 ± 8.167
R. stricta	25	HPR	0.498 ± 0.061	37.083 ± 10.183
R. stricta	35	HPR	0.697 ± 0.106	51.889 ± 17.672
N. tabacum	25	GLYK	0.12 ± 0.006	8.061 ± 0.729
N. tabacum	35	GLYK	0.168 ± 0.007	11.232 ± 0.847
R. stricta	25	GLYK	0.123 ± 0.010	9.137 ± 1.275
R. stricta	35	GLYK	0.168 ± 0.015	12.487 ± 1.916

LITERATURE CITED

Abadie, C., Boex-Fontvieille, E. R., Carroll, A. J., & Tcherkez, G. (2016). In vivo stoichiometry of photorespiratory metabolism. *Nature Plants, 2*(2), 1-4.

Aebi, H. E. (1983). Catalase. In: Bergmeyer, H.U., Ed., Methods of Enzymatic Analysis. *Verlag Chemie, Weinheim*, 273-286.

Anderson, L. E. (1971). Chloroplast and cytoplasmic enzymes II. Pea leaf triose phosphate isomerases. *Biochimica et Biophysica Acta (BBA) - Enzymology, 235*(1), 237-244. doi:https://doi.org/10.1016/0005-2744(71)90051-9

Baker, A. L., & Tolbert, N. E. (1966). Glycolate oxidase (ferredoxin containing form). Methods in Enzymology. *Academic Press, 9*, 339-342.

Bao, H., Morency, M., Rianti, W., Saeheng, S., Roje, S., Weber, A. P. M., & Walker, B. J. (2021). Catalase protects against nonenzymatic decarboxylations during photorespiration in Arabidopsis thaliana. *Plant Direct, 5*(12), e366. doi:https://doi.org/10.1002/pld3.366

Barbour, M. M., McDowell, N. G., Tcherkez, G., Bickford, C. P., & Hanson, D. T. (2007). A new measurement technique reveals rapid post-illumination changes in the carbon isotope composition of leaf-respired CO2. *Plant, Cell & Environment, 30*(4), 469-482. doi:https://doi.org/10.1111/j.1365-3040.2007.01634.x

Bauwe, H., Hagemann, M., Kern, R., & Timm, S. (2012). Photorespiration has a dual origin and manifold links to central metabolism. *Current Opinion in Plant Biology, 15*(3), 269-275. doi:10.1016/j.pbi.2012.01.008

Cousins, A. B., Pracharoenwattana, I., Zhou, W., Smith, S. M., & Badger, M. R. (2008). Peroxisomal malate dehydrogenase is not essential for photorespiration in Arabidopsis but its absence causes an increase in the stoichiometry of photorespiratory CO2 release. *Plant Physiology, 148*(2), 786-795. doi:10.1104/pp.108.122622

Dat, J. F., Pellinen, R., Beeckman, T., Van De Cotte, B., Langebartels, C., Kangasjärvi, J., . . . Van Breusegem, F. (2003). Changes in hydrogen peroxide homeostasis trigger an active cell death process in tobacco. *The Plant Journal, 33*(4), 621-632. doi:https://doi.org/10.1046/j.1365-313X.2003.01655.x

De Souza, A. P., Burgess, S. J., Doran, L., Hansen, J., Manukyan, L., Maryn, N., . . . Long, S. P. (2022). Soybean photosynthesis and crop yield are improved by accelerating recovery from photoprotection. *Science, 377*(6608), 851-854. doi:doi:10.1126/science.adc9831

Driscoll, A. W., Bitter, N. Q., & Ehleringer, J. R. (2021). Interactions among intrinsic water-use efficiency and climate influence growth and flowering in a common desert shrub. *Oecologia, 197*(4), 1027-1038. doi:10.1007/s00442-020-04825-3

Driscoll, A. W., Bitter, N. Q., Sandquist, D. R., & Ehleringer, J. R. (2020). Multidecadal records of intrinsic water-use efficiency in the desert shrub Encelia farinosa reveal strong responses to climate change. *Proceedings of the National Academy of Sciences, 117*(31), 18161-18168. doi:doi:10.1073/pnas.2008345117

Eberhard, S., Finazzi, G., & Wollman, F. A. (2008). The dynamics of photosynthesis. *Annu Rev Genet, 42*, 463-515. doi:10.1146/annurev.genet.42.110807.091452

Ely, K. S., Rogers, A., Agarwal, D. A., Ainsworth, E. A., Albert, L. P., Ali, A., . . . Yang, D. (2021). A reporting format for leaf-level gas exchange data and metadata. *Ecological Informatics, 61*, 101232. doi:https://doi.org/10.1016/j.ecoinf.2021.101232

Evans, J. R., Sharkey, T. D., Berry, J. A., & Farquhar, G. D. (1986). Carbon Isotope Discrimination measured Concurrently with Gas Exchange to Investigate CO2 Diffusion in Leaves of Higher Plants. *Functional Plant Biology, 13*(2), 281-292. doi:https://doi.org/10.1071/PP9860281

Evans, J. R., & von Caemmerer, S. (2013). Temperature response of carbon isotope discrimination and mesophyll conductance in tobacco. *Plant Cell Environ, 36*(4), 745-756. doi:10.1111/j.1365-3040.2012.02591.x

Farquhar, G., O'Leary, M., & Berry, J. (1982). On the Relationship Between Carbon Isotope Discrimination and the Intercellular Carbon Dioxide Concentration in Leaves. *Functional Plant Biology, 9*(2), 121-137. doi:https://doi.org/10.1071/PP9820121

Farquhar, G. D., & Cernusak, L. A. (2012). Ternary effects on the gas exchange of isotopologues of carbon dioxide. *Plant, Cell & Environment, 35*(7), 1221-1231. doi:https://doi.org/10.1111/j.1365-3040.2012.02484.x

Flamholz, A. I., Prywes, N., Moran, U., Davidi, D., Bar-On, Y. M., Oltrogge, L. M., . . . Milo, R. (2019). Revisiting Trade-offs between Rubisco Kinetic Parameters. *Biochemistry, 58*(31), 3365-3376. doi:10.1021/acs.biochem.9b00237

Flügel, F., Timm, S., Arrivault, S., Florian, A., Stitt, M., Fernie, A. R., & Bauwe, H. (2017). The Photorespiratory Metabolite 2-Phosphoglycolate Regulates Photosynthesis and Starch Accumulation in Arabidopsis. *The Plant Cell, 29*(10), 2537-2551. doi:10.1105/tpc.17.00256

Fu, X., Gregory, L. M., Weise, S. E., & Walker, B. J. (2023). Integrated flux and pool size analysis in plant central metabolism reveals unique roles of glycine and serine during photorespiration. *Nature Plants, 9*(1), 169-178. doi:10.1038/s41477-022-01294-9

Giuliani, R., Karki, S., Covshoff, S., Lin, H.-C., Coe, R. A., Koteyeva, N. K., . . . Cousins, A. B. (2019). Knockdown of glycine decarboxylase complex alters

photorespiratory carbon isotope fractionation in Oryza sativa leaves. *Journal of Experimental Botany, 70*(10), 2773-2786. doi:10.1093/jxb/erz083

Gregory, L. M., McClain, A. M., Kramer, D. M., Pardo, J. D., Smith, K. E., Tessmer, O. L., . . . Sharkey, T. D. (2021). The triose phosphate utilization limitation of photosynthetic rate: Out of global models but important for leaf models. *Plant Cell Environ, 44*(10), 3223-3226. doi:10.1111/pce.14153

Grodzinski, B. (1978). Glyoxylate decarboxylation during photorespiration. *Planta, 144*(1), 31-37. doi:10.1007/BF00385004

Hall, N. P., & Keys, A. J. (1983). Temperature dependence of the enzymic carboxylation and oxygenation of ribulose 1, 5-bisphosphate in relation to effects of temperature on photosynthesis. *Plant Physiology, 72*(4), 945-948.

Halliwell, B., & Butt, V. S. (1974). Oxidative decarboxylation of glycollate and glyoxylate by leaf peroxisomes. *The Biochemical journal, 138*(2), 217-224. doi:10.1042/bj1380217

Heinze, M., & Gerhardt, B. (2002). Plant Catalases. In A. Baker & I. A. Graham (Eds.), *Plant Peroxisomes: Biochemistry, Cell Biology and Biotechnological Applications* (pp. 103-140). Dordrecht: Springer Netherlands.

Hermida-Carrera, C., Kapralov, M. V., & Galmés, J. (2016). Rubisco Catalytic Properties and Temperature Response in Crops. *Plant Physiology, 171*(4), 2549-2561. doi:10.1104/pp.16.01846

Jordan, D. B., & Ogren, W. L. (1984). The CO2/O2 specificity of ribulose 1,5-bisphosphate carboxylase/oxygenase. *Planta, 161*(4), 308-313. doi:10.1007/BF00398720

Kannenberg, S. A., Driscoll, A. W., Szejner, P., Anderegg, W. R. L., & Ehleringer, J. R. (2021). Rapid increases in shrubland and forest intrinsic water-use efficiency during an ongoing megadrought. *Proceedings of the National Academy of Sciences, 118*(52), e2118052118. doi:doi:10.1073/pnas.2118052118

Keech, O., Zhou, W., Fenske, R., Colas-des-Francs-Small, C., Bussell, J. D., Badger, M. R., & Smith, S. M. (2012). The Genetic Dissection of a Short-Term Response to Low CO₂ Supports the Possibility for Peroxide-Mediated Decarboxylation of Photorespiratory Intermediates in the Peroxisome. *Molecular Plant, 5*(6), 1413-1416. doi:10.1093/mp/sss104

Kendziorek, M., & Paszkowski, A. (2008). Properties of serine:glyoxylate aminotransferase purified from Arabidopsis thaliana leaves. *Acta Biochimica et Biophysica Sinica, 40*(2), 102-110. doi:10.1111/j.1745-7270.2008.00383.x

Kozaki, A., & Takeba, G. (1996). Photorespiration protects C3 plants from photooxidation. *Nature, 384*(6609), 557-560. doi:10.1038/384557a0

Kromdijk, J., Głowacka, K., Leonelli, L., Gabilly, S. T., Iwai, M., Niyogi, K. K., & Long, S. P. (2016). Improving photosynthesis and crop productivity by accelerating recovery from photoprotection. *Science, 354*(6314), 857-861. doi:doi:10.1126/science.aai8878

Laisk, A. K. (1977). Kinetics of photosynthesis and photorespiration of C3 in plants.

Larkindale, J., & Huang, B. (2004). Changes of lipid composition and saturation level in leaves and roots for heat-stressed and heat-acclimated creeping bentgrass (Agrostis stolonifera). *Environmental and Experimental Botany, 51*(1), 57-67. doi:https://doi.org/10.1016/S0098-8472(03)00060-1

Lawrence, M. G. (2005). The Relationship between Relative Humidity and the Dewpoint Temperature in Moist Air: A Simple Conversion and Applications. *Bulletin of the American Meteorological Society, 86*(2), 225-234. doi:10.1175/bams-86-2-225

Lawson, T., Davey, P. A., Yates, S. A., Bechtold, U., Baeshen, M., Baeshen, N., . . . Mullineaux, P. M. (2014). C3 photosynthesis in the desert plant Rhazya stricta is fully functional at high temperatures and light intensities. *New Phytologist, 201*(3), 862-873. doi:https://doi.org/10.1111/nph.12559

Liepman, A. H., & Olsen, L. J. (2001). Peroxisomal alanine : glyoxylate aminotransferase (AGT1) is a photorespiratory enzyme with multiple substrates in Arabidopsis thaliana. *The Plant Journal, 25*(5), 487-498. doi:https://doi.org/10.1046/j.1365-313x.2001.00961.x

Liepman, A. H., & Olsen, L. J. (2003). Alanine Aminotransferase Homologs Catalyze the Glutamate:Glyoxylate Aminotransferase Reaction in Peroxisomes of Arabidopsis. *Plant Physiology, 131*(1), 215-227. doi:10.1104/pp.011460

Liu, L., Zhong, S., Yang, R., Hu, H., Yu, D., Zhu, D., . . . Gong, D. (2008). Expression, purification, and initial characterization of human alanine aminotransferase (ALT) isoenzyme 1 and 2 in High-five insect cells. *Protein Expression and Purification, 60*(2), 225-231. doi:https://doi.org/10.1016/j.pep.2008.04.006

Liu, Y., Guérard, F., Hodges, M., & Jossier, M. (2020). Phosphomimetic T335D Mutation of Hydroxypyruvate Reductase 1 Modifies Cofactor Specificity and Impacts Arabidopsis Growth in Air1. *Plant Physiology, 183*(1), 194-205. doi:10.1104/pp.19.01225

Marcum, K. B. (1998). Cell Membrane Thermostability and Whole-Plant Heat Tolerance of Kentucky Bluegrass. *Crop Science, 38*(5), cropsci1998.0011183X003800050017x. doi:https://doi.org/10.2135/cropsci1998.0011183X003800050017x

McClain, A. M., & Sharkey, T. D. (2023). Rapid CO2 changes cause oscillations in photosynthesis that implicate PSI acceptor-side limitations. *Journal of Experimental Botany*. doi:10.1093/jxb/erad084

Moore, C. E., Meacham-Hensold, K., Lemonnier, P., Slattery, R. A., Benjamin, C., Bernacchi, C. J., . . . Cavanagh, A. P. (2021). The effect of increasing temperature on crop photosynthesis: from enzymes to ecosystems. *Journal of Experimental Botany, 72*(8), 2822-2844. doi:10.1093/jxb/erab090

Ogle, K., Lucas, R. W., Bentley, L. P., Cable, J. M., Barron-Gafford, G. A., Griffith, A., . . . Tissue, D. T. (2012). Differential daytime and night-time stomatal behavior in plants from North American deserts. *New Phytologist, 194*(2), 464-476. doi:https://doi.org/10.1111/j.1469-8137.2012.04068.x

Pai, S.-C., Yang, C.-C., & Riley, J. P. (1990). Effects of acidity and molybdate concentration on the kinetics of the formation of the phosphoantimonylmolybdenum blue complex. *Analytica Chimica Acta, 229*, 115-120.

Pörtner, H. O., Roberts, D. C., Tignor, M., Poloczanska, E. S., Mintenbeck, K., Alegría, A., . . . (eds.). (2022). IPCC, 2022: Climate Change 2022: Impacts, Adaptation, and Vulnerability. *Cambridge Univeristy Press*.

Prasertthai, P., Paethaisong, W., Theerakulpisut, P., & Dongsansuk, A. (2022). High Temperature Alters Leaf Lipid Membrane Composition Associated with Photochemistry of PSII and Membrane Thermostability in Rice Seedlings. *Plants (Basel), 11*(11). doi:10.3390/plants11111454

Queval, G., Hager, J., Gakière, B., & Noctor, G. (2008). Why are literature data for H2O2 contents so variable? A discussion of potential difficulties in the quantitative assay of leaf extracts. *Journal of Experimental Botany, 59*(2), 135-146. doi:10.1093/jxb/erm193

Queval, G., Issakidis-Bourguet, E., Hoeberichts, F. A., Vandorpe, M., Gakière, B., Vanacker, H., . . . Noctor, G. (2007). Conditional oxidative stress responses in the Arabidopsis photorespiratory mutant cat2 demonstrate that redox state is a key modulator of daylength-dependent gene expression, and define photoperiod as a crucial factor in the regulation of H2O2-induced cell death. *The Plant Journal, 52*(4), 640-657. doi:https://doi.org/10.1111/j.1365-313X.2007.03263.x

R Core Team. (2021). R: A Language and Environment for Statistical Computing. Vienna, Austria: R Foundation for Statistical Computing. Retrieved from https://www.R-project.org

Rawson, H. M., Begg, J. E., & Woodward, R. G. (1977). The effect of atmospheric humidity on photosynthesis, transpiration and water use efficiency of leaves of several plant species. *Planta, 134*(1), 5-10. doi:10.1007/BF00390086

RStudio Team. (2021). RStudio: Integrated Development Environment for R. Boston, MA: RStudio, PBC. Retrieved from http://www.rstudio.com/

Saathoff, A. J., & Welles, J. (2021). Gas exchange measurements in the unsteady state. *Plant, Cell & Environment, 44*(11), 3509-3523. doi:https://doi.org/10.1111/pce.14178

Schwarte, S., & Bauwe, H. (2007). Identification of the Photorespiratory 2-Phosphoglycolate Phosphatase, PGLP1, in Arabidopsis. *Plant Physiology, 144*(3), 1580-1586. doi:10.1104/pp.107.099192

Shen, J., Zeng, Y., Zhuang, X., Sun, L., Yao, X., Pimpl, P., & Jiang, L. (2013). Organelle pH in the Arabidopsis Endomembrane System. *Molecular Plant, 6*(5), 1419-1437. doi:https://doi.org/10.1093/mp/sst079

Somerville, C. R. (2001). An early Arabidopsis demonstration. Resolving a few issues concerning photorespiration. *Plant Physiology, 125*(1), 20-24.

Somerville, C. R., & Ogren, W. L. (1980). Photorespiration mutants of Arabidopsis thaliana deficient in serine-glyoxylate aminotransferase activity. *Proceedings of the National Academy of Sciences, 77*(5), 2684-2687.

South, P. F., Cavanagh, A. P., Lopez-Calcagno, P. E., Raines, C. A., & Ort, D. R. (2018). Optimizing photorespiration for improved crop productivity. *Journal of Integrative Plant Biology, 60*(12), 1217-1230. doi:https://doi.org/10.1111/jipb.12709

Stinziano, J. R., Morgan, P. B., Lynch, D. J., Saathoff, A. J., McDermitt, D. K., & Hanson, D. T. (2017). The rapid A–Ci response: photosynthesis in the phenomic era. *Plant, Cell & Environment, 40*(8), 1256-1262. doi:https://doi.org/10.1111/pce.12911

Strand, D. D., Karcher, D., Ruf, S., Schadach, A., Schöttler, M. A., Sandoval-Ibañez, O., . . . Bock, R. (2023). Characterization of mutants deficient in N-terminal phosphorylation of the chloroplast ATP synthase subunit β. *Plant Physiol, 191*(3), 1818-1835. doi:10.1093/plphys/kiad013

Tazoe, Y., von Caemmerer, S., Estavillo, G. M., & Evans, J. R. (2011). Using tunable diode laser spectroscopy to measure carbon isotope discrimination and mesophyll conductance to CO2 diffusion dynamically at different CO2 concentrations. *Plant, Cell & Environment, 34*(4), 580-591. doi:https://doi.org/10.1111/j.1365-3040.2010.02264.x

Tcherkez, G. (2006). How large is the carbon isotope fractionation of the photorespiratory enzyme glycine decarboxylase? *Functional Plant Biology, 33*(10), 911-920. doi:https://doi.org/10.1071/FP06098

Timm, S., Woitschach, F., Heise, C., Hagemann, M., & Bauwe, H. (2019). Faster removal of 2-phosphoglycolate through photorespiration improves abiotic stress tolerance of arabidopsis. *Plants, 8*(12). doi:10.3390/plants8120563

Tolbert, N. E., Yamazaki, R. K., & Oeser, A. (1970). Localization and Properties of Hydroxypyruvate and Glyoxylate Reductases in Spinach Leaf Particles. *Journal of Biological Chemistry, 245*(19), 5129-5136. doi:https://doi.org/10.1016/S0021-9258(18)62827-3

Ubierna, N., Holloway-Phillips, M.-M., & Farquhar, G. D. (2018). Using Stable Carbon Isotopes to Study C3 and C4 Photosynthesis: Models and Calculations. In S. Covshoff (Ed.), *Photosynthesis: Methods and Protocols* (pp. 155-196). New York, NY: Springer New York.

Urban, J., Ingwers, M., McGuire, M. A., & Teskey, R. O. (2017a). Stomatal conductance increases with rising temperature. *Plant Signal Behav, 12*(8), e1356534. doi:10.1080/15592324.2017.1356534

Urban, J., Ingwers, M. W., McGuire, M. A., & Teskey, R. O. (2017b). Increase in leaf temperature opens stomata and decouples net photosynthesis from stomatal conductance in Pinus taeda and Populus deltoides x nigra. *J Exp Bot, 68*(7), 1757-1767. doi:10.1093/jxb/erx052

Vialet-Chabrand, S., Matthews, J. S. A., Brendel, O., Blatt, M. R., Wang, Y., Hills, A., . . . Lawson, T. (2016). Modelling water use efficiency in a dynamic environment: An example using Arabidopsis thaliana. *Plant Science, 251*, 65-74. doi:https://doi.org/10.1016/j.plantsci.2016.06.016

Von Caemmerer, S. (2000). *Biochemical models of leaf photosynthesis*: Csiro publishing.

von Caemmerer, S., & Evans, J. R. (2015). Temperature responses of mesophyll conductance differ greatly between species. *Plant, Cell & Environment, 38*(4), 629-637. doi:https://doi.org/10.1111/pce.12449

Walker, B. J., & Cousins, A. B. (2013). Influence of temperature on measurements of the CO2 compensation point: differences between the Laisk and O2-exchange methods. *J Exp Bot, 64*(7), 1893-1905. doi:10.1093/jxb/ert058

Walker, B. J., Kramer, D. M., Fisher, N., & Fu, X. (2020). Flexibility in the Energy Balancing Network of Photosynthesis Enables Safe Operation under Changing Environmental Conditions. *Plants, 9*(3), 301. Retrieved from https://www.mdpi.com/2223-7747/9/3/301

Walker, B. J., Skabelund, D. C., Busch, F. A., & Ort, D. R. (2016a). An improved approach for measuring the impact of multiple CO2 conductances on the apparent photorespiratory CO2 compensation point through slope–intercept regression. *Plant, Cell & Environment, 39*(6), 1198-1203. doi:https://doi.org/10.1111/pce.12722

Walker, B. J., South, P. F., & Ort, D. R. (2016b). Physiological evidence for plasticity in glycolate/glycerate transport during photorespiration. *Photosynthesis Research, 129*(1), 93-103. doi:10.1007/s11120-016-0277-3

Warren, C. R. (2004). The photosynthetic limitation posed by internal conductance to CO2 movement is increased by nutrient supply. *Journal of Experimental Botany, 55*(406), 2313-2321. doi:10.1093/jxb/erh239

Willekens, H., Chamnongpol, S., Davey, M., Schraudner, M., Langebartels, C., Van Montagu, M., . . . Van Camp, W. (1997). Catalase is a sink for H2O2 and is indispensable for stress defence in C3 plants. *The EMBO Journal, 16*(16), 4806-4816. doi:https://doi.org/10.1093/emboj/16.16.4806

Zelitch, I. (1989). Selection and Characterization of Tobacco Plants with Novel O2-Resistant Photosynthesis. *Plant Physiology, 90*(4), 1457-1464. doi:10.1104/pp.90.4.1457

Zelitch, I. (1992). Factors Affecting Expression of Enhanced Catalase Activity in a Tobacco Mutant with O2-Resistant Photosynthesis. *Plant Physiology, 98*(4), 1330-1335. doi:10.1104/pp.98.4.1330

Zelitch, I., Schultes, N. P., Peterson, R. B., Brown, P., & Brutnell, T. P. (2008). High Glycolate Oxidase Activity Is Required for Survival of Maize in Normal Air *Plant Physiology, 149*(1), 195-204. doi:10.1104/pp.108.128439

CHAPTER 3: Rubisco activity and activation state dictate photorespiratory plasticity in *Betula papyrifera* acclimated to future climate conditions

This research was submitted to:

Gregory, L.M., Scott, K.F., Sharpe, L.A., Roze, L.V., Schmiege, S.C., Way D.A., & Walker, B.J. Rubisco activity and activation state dictate photorespiratory plasticity in *Betula papyrifera* acclimated to future climate conditions. (Submitted to Scientific Reports)

Abstract

Plant metabolism faces a challenge of investing enough enzymatic capacity to a pathway without overinvestment. As it takes energy and resources to build, operate, and maintain enzymes, there are benefits and drawbacks to accurately matching capacity to the pathway influx. The relationship between functional capacity and physiological load could be explained through symmorphosis, which would quantitatively match enzymatic capacity to pathway influx. Alternatively, plants could maintain excess enzymatic capacity to manage unpredictable pathway influx. In this study, we use photorespiration as a case study to investigate these two hypotheses in *Betula papyrifera*. This involves altering photorespiratory influx by manipulating the growth environment, via changes in CO_2 concentration and temperature, to determine how photorespiratory capacity acclimates to environmental treatments. Surprisingly, the results from these measurements indicate that there is no plasticity in photorespiratory capacity in *B. papyrifera*, and that a fixed capacity is maintained under each growth condition. The fixed capacity is likely due to the existence of reserve capacity in the pathway that manages unpredictable photorespiratory influx in dynamic environments. Additionally, we found that *B. papyrifera* had a constant net carbon assimilation under each growth condition due to an adjustment of functional rubisco activity driven by changes in activation state. These results provide the acclimation ability and limitations of *B. papyrifera* to future climate scenarios currently predicted in the next century.

Keywords:

acclimation, photorespiratory capacity, rubisco activation state, *B. papyrifera*

Introduction

Anthropogenic activities are rapidly changing the composition and thermal conditions of the global atmosphere, leading to fundamental trade-offs in photosynthetic carbon metabolism. Burning fossil fuels has and continues to liberate enormous quantities of CO_2 and other greenhouse gases into the atmosphere, which has increased global temperatures due to their role in radiative heat transfer (Wei *et al.*, 2018). The most recent Intergovernmental Panel on Climate Change (IPCC) report indicates that global surface temperatures have increased faster in the last 50 years due to anthropogenic greenhouse gas release than in any other 50-year period in the previous 2000 years (Lee *et al.*, 2023). The influx of CO_2 into the atmosphere will directly alter photosynthetic carbon metabolism, in addition to operating at elevated temperatures, as atmospheric CO_2 and O_2 are substrates for the initial carbon-fixing enzyme of photosynthesis, rubisco.

Rubisco has dual substrate affinity for both CO_2 and O_2, with each acting as a competitive inhibitor to the other (Badger *et al.*, 1974; Bowes *et al.*, 1972; Bowes *et al.*, 1971; Laing, 1974; Peisker, 1974). The fixation of CO_2 through rubisco carboxylation (v_c) initiates net carbon assimilation (A) through the Calvin-Benson cycle, while the fixation of O_2 through rubisco oxygenation (v_o) initiates photorespiration (see Figure 1 in chapter 1) (Bassham *et al.*, 1950; Bowes *et al.*, 1971; Laing, 1974). The enrichment of atmospheric CO_2 concentrations and warming of the atmosphere exert opposite effects on rates of rubisco v_c and v_o. Considering just an increase in CO_2 concentration, rubisco catalyzes more carboxylation reactions due to the heightened partial pressure of CO_2 surrounding the enzyme (Drake *et al.*, 1997). Conversely, a warmer atmosphere enhances rates of rubisco oxygenation through temperature-dependent shifts in rubisco specificity for CO_2 relative to $O_2$and a decrease in CO_2/ O_2 gas solubility (Hall *et al.*, 1983; Hermida-Carrera *et al.*, 2016; Jordan *et al.*, 1984). Additionally, prior to rubisco v_c or v_o, rubisco must be carbamylated to prime the catalytic sites of the enzyme to accept CO_2 or O_2 (Hammond *et al.*, 1998; Lorimer *et al.*, 1980). The generation of misfire products which prevent further reactions in the active site of rubisco can reduce the efficiency of the enzyme, and conformational changes are required by rubisco activase to restore functionality (Bhat *et al.*, 2017; Portis, 2003; Spreitzer *et al.*, 2002). Rubisco

activase, the chaperone protein that promotes these conformational changes, heavy regulates functional rubisco activity and is also impacted by changing CO_2 concentrations and temperature (Carmo-Silva *et al.*, 2013; Cen *et al.*, 2005; Crafts-Brandner *et al.*, 2000; Galmés *et al.*, 2013; Kim *et al.*, 2005; Portis, 2003; Salvucci *et al.*, 2004b). Although past research has elucidated the mechanisms of rubisco under elevated CO_2 concentrations and increased temperatures, our understanding of how/if photorespiration, downstream of rubisco, acclimates to these environmental changes is limited.

Specifically, it is unknown whether photorespiratory capacity downstream of rubisco acclimates to changes in growth CO_2 concentration and temperature to maintain v_o or whether excess capacity exists in photorespiration constitutively. This capacity of photorespiration is set by the maximal reaction velocity (V_{max}) for the enzymes downstream of rubisco. While rubisco sets the rate of 2-phosphoglycolate (2-PG) production through v_o (photorespiratory influx), the enzymes downstream of rubisco must process the subsequent photorespiratory intermediates that are produced. Some of these reactions process biologically inert photorespiratory intermediates, like glycine, but others degrade biologically active intermediates, such as 2-phosphoglycolate (2-PG), glycolate, and H_2O_2. If there is mismatch between photorespiratory influx and the capacities of downstream photorespiratory reactions, photorespiratory intermediates are likely to accumulate due to insufficient conversion rates. Accumulation of either 2-PG or glycolate under photorespiratory pressure can lead to a decrease in *A* through inhibition of triose phosphate isomerase and sedoheptulose-1,7-bisphosphate, or through interference with rubisco activity and RuBP regeneration, respectively (Anderson, 1971; Campbell *et al.*, 1990; Chastain *et al.*, 1989; Cook *et al.*, 1985; Dellero *et al.*, 2016; Flügel *et al.*, 2017; Mulligan *et al.*, 1983). Accumulation of H_2O_2, a signaling molecule involved in both stress and developmental processes, leads to cell death when catalase-deficient *Nicotiana tabacum* mutant plants were exposed to high photorespiratory pressure (Dat *et al.*, 2003). Managing these intermediates is thus important to maintain plant vigor, especially in changing environments where photorespiratory influx is highly dynamic.

Photorespiratory influx can change in short- (seconds to days) or long-term (weeks-years) time scales depending on the growth environment. Daily photorespiratory influx can increase due to heat wave anomalies, causing a greater carbon efflux associated with photorespiration compared to historic averages (Cavanagh *et al.*, 2023). While at the opposite end, C_3 plants adapted to hot-arid environments, like *Rhazya stricta*, has double the rates of v_o compared to *Nicotiana tabacum* when grown together at similar growth temperatures in a glasshouse (Gregory *et al.*, 2023). Whether there are rapid or permanent changes to photorespiratory influx, it is unclear if there is acclimation in the pathway metabolic capacity downstream of rubisco.

There are two main hypotheses that could explain the relationship between photorespiratory influx and downstream metabolic capacity. One concept to describe the relationship between functional capacity and physiological load is symmorphosis. Symmorphosis means that the structure optimally matches the demand placed on the system (Suarez *et al.*, 1997; Taylor *et al.*, 1981; Weibel *et al.*, 1991). Symmorphosis in the case of photorespiration would exist if the enzymatic capacities (V_{max}) quantitatively match the v_o pressure tied to growth conditions, such that photorespiratory capacity would be optimized to photorespiratory influx. A benefit to symmorphosis for photorespiratory capacity is optimal energy expenditure. As it takes energy and resources to build, operate, and maintain enzymes, optimally matching capacity to influx would alleviate wasted energy that could go into growth or fitness. Alternatively, another hypothesis to explain the structure-function relationship would be the presence of a reserve capacity embedded into the pathway (Alexander, 1981; Diamond, 2002). We will refer to this reserve or excess capacity as a “safety factor”. The presence of safety factors in the photorespiratory pathway would appear as higher capacities (V_{max}) of the downstream enzymes than appears to be needed, but that could manage dynamic photorespiratory influx in fluctuating conditions, while maintaining *A*. The benefit of overinvestment in photorespiratory capacity would be efficient degradation of photorespiratory intermediates so that minimal to no accumulation of these intermediates would occur. A downside to this overinvestment would be that the excess energy needed for photorespiratory enzyme synthesis, operation, regulation, and maintenance to keep capacity high could otherwise be devoted elsewhere in the plant.

To explore these hypotheses, we determined the plasticity of enzyme capacity across the photorespiratory pathway over six different CO_2 concentration and temperature growth environments in *B. papyrifera*. *B. papyrifera* is ideal for studying plasticity of photorespiration under future conditions as it is native to the boreal forest, a biome predicted to experience the most significant increase in temperature compared to all forest biomes by 2100, concurrent with rising atmospheric CO_2 concentrations (Collins *et al.*, 2013; Gauthier *et al.*, 2015; Price *et al.*, 2013). Since v_o in absolute terms and the ratio of v_o/v_c are sensitive to both CO_2 concentration and temperature, these environmental shifts should influence photorespiratory influx during growth. The growth environments were designed using a factorial approach which aimed to mimic current, moderate, and extreme climate change scenarios for the boreal region (Collins *et al.*, 2013; Dusenge *et al.*, 2020). To test the validity of these hypotheses in *B. papyrifera*, biochemical and physiological mechanisms were probed using biochemical assays with gas-exchange data from a previous study to determine if photorespiratory capacity acclimates to environmental treatments.

In this paper, we determined there is no plasticity in photorespiratory capacity in *B. papyrifera* grown under different CO_2 concentrations and temperatures. Instead, a fixed photorespiratory capacity is maintained, likely due to the existence of safety factors embedded in the pathway. Interestingly, the initial reactions in the photorespiratory pathway have lower safety factors than later ones, highlighting potential enzymatic bottlenecks that may limit the rate of reaction due to low enzyme activities. Additionally, we found that *B. papyrifera* had a constant *A* under each growth condition due to an adjustment of functional rubisco activity driven by changes in activation state. These results provide insight into the acclimation ability and limitations of *B. papyrifera* to future climate scenarios currently predicted in the next century.

Results

B. papyrifera photorespiratory enzyme activity across six growth environments

To assess the acclimation potential of photorespiratory capacity in *B. papyrifera,* we measured chloroplastic and peroxisomal enzyme activities under saturating substrate concentration to determine an *in vitro* V_{max} (Figure 3.1 & 3.2; Table 3.1 & 3.2). These enzyme activities were measured in leaves of *B. papyrifera* grown under 6 different environmental conditions at 25◦C and 35◦C using crude protein extract. The environmental treatments mimics ambient or elevated CO_2 concentrations (AC or EC) and under 1 of 3 temperature treatments (T0, T4, T8). The enzyme assayed were rubisco (RBC), phosphoglycolate phosphatase (PGP), glycolate oxidase (GO), catalase (CAT), glutamate glyoxylate aminotransferase (GGAT), alanine glyoxylate aminotransferase (AGAT), serine glyoxylate aminotransferase (SGAT), hydroxypyruvate reductase (HPR), and glycerate kinase (GLYK). *B. papyrifera* had greater total rubisco activity when grown under T0AC than when grown at T8AC, T4AC, and T8EC at both 25◦C and 35◦C assay temperatures. *B. papyrifera* had greater GO activities when grown under T0EC, than under T4AC, T8AC, and T8EC at 35◦C. Additionally, *B. papyrifera* had greater CAT activities when grown under T0AC than under T4EC at 25◦C, and under T4EC and T8EC at 35◦C. *B. papyrifera* had similar PGP, GO, GGAT, AGAT, SGAT, HPR, and GLYK activities when grown under any of the six growth environments. The two-way ANOVA reveals a significant temperature effect with RBC, GO, CAT, and HPR at 25◦C, while RBC, GO, and CAT have a significant temperature effect at 35◦C. CAT and GGAT has a significant CO_2 concertation effect under 35◦C assay temperature. RBC was the only photorespiratory enzyme with an interactive effect between CO_2 concentration and temperature at 25◦C, but not at 35◦C (Table 3.3). Thus, the photorespiratory enzyme activity downstream of rubisco does not acclimate in parallel to v_o and appears to have the same enzymatic photorespiratory capacity regardless of environmental growth conditions.

To determine whether downstream enzyme activities scale with rubisco activity, the initial enzyme of the photorespiratory pathway, downstream enzyme's activities were plotted against total rubisco activity using the entire kinetic dataset measured for each enzyme (Figure 3.3). Linear regressions were fitted to establish correlation to total

rubisco activity. The activity of the enzymes PGP, GO, CAT, SGAT, HPR, and GLYK all had significant (*p-value* < 0.01) positive correlations to rubisco activity, while the activity of GGAT, AGAT, and SGAT were not correlated with rubisco activity.

The temperature response ratio (or Q_{10}) of the enzyme activities were calculated by dividing the activity at 35◦C by the activity at 25◦C (Figure 3.9). The Q_{10} of RBC, PGP, GO, CAT, GGAT, AGAT, SGAT, HPR, and GLYK were not affected by growth CO_2 concentration or temperature. RBC, PGP, GO, CAT, HPR, and GLYK had Q_{10} above 1, indicating a thermal dependence with enzyme activity. However, the GGAT, AGAT, and SGAT had Q_{10} equal to or below 1, indicating aminotransferases activity is likely temperature independent in *B. papyrifera*.

***B. papyrifera* rubisco deactivates across ambient and elevated CO_2, but not across temperature gradients**

In vivo net carbon fixation is driven by functional rubisco activity rather than total rubisco activity, which is heavily regulated and only considers the activity of rubisco with open active sites. To evaluate the response of *in vivo* rubisco activity to different growth environments in *B. papyrifera*, rubisco activation state was measured (Figure 3.4). The initial and chemically activated enzyme activities were measured in leaves of *B. papyrifera* at 25◦C from crude protein extract. The initial rubisco activity was divided by the chemically activated rubisco activity to determine functionally active rubisco. *B. papyrifera* grown under T0AC and T4AC had a higher rubisco activation state than trees grown under T4EC and T8EC conditions. When compared against the active rubisco at current climate conditions (T0AC), rubisco deactivates by 3.3% (T4AC), 13.1% (T8AC), 15.6% (T0EC), 24.7% (T4EC), and 31.4% (T8EC). The two-way ANOVA reveals a clear CO_2 concentration effect (*p*-value = < 0.001) and a temperature effect (*p*-value = 0.024), but no interactive effect (Table 3.4).

***B. papyrifera* rubisco carboxylation responds similar across growth environments, but oxygenation pressure varies**

To assess the ability of *B. papyrifera* to fix carbon under the six different growth environments, A, v_o, v_c, v_o/v_c were resolve at the time of leaf development using temperature response curves (Figure 3.5 & 3.6). 10-days prior to leaf harvest the average growth temperatures were 19.2◦C (T0AC), 19.4◦C (T0EC), 23.0◦C (T4AC),

23.1°C (T4EC), 26.8°C (T8AC), 26.4°C (T8EC). Changing CO_2 and temperature during growth did not cause significant differences in *A,* v_c, or v_o, but did cause a significant difference in v_o/v_c at the time of leaf harvest. *B. papyrifera* v_o and v_o/v_c are sensitive to CO_2 concentration (*p*-value = 0.003 & < 0.000), but not to temperature (Table 3.5). Thus, these environmental conditions altered photorespiratory influx in *B. papyrifera* within CO_2 conditions. However, the change in photorespiratory influx did not alter *A* across growth conditions.

Three output parameters (i.e., the maximum rate on the temperature response curve, V_{max}; the temperature optimum, T_{opt}, and the maximum temperature, T_{max}) were additionally solved from the temperature response curves for *A*, v_o, and v_c and compared between the *B. papyrifera* growth environments (Figure 3.10 A-I). No significant differences were reveals across growth conditions for any of the parameters.

***B. papyrifera* photorespiratory safety factors across six growth environments**

To evaluate the relationship between photorespiratory influx and downstream metabolic capacities, safety factors were calculated under each growth environment in *B. papyrifera* at 25°C to quantify the excess capacity (Figure 3.7). To calculate "safety factors", downstream photorespiratory enzyme activities m^{-2} s^{-1} at 25°C were divided by v_o estimated at 25°C using the temperature response curve. If a safety factor is below 1, then photorespiratory influx is greater than enzymatic capacity. If a safety factor is equal to 1, then photorespiratory influx is accurately matched to the enzymatic capacity and indicates symmorphosis. If a safety factor is above 1, then photorespiratory influx is less than the enzymatic capacity and indicates a reserve capacity. Broadly, plants grown under ambient CO_2 concentrations had lower safety factors across the downstream enzymes than plants that grew under elevated CO_2 conditions due to the decrease in v_o in plants from the high CO_2 concentrations. In particular, PGP, GO, and GGAT had safety factors of ~1 under T0AC, T4AC, and T8AC growth conditions, which suggest symmorphosis, but safety factors above 1 under T0EC, T4EC, and T8EC growth conditions. CAT, AGAT, SGAT, HPR, and GLYK had safety factors above 1 for all growth conditions, revealing the reserve capacity. The two-way ANOVA reveals a clear CO_2 concentration effect (*p*-value = < 0.001) in all enzyme safety factors, and a

temperature effect in CAT, AGAT, SGAT, and GLYK (*p*-value = 0.007, 0.033, 0.001, 0.003, respectively), but no interactive effect (Table 3.6).

Discussion

This study demonstrates that photorespiratory enzyme activity has predominately a fixed capacity, rather than an acclimation response, to changing CO_2 and temperature in *B. papyrifera* (Figure 3.1 & 3.2). Changing CO_2 and temperature during growth did not cause a significant difference in photorespiratory influx between the six growth conditions but did significantly alter the v_o/v_c as estimated from previously measured gas exchange during this experiment (Figure 3.6D & F). However, significant CO_2 concentration effect was identified in the absolute rates of v_o and v_o/v_c, but no temperature effect was found (Table 3.5). Trends in this experiment are consistent with increased CO_2 decreasing rates of rubisco oxygenation due to elevated CO_2, and a slight decrease with temperature caused by decreases in rubisco activation state (Figure 3.4 and 3.6). This indicates that the regulation of photorespiratory enzymes is not tied simply to temperature during development. The inability of photorespiratory enzymes, downstream of rubisco, to acclimate to environmental conditions raises the question: does photorespiratory enzymatic capacity need to acclimate to maintain optimal v_o, or does excess photorespiratory capacity already exist?

If photorespiratory capacity needs to acclimate to maintain a new v_o, then the kinetic properties of the enzyme activities in *B. papyrifera* may be optimized. An optimized photorespiratory pathway would adhere to the symmorphosis hypothesis, where the enzyme activities resulting from morphogenesis would quantitatively match the v_o (Suarez *et al.*, 1997; Taylor *et al.*, 1981; Weibel *et al.*, 1991). Historically, *B. papyrifera* trees inhabit high latitude regions and are frequently found in boreal forests biomes that experience cold-moderate temperatures, with freezing temperatures for over half the year (Gauthier *et al.*, 2015). Under a boreal forest environment, we would expect *B. papyrifera* to be adapted to low photorespiratory pressure, therefore a minimal photorespiratory capacity should be maintained. In this study, where *B. papyrifera* is exposed to different CO_2 and temperature conditions during growth, we would expect changes in v_o to adjust photorespiratory capacity in parallel. Based on the mean v_o at 25°C, which are 5.96 μmol m^{-2} s^{-1} (T0AC), 4.63 μmol m^{-2} s^{-1} (T4AC), 3.94 μmol m^{-2} s^{-1} (T8AC), 2.64 μmol m^{-2} s^{-1} (T0EC), 2.58 μmol m^{-2} s^{-1} (T4EC), 1.75 μmol m^{-2} s^{-1} (T8EC), the downstream enzyme activities at 25°C would need to be ~6 μmol m^{-2} s^{-1} (T0AC), ~5μmol

m^{-2} s^{-1} (T4AC), ~4 µmol m^{-2} s^{-1} (T8AC), ~3 µmol m^{-2} s^{-1} (T0EC & T4EC), ~2 µmol m^{-2} s^{-1} (T8EC) to manage this carbon influx following rubisco oxygenation. Under ambient CO_2 conditions, the activities of PGP, GO, GGAT are near 5 µmol m^{-2} s^{-1} and broadly match the photorespiratory influx, but the other downstream enzymes have activities greater than this. In contrast, under elevated CO_2 conditions we would expect enzyme activities closer to 3 µmol m^{-2} s^{-1}, to match the v_o, but we do not see this. Instead, the enzyme activities have no significant changes to what is measured under ambient conditions (T0AC). Since photorespiration does not acclimate distinct enzyme activities to maintain v_o in *B. papyrifera*, adjustment of photorespiratory capacity through symmorphosis alone is not supported in *B. papyrifera* at the tested growth conditions.

An alternative hypothesis to describe the fixed capacity of the photorespiratory enzymes is the existence of "safety factors" embedded into the pathway (Salvador *et al.*, 2003). With this hypothesis, the photorespiratory pathway has a reserve capacity to handle photorespiratory influx under dynamic conditions. Therefore, we would expect greater photorespiratory enzyme capacities in *B. papyrifera* than are required by "typical" physiological demand to manage rapid changes in v_o without compromising *A*. In all environmental conditions *B. papyrifera* were grown under, photorespiratory enzymes' activities matched or exceeded v_o and were not significantly altered by differences in photorespiratory influx brought by changes in CO_2 or temperature. Additionally, we find that *A* is consistent between the six growth conditions (Figure 3.5B). The inability to acclimate photorespiratory capacity to growth conditions is evidence for safety factors within the pathway constitutively. Interestingly, the initial reactions of photorespiration have lower safety factors (Enzyme activity / v_o) than the reactions later in the pathway (Figure 3.7). This is primarily due to the larger photorespiratory influx under ambient CO_2 conditions (T0AC, T4AC, T8AC), compared to elevated CO_2 conditions (T0EC, T4EC, T8EC), in tandem with the fixed absolute activities of the photorespiratory enzymes (Figure 3.1 & 3.2 and Table 3.6). Since *B. papyrifera* had lower absolute activities of PGP, GO, and GGAT compared to CAT, AGAT, SGAT, HPR, and GLYK across growth conditions, the safety factors calculated for these initial enzymes were lower. In particular, when *B. papyrifera* was grown under

T0AC, T4AC, and T8AC, the safety factor ranged from 0.787-1.267 in PGP, GO, and GGAT, but ranged from 1.751-3.314 under T0EC, T4EC, and T8EC.

Low safety factors in the initial photorespiratory enzymes suggest that these reactions may be rate limiting in *B. papyrifera* and potential enzymatic bottlenecks in the pathway. Enzymatic bottlenecks are defined here as steps in a metabolic pathway where the rate of the reaction is significantly limited by the activity of the enzyme. The pattern of underinvestment in enzyme activity in the initial reactions of photorespiration in *B. papyrifera* may apply universally to C_3 species and increasing the activity of these enzymes may improve photosynthetic efficiency when photorespiratory influx is unpredictable. Past work supports this hypothesis generally, for example, in *Rhazya stricta*, a C_3 desert extremophile, the early photorespiratory enzymes PGP and CAT had elevated activities when compared to *Nicotiana tabacum* (Gregory *et al.*, 2023). *R. stricta* is adapted to hot-arid environments, where temperatures range from 26°C to 43°C, that promote an increase of photorespiratory influx (Lawson *et al.*, 2014). The increased activity of PGP and CAT adapted in *R. stricta* may provide an increase in safety factor in these initial enzymes to reduce enzymatic bottlenecks and maintain minimal inhibitor or H_2O_2 accumulation during periods of high v_o in this species. Interestingly, species that do not show this constitutive safety factor, may have increased photosynthetic resilience by increasing enzyme capacity. For example, PGP overexpression in *Arabidopsis thaliana* improved *A* likely by maintaining lower steady-state pools of 2-phosphoglycolate after short- and long-term exposure to elevated temperatures (Flügel *et al.*, 2017; Timm *et al.*, 2019). Another photorespiratory enzyme, glycine decarboxylates complex (GDC), is expected to have a low safety factor, although it was not measured in this study. Overexpression of one of the four protein that compose the complex, H-protein, enhance GDC activity and is associated with an increase in *A* in *Arabidopsis thaliana* (Timm *et al.*, 2012). Other researchers, have overexpressed H-protein in *Nicotiana tabacum* and have similarly shown an increases plant biomass (López-Calcagno *et al.*, 2019).

The decrease in CAT activities with increasing growth temperatures in *B. papyrifera* may be attributed to a decline in enzyme synthesis due to oxidative damage. Oxidative stress caused by high temperatures or heat shock enhance catalase

inactivation by preventing the resynthesis of new enzymes (Dat *et al.*, 1998; Feierabend *et al.*, 1992; Streb *et al.*, 1993; Willekens *et al.*, 1995). This inhibition of catalase synthesis lowers the steady-state concentration of the enzyme, resulting in a decline in catalase activity with increasing temperatures (Streb *et al.*, 1996). Previous work identified a sharp decline in catalase activity after exposure to 24◦C, 48◦C, and 54◦C in *Capsicum annuum L.* (Anderson, 2002). In *Zea mays*, low catalase activity was attributed to lower amounts of cat2 protein due to higher degradation rates (Matters *et al.*, 1986).

It is also worth noting the difference in the safety factor between GGAT and AGAT in *B. papyrifera*, as it might be suggestive of the amino donor *B. papyrifera* uses to facilitate the transamination reaction (Figure 3.7D & E). Peroxisomal aminotransferases in the photorespiratory pathway utilize glycolate as an amino acceptor, yet the specific amino donor across species remains unknown due to promiscuity (Husic *et al.*, 1987; Leegood *et al.*, 1995; Liepman *et al.*, 2003; Somerville *et al.*, 1980). In various plant species, glutamate and alanine are supported to be the main donor for glycine production from glycolate (Betsche, 1983). In *Arabidopsis thaliana*, glutamate is supported to be the main donor as GGAT-KO mutants reveal photorespiratory phenotype (Somerville *et al.*, 1980). In our work, the larger safety factor in AGAT is caused by the higher absolute activity of AGAT (~15 μmol Alanine m^{-2} s^{-1}), than GGAT (~4 μmol Glutamate m^{-2} s^{-1}) across growth environments. The larger activity may indicate the preference for alanine as the amino doner during periods of high photorespiratory influx (Figure 3.2D & E). In agreement with this, past work in *R. stricta* and *N. tabacum* have greater absolute activities of AGAT (~20 & ~9 μmol Alanine m^{-2} s^{-1}, respectively), than GGAT (~2 & ~2 μmol Glutamate m^{-2} s^{-1}, respectively), suggesting that alanine may be the amino donor in these species as well (Gregory *et al.*, 2023).

Although outside of the scope of this study, it is also likely that some photorespiratory enzymes in *B. papyrifera* are subject to posttranslational modifications (PTM) that further regulate enzyme activity *in vivo*. We recognize that photorespiratory capacity measured *in vitro* in this study is different than the enzymatic rates under physiologically-relevant substrate concentrations *in vivo.* PTMs might provide fine-tune

metabolic control of the photorespiratory system by transient inactivation of a particular enzyme, or positively or negatively alter enzyme activity in relation to environmental pressure (Friso *et al.*, 2015; Keech *et al.*, 2017). Recently, regulation of the photorespiratory pathway has been found to include protein phosphorylation, ubiquitination, acetylation, and redox modifications (Hodges, 2022; Hodges *et al.*, 2013; Keech *et al.*, 2017; Timm *et al.*, 2020).

Although many of the enzymes downstream of rubisco do not adjust their activities to environmental pressure, we identified that the activities of many downstream photorespiratory enzymes scaling to total rubisco activity (Figure 3.3). Our results demonstrate a significant correlation of PGP, GO, CAT, SGAT, HPR, and GLYK to total rubisco activity, however no correlation of GGAT, and AGAT to rubisco activity. The coordinated change of PGP, GO, CAT, SGAT, HPR, and GLYK activities associated with rubisco may be an effective strategy to alter pathway capacity. Especially when considering the safety factor of PGP and GO, tight coordination may circumvent the underinvestment in enzyme capacity early in the photorespiratory pathway. The mechanism that causes this coordinated regulation may be at the transcript-level via co-expression of multiple photorespiratory genes (Laxa *et al.*, 2018). The activities of the aminotransferase enzymes (GGAT, AGAT, and SGAT) are not well explained by the variation seen in rubisco activity.

The results from this work suggest *B. papyrifera* acclimates functional rubisco capacity (total activity * activation state) to growth conditions through adjustments in rubisco activation state (Figure 3.1 & 3.4). When compared to active rubisco at current climate conditions (T0AC), rubisco deactivates by 3.3% (T4AC), 13.1% (T8AC), 15.6% (T0EC), 24.7% (T4EC), and 31.4% (T8EC). The deactivation of rubisco is largest when compared within the CO_2 concentrations. Both a CO_2 effect (p-value = < 0.000) and temperature effect (p-value = < 0.024) were identified (Table 3.4). Our activation state data in *B. papyrifera* agree with what is universally observed when rubisco is exposed to increasing CO_2 and/or temperature treatments (Cen *et al.*, 2005; Crafts-Brandner *et al.*, 2000; Kim *et al.*, 2005; Salvucci *et al.*, 2006; Scafaro *et al.*, 2023). The deactivation of rubisco associated with elevated CO_2 is likely driven by a combination of a regulated response in RuBP regeneration, and possibly rubisco activase sensitivity to high

temperature in *B. papyrifera* (Cen et al., 2005). Under elevated CO_2 conditions, rubisco consumes RuBP faster than it is regenerated, which reduces the ATP:ADP ratio, compared to ambient CO_2 conditions. The ATP:ADP ratio regulates the activity of rubisco activase and reduces the catalytic capacity of rubisco to rebalance the RuBP regeneration to consumption capacity (Portis, 2003; Ruuska *et al.*, 2000; Sage *et al.*, 1990). The decrease in activation state with temperature coincides with a decrease in rubisco activase activity under elevated temperatures (Kim *et al.*, 2005; Portis, 2003; Salvucci *et al.*, 2004a, 2004b, 2004c).

With the differences in active rubisco within the 6 climate scenarios, *in vivo A,* v_c, and v_o estimated during leaf development remains constant (Figure 3.5B and 3.6B & D). We show that *in vitro* rubisco activity for CO_2 in *B. papyrifera* has lower activity under T4AC, T8AC, and T8EC scenarios at both 25°C and 35°C assay temperatures, which is explained by its activation state (Figure 3.1A & Figure 3.4). Rubisco activity to O_2 ($v_{o,max}$), although not measured, is anticipated to be lower, with similar trends that as rubisco activity to CO_2, as both of these reactions occur in the same active enzyme.

Conclusion

In summary, these results suggest that photorespiration, downstream of rubisco, does not acclimate distinct enzyme activities to environmental pressures in parallel to photorespiratory influx, but instead has a fixed capacity that scales relative to total rubisco activity. This fixed capacity is due to safety factors embedded into the photorespiratory pathway, although initial reactions have a lower safety factor than later ones, potentially revealing enzymatic bottlenecks. A majority of downstream photorespiratory enzyme activities correlated to total rubisco activity indicating that rubisco, instead of the environmental factors, sets the capacity for photorespiration. Additionally, *A* remained consistent between environmental pressures as a consequence of acclimation of rubisco activation state in *B. papyrifera*. This work provides physiological and biochemical mechanisms for the acclimation ability and limitations in *B. papyrifera* to future climate scenarios.

Material and Methods

Plant Material and Growth Conditions

Leaf material of paper birch (*B. papyrifera* [Marshall]) were harvested from 6 climate treatments from the Biotron Experimental Climate Change Research Centre of Western University (Figure 3.8) (Schmiege *et al.*, 2023)(Hammer *et al.,* unpublished). In brief, growth conditions for each glasshouse were set to the following 6 climate treatments: Ambient CO_2 (398 ± 54 ppm) or Elevated CO_2 (739 ± 48 ppm; elevated CO_2 treatments were maintained by adding pure CO_2 to the chambers until the elevated setpoint was reached), with 1 of 3 temperature treatments: ambient temperature, ambient + 4◦C, or ambient + 8◦C. Ambient temperature conditions were set to a 5-year day/ night average for Algonquin Park, ON (45◦58′N, 78◦48′W). Plants grew in the glasshouses for 5 months before the youngest, fully expanded leaves of *B. papyrifera* were harvested from each treatment, frozen in liquid N_2, and stored at -80◦C.

Preparing crude protein extract for protein quantification, total chlorophyll content, enzyme activity assays

Crude protein extracts were prepared from the youngest, fully expanded leaves of *B. papyrifera*. Leaf material was homogenize on ice with 1.5 mL of the Extraction buffer (50 mM EPPS buffer, pH 8.0, containing 1 mM EDTA, 10 mM DTT, 0.1% Triton X-100 [v/v], 0.5% polyvinylpyrrolidone, and 20 µL 1X SigmaFAST Protease Inhibitor Cocktail, EDTA Free (Sigma, St. Louis, MO, USA)), using a 2 mL glass-to-glass homogenizer (Kontes Glass Co., Vineland, NJ, USA). The homogenate was transferred into a 2 mL plastic Eppendorf tube and clarified by centrifugation for 15 min at 15,000 g and 4◦C (Eppendorf Centrifuge 5424R, Eppendorf, Enfield, CT, USA). The supernatant, containing the clarified crude protein extract, was used for protein quantification, and enzyme activity assays. Both the supernatant and insoluble pellet were used to quantify total chlorophyll content.

Protein quantification

Soluble protein content was determined in crude protein extract (Bio-Rad Protein Assay; BIO-RAD, USA) according to the manufacturer instructions using a SpectraMax M2 Microplate Reader (Molecular Devices, San Jose, CA, USA).

Total Chlorophyll Content

Soluble chlorophyll content was determined in clarified crude protein extract and the insoluble pellet using a SpectraMax M2 Microplate Reader (Molecular Devices, San Jose, CA, USA). Chlorophyll content in the crude protein extract was determined by mixing 40 µL of the crude protein extract with 960 µL of 100% Ethanol. Following a few inversions, the solution was centrifuged to gather the precipitate at the bottom of the tube, and the clarified supernatant was measured at 649 nm and 665 nm. Chlorophyll content in the insoluble pellet was determined by adding 1 mL of 100% Ethanol to the pellet and vortexing to homogenize the solution for 30-45 seconds. Following a centrifugation step, 40 µL of the clarified supernatant was measured at 649 nm and 665 nm. The absorption coefficient for 100% ethanol were taken from Table 1 of (Ritchie, 2008). *Chl a* and *Chl b* equations used are below (Porra, 2002; Porra *et al.*, 1989; Ritchie, 2006):

$$Chl\ a = (13.2969 * Abs_{665}) - (4.5224 *\ Abs_{649}) \quad (1)$$

$$Chl\ b = (-7.4096 * Abs_{665}) + (25.7205 *\ Abs_{649}) \quad (2)$$

$$Total\ Chl\ Content = Chl\ a + Chl\ b \quad (3)$$

Enzyme Activity Assays

All enzyme activities (except for RBC and CAT) were measured by *spectrophotometric* assays with the use of SpectraMax M2 Plate reader and SoftMax Pro7 software (Molecular Devices, San Jose, CA, USA). PGP, GO, GGAT, AGAT, SGAT, HPR, and GLYK assays were performed in a 200 µL total reaction mix using polystyrene or acrylic UV transparent 96-well microplates (Corning, Kennebunk, ME, USA) as described in (Gregory *et al.*, 2023). While the RBC and CAT assay was performed in 1 mL reaction mix using an Cary60 UV-Vis Spectrophotometer (Agilent Technologies, Santa Clara, California, USA) and Oxygraph+ Oxygen Monitoring System and Oxytrace+ software (Hansatech Instruments, Penteny, UK). The pH of reactions was selected based on the organellar pH where the reaction occurs (Heinze *et al.*, 2002; Kendziorek *et al.*, 2008; Liu *et al.*, 2008; Shen *et al.*, 2013). All enzyme assays

were performed with 2-3 technical replicates on 5-6 independent biological replicates using leaf tissue from different plants.

Rubisco Activity and Activation State Assays

The activity of RBC was determined by linking the formation of 3-phosphoglcerate to NADH oxidation in chemical activated crude protein extracted from *B. papyrifera* leaves, and was identical to GLYK activity described in (Gregory *et al.*, 2023). The initial rate of reaction was determined during first 20 sec. The initial rate of the reaction was used to express the specific activity as μmoles CO_2 m^{-2} s^{-1}.

The activity and activation state of rubisco was determined by measuring the initial and chemically activated rubisco as described in (Walker *et al.*, 2016b). The activity of RBC was determined by linking the formation of 3-phosphoglcerate to NADH oxidation in chemical activated crude protein extracted from *B. papyrifera* leaves. For this the extraction buffer was prepared CO_2-free (via N_2 sparging), and the initial reaction mix containing 908 μL rubisco reaction buffer (containing 50 mM HEPES, pH 7.8, 20 mM $MgCl_2$, 1 mM ETDA, 1 mM ATP, 5 mM Creatine Phosphate, 20 mM $NaHCO_3$, 0.2 mM NADH), 20 μL of coupling enzyme, 32 μL 16.04 mM RuBP was incubated for 1 min to determine the NADH baseline. The reaction was initiated with 40 μL crude protein extract, and the NADH consumption was observed for 3 min with 0.1 sec interval. The initial rate of the reaction was determined during first 20 sec. The chemically activated assay followed the same steps as the initial, but the crude protein extract was initially activated with 15 mM $NaHCO_3$ and 15 mM $MgCl_2$ for 15 minutes before starting the reaction. The rate of the reaction was used to express the specific activity as μmoles CO_2 m^{-2} s^{-1}. The ratio of the initial and chemical activated rates were multiplied by 100 to resolve the activation state of rubisco on a percentage basis (Sales *et al.*, 2018). Activation state assays were performed with 2 technical replicates on 5 independent biological replicates using leaf tissue from different plants.

Catalase Activity Assay

The activity of CAT was determined in *B. papyrifera* by the production of O_2 (Aebi, 1983; Zelitch, 1989) with the following modifications. The reaction mix containing 946 μL 50 mM K-phosphate buffer, pH 8.1, and 20 μL crude protein extract, was incubated for 1.5 min to determine the O_2 baseline. The reaction was initiated with 34 μL

30 mM H_2O_2 and the increase in O_2 production (nmol/mL) was observed for 1.5 min with 1 sec interval using a Oxygraph+ Oxygen Monitoring System. The initial rate of reaction was determined during the first 10 seconds and the specific activity was expressed as μmoles O_2 produced m^{-2} s^{-1} (Escobar *et al.*, 1990; Szczepanczyk *et al.*, 2023).

Gas Exchange

Temperature response data (10°C, 20°C, 30°C, and 40°C) of net carbon assimilation (*A*) under ambient oxygen conditions (21%) at high light (1800 μmol PAR m^{-2} s^{-1}) intensity measured on the youngest, fully expanded leaves of *B. papyrifera* were provided by (Hammer *et al.,* unpublished) using a LI-6800 or a LI-6400XT (LI-COR Biosciences, USA). Data of the rates of CO_2 release from non-photorespiratory processes in the light (R_L) at 25°C measured using the common intersection method (Laisk, 1977; Walker *et al.*, 2016a) were taken from (Schmiege *et al.*, 2023). The temperature response of R_L was estimated according to the Arrhenius equation,

$$R_L = exp^{\frac{c-\Delta H_a}{R*T_k}} \quad (4)$$

(Bernacchi *et al.*, 2001). Where, c is the scaling constant (18.72), ΔH_a is the activation energy (46.39 J), R is the molar gas constant (8.314 J mol^{-1} K), and T_k is the leaf temperature. The photorespiratory CO_2 compensation point (Γ^*) of *B. papyrifera* has not been measured, therefore was assumed to be similar to *N. tabacum*. The temperature response of Γ^* was solved using an Arrhenius equation (above) with a c of 13.49 and a ΔH_a of 24.46 (Bernacchi *et al.*, 2002). CO_2 response curves at 10°C, 20°C, 30°C, and 40°C were fit using an R-based *ACi* fitting tool to estimate mesophyll conductance (g_m) while constraining previously resolved R_L and Γ^* parameters (Gregory *et al.*, 2021) (see http://github.com/poales/msuRACiFit to access Rscript with user-friendly interface).

Estimating rates of v_c and v_o

v_c and v_o for *B. papyrifera* were estimated according to

$$v_c = \frac{A + R_L}{1 - \Gamma^*/C_c} \quad (5)$$

$$v_o = \frac{v_c - A - R_L}{0.5} \quad (6)$$

(Walker *et al.*, 2020). Where, the partial pressure of CO_2 at the site of rubisco catalysis (C_c) was determined by

$$C_c = C_i - \frac{A}{g_m} \quad (7)$$

Modelling the Temperature Response of *A*, v_c, and v_o

The temperature response of *A*, v_c, and v_o were modelled to estimate key parameters (V_{max}, T_{opt}, T_{max}) with the following equation

$$Param = V_{max} * (\frac{T_{max} - T_{leaf}}{T_{max} - T_{opt}}) * (\frac{T_{leaf}}{T_{opt}})^{\frac{T_{opt}}{T_{max} - T_{opt}}} \quad (8)$$

(Collier *et al.*, 2017). Where, $Param$ is either *A*, v_c, or v_o, V_{max} is an estimation of the maximum rate of the parameter of interest on the temperature response curve, T_{opt} is the temperature optimum, T_{max} is the maximum temperature, and T_{leaf} is the leaf temperature (i.e., 10°C, 20°C, 30°C, or 40°C). The three output parameters were compared between the *B. papyrifera* growth environments (Figure 3.10 A-I).

Determining *A*, v_c, and v_o at leaf harvest

The *B. papyrifera* plants in this experiment took approximately 10 days to develop from young to fully expanded leaves. To establish the growth temperature of the leaves during their development, the temperature at solar noon (12:00pm) across the 10-day range (i.e., September 27th to September 17th) was averaged. The average growth temperatures were 19.2°C (T0AC), 19.4°C (T0EC), 23.0°C (T4AC), 23.1°C (T4EC), 26.8°C (T8AC), 26.4°C (T8EC).

With this temperature information and the temperature response models, we resolved the photosynthetic parameters (i.e., *A*, v_c, v_o, and v_o/v_c) the leaves were reasonably experiencing at the time of harvest.

Determining Safety Factors of Downstream Photorespiratory Enzymes

Safety factor was calculated using the equation below:

$$Safety\ Factor = \frac{Capacity}{Load} \quad (9)$$

Where, *Capacity* is enzyme activity and *Load* is v_o (Diamond, 2002).

Data Analysis

Gas exchange and biochemical data were analyzed and visualized using custom scripts in R (R Core Team, 2021). We used lm() in the stats package to fit linear models, gnls() in the nlme package to fit non-linear models, and emmeans() in the emmeans package for mean and parameter comparison. Gas-exchange and Biochemical data were analyzed using Two-way analysis of variance (ANOVA), accounting for growth CO_2 concentration and temperature, to measure significance. All ANOVA tests were followed with a Tukey's post hoc test.

Acknowledgement

We would like to thank Julia Hammer for providing the leaf material and gas-exchange data for the study. We additionally thank Mauricio Tejera-Nieves for help with non-linear models for the temperature response curves.

Figures

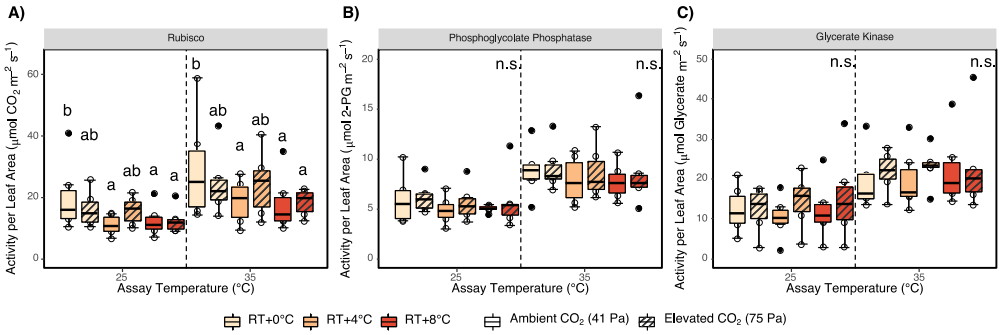

Figure 3.1. Chloroplastic Photorespiratory Enzyme Activities in *B. papyrifera* at 25°C and 35°C. Specific activities per m² leaf area were measured in *B. papyrifera* using crude protein extract for rubisco, phosphoglycolate phosphatase, and glycerate kinase. Colors represent temperature treatments, with ambient temperature in yellow, ambient temperature +4°C in orange, and ambient temperature +8°C in red. No hatching pattern denotes ambient CO_2 concentration, while hatching represents elevated CO_2. Shown are the boxplots as well as the points indicating the biological replicates (n = 6). Significant difference between treatment types is indicated by letters as determined by Two-way ANOVA with $p < 0.05$.

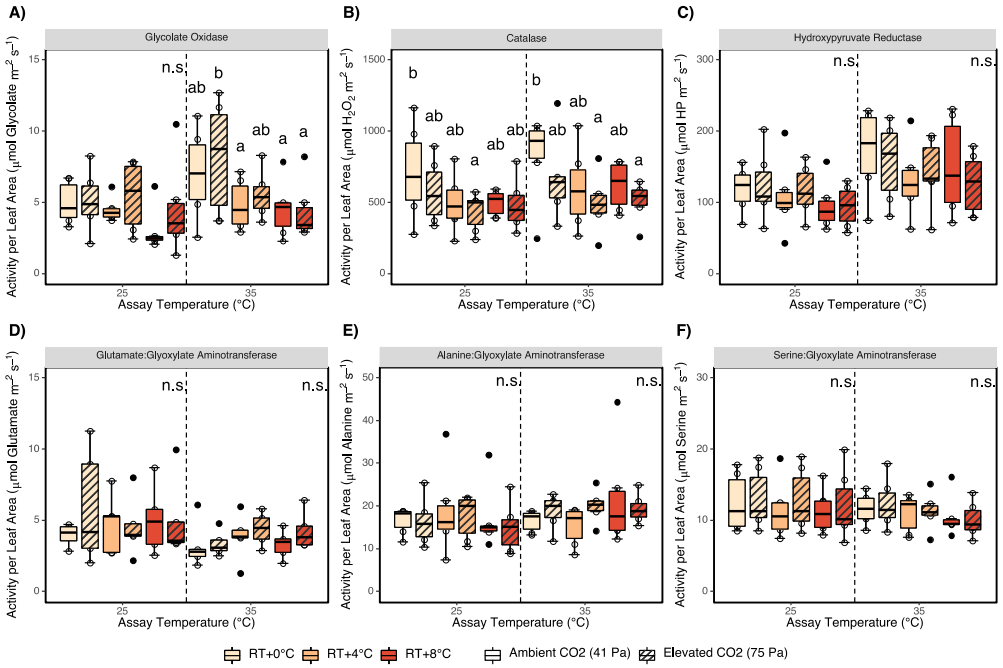

Figure 3.2. Peroxisomal Photorespiratory Enzyme Activities in *B. papyrifera* at 25°C and 35°C. Specific activities per m^2 leaf area were measured in *B. papyrifera* using crude protein extract for peroxisomal enzymes glycolate oxidase, catalase, hydroxypyruvate reductase, glutamate glyoxylate aminotransferase, alanine glyoxylate aminotransferase, and serine glyoxylate aminotransferase. Colors represent temperature treatments, with ambient temperature in yellow, ambient temperature +4°C in orange, and ambient temperature +8°C in red. No hatching pattern denotes ambient CO_2 concentration, while hatching represents elevated CO_2. Shown are the boxplots as well as the points indicating the biological replicates (n = 6). Significant difference between treatment types is indicated by letters as determined by Two-way ANOVA with $p < 0.05$.

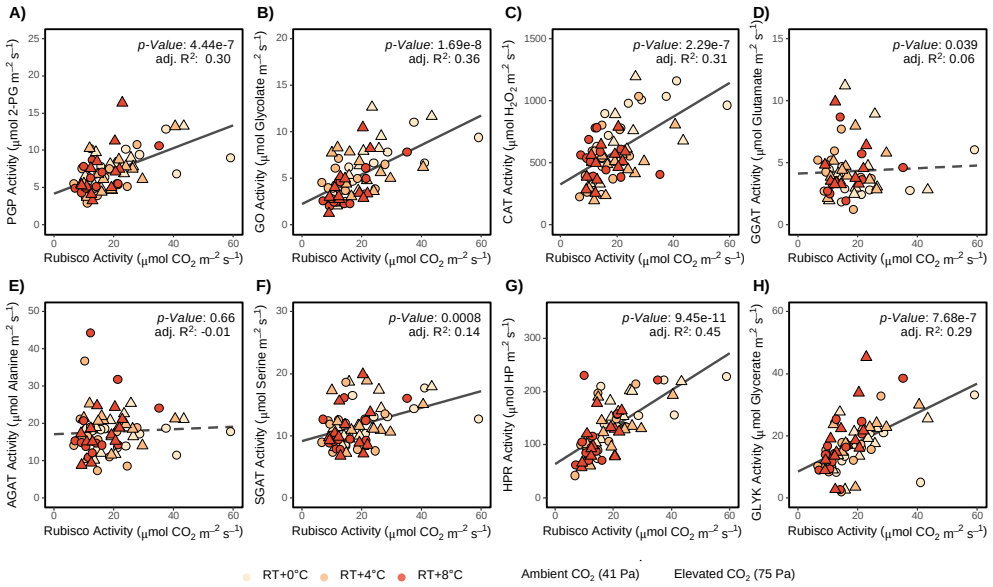

Figure 3.3. Downstream Photorespiratory Enzyme Activities Correlation to Rubisco Activity in *B. papyrifera*. A correlation of the specific activities per m^2 leaf area of the 8 downstream photorespiratory enzymes (phosphoglycolate phosphatase, glycolate oxidase, catalase, glutamate glyoxylate aminotransferase, alanine glyoxylate aminotransferase, serine glyoxylate aminotransferase, hydroxypyruvate reductase, and glycerate kinase) versus rubisco are visualized in *B. papyrifera* using crude protein extract. Colors represent temperature treatments, with ambient temperature in yellow, ambient temperature +4°C in orange, and ambient temperature +8°C in red. Shape represents CO_2 concentration, with ambient CO_2 being circles and elevated CO_2 being triangles. Linear regressions are fitted with the corresponding *p-values* ($p < 0.01$) and adjusted R^2.

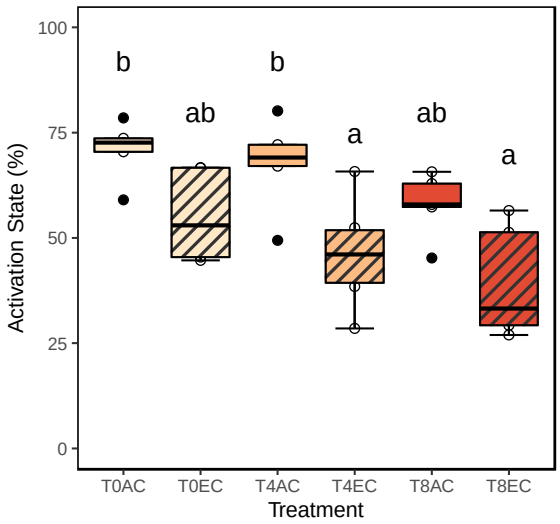

Figure 3.4. Rubisco Activation State. Initial and chemically activated Specific activities per m^2 leaf area were measured in *B. papyrifera* using crude protein extract for rubisco and divided to give activation state on a percentage basis. Colors represent temperature treatments, with ambient temperature in yellow, ambient temperature +4°C in orange, and ambient temperature +8°C in red. No hatching pattern denotes ambient CO_2 concentration, while hatching pattern represents elevated CO_2. Significant difference between treatment types is indicated by letters as determined by Two-way ANOVA with $p < 0.05$.

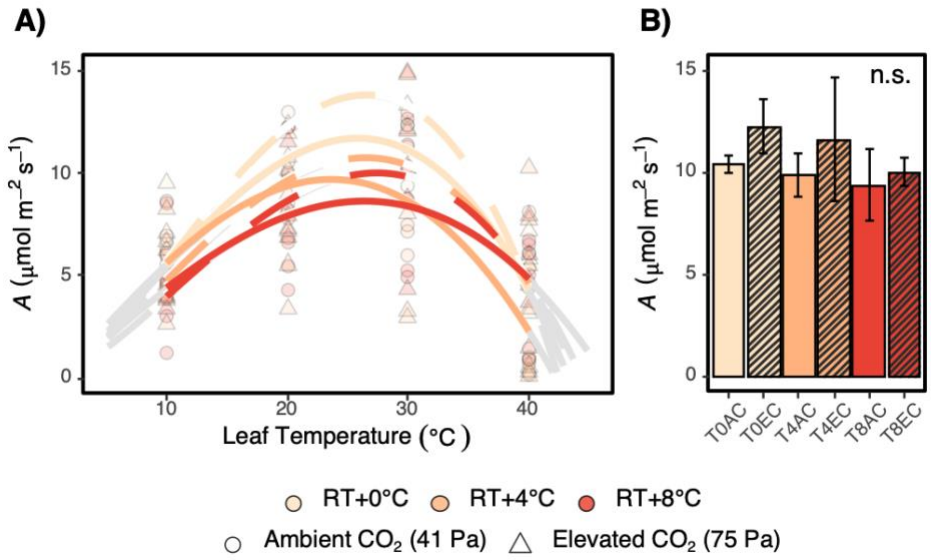

Figure 3.5. Net Carbon Fixation in *B. papyrifera*. The temperature response of net carbon assimilation (*A*; A), and the *A* rate at the time of leaf harvest (B). Colors represent temperature treatments, with ambient temperature in yellow, orange, ambient temperature +4°C in orange, and ambient temperature +8°C in red. Solid line and no hatching pattern denotes ambient CO_2 concentration, while dotted line and hatching pattern represents elevated CO_2. Shown are A) non-linear temperature response model of *A* at 10°C, 20°C, 30°C, and 40°C (interpolation and extrapolation are indicated with color and gray scales, respectively), and B) bar plot with ± SE bars representing *A* rates from 3-5 biological replicates. Significant difference between the harvest *A* rates treatment types is indicated by letters as determined by Two-way ANOVA with $p < 0.05$.

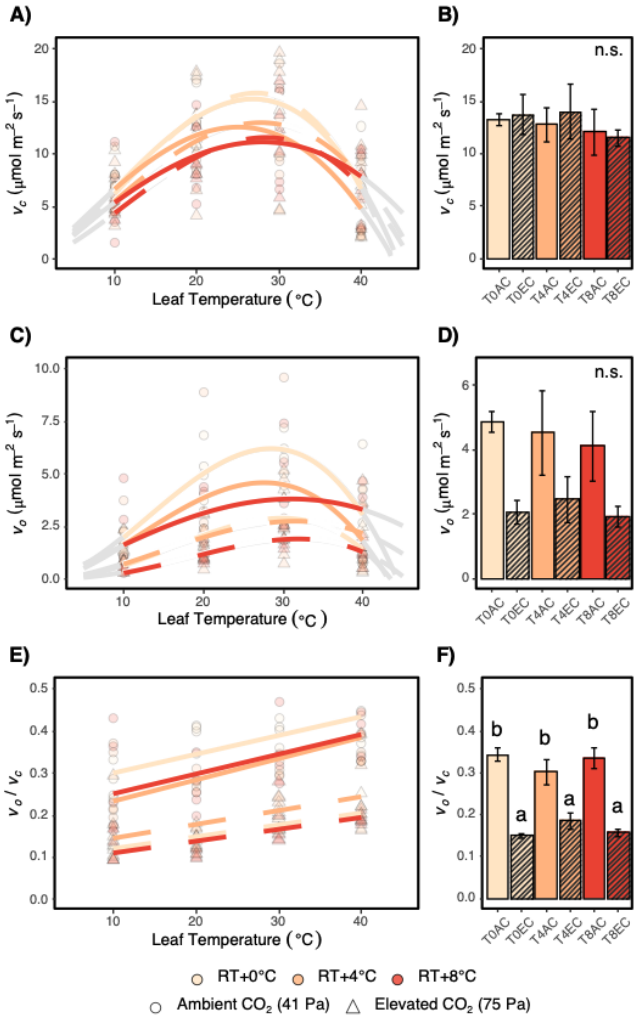

Figure 3.6. Rubisco carboxylation and oxygenation in *B. papyrifera*. The temperature response of rubisco oxygenation rate (v_o, A), rubisco carboxylation rate (v_c, C), and rubisco oxygenation per carboxylation (v_o/v_c, E). The v_c (B), v_o (D), and v_o/v_c (F) rate at the time of leaf harvest. Colors represent temperature treatments, with ambient temperature in yellow, ambient temperature +4°C in orange, and ambient temperature +8°C in red. Solid line and no hatching pattern denotes ambient CO_2 concentration, while dotted line and hatching pattern represents elevated CO_2. Shown are A) non-linear temperature response models of v_o, v_c and v_o/v_c at 10°C, 20°C, 30°C, and 40°C (interpolation and extrapolation are indicated with color and gray scales, respectively), and B) bar plot with ± SE bars representing v_o, v_c and v_o/v_c rates from 3-5 biological replicates. Significant difference between the harvest *A* rates treatment types is indicated by an asterisk as determined by Two-way ANOVA with $p < 0.05$.

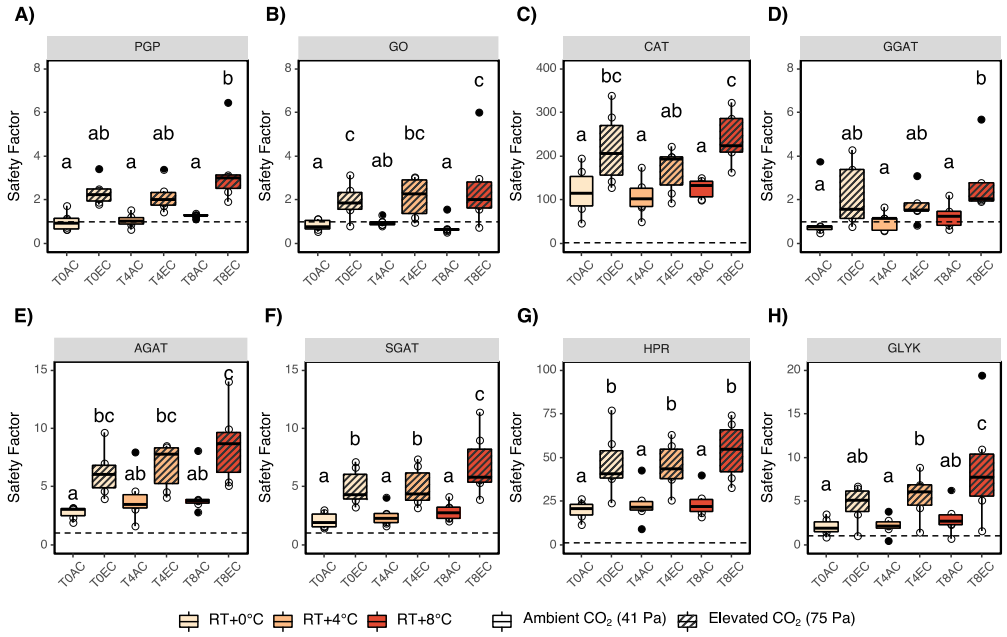

Figure 3.7. Safety Factors of Downstream Photorespiratory Enzymes at 25°C in *B. papyrifera*. Safety factors (specific activities per m² leaf area measured at 25°C divided by corresponding mean v_o at 25°C) of downstream photorespiratory enzymes (PGP, GO, CAT, GGAT, AGAT, SGAT, HPR, and GLYK) were calculated in *B. papyrifera*. Colors represent temperature treatments, with ambient temperature in yellow, ambient temperature +4°C in orange, and ambient temperature +8°C in red. No hatching pattern denotes ambient CO_2 concentration, while hatching pattern represents elevated CO_2. Shown are the boxplots as well as the points indicating the biological replicates (n = 6). Significant difference between treatment types is indicated by letters as determined by Two-way ANOVA with $p < 0.05$.

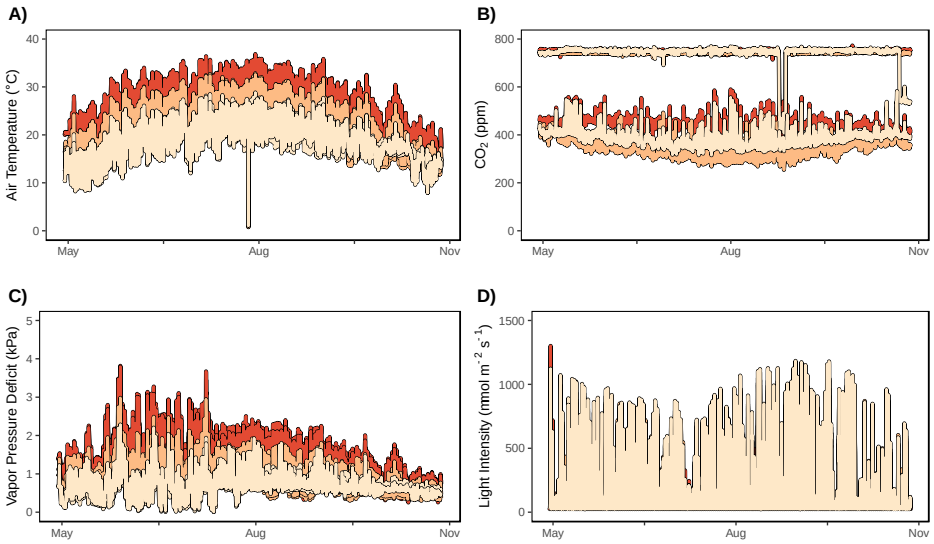

Figure 3.8. Environmental treatments the six glasshouses in the Biotron Experimental Climate Change Research Centre. Air temperature (◦C; A), CO_2 concentration (ppm; B), Vapor Pressure Deficit (kPa; C), and Light Intensity (µmol m^{-2} s^{-1}; D). Colors represent temperature treatments, with ambient temperature in yellow, ambient temperature +4◦C in orange, and ambient temperature +8◦C in red, while solid and dashed pattern represent ambient or elevated CO_2 concentration, respectively (not visible).

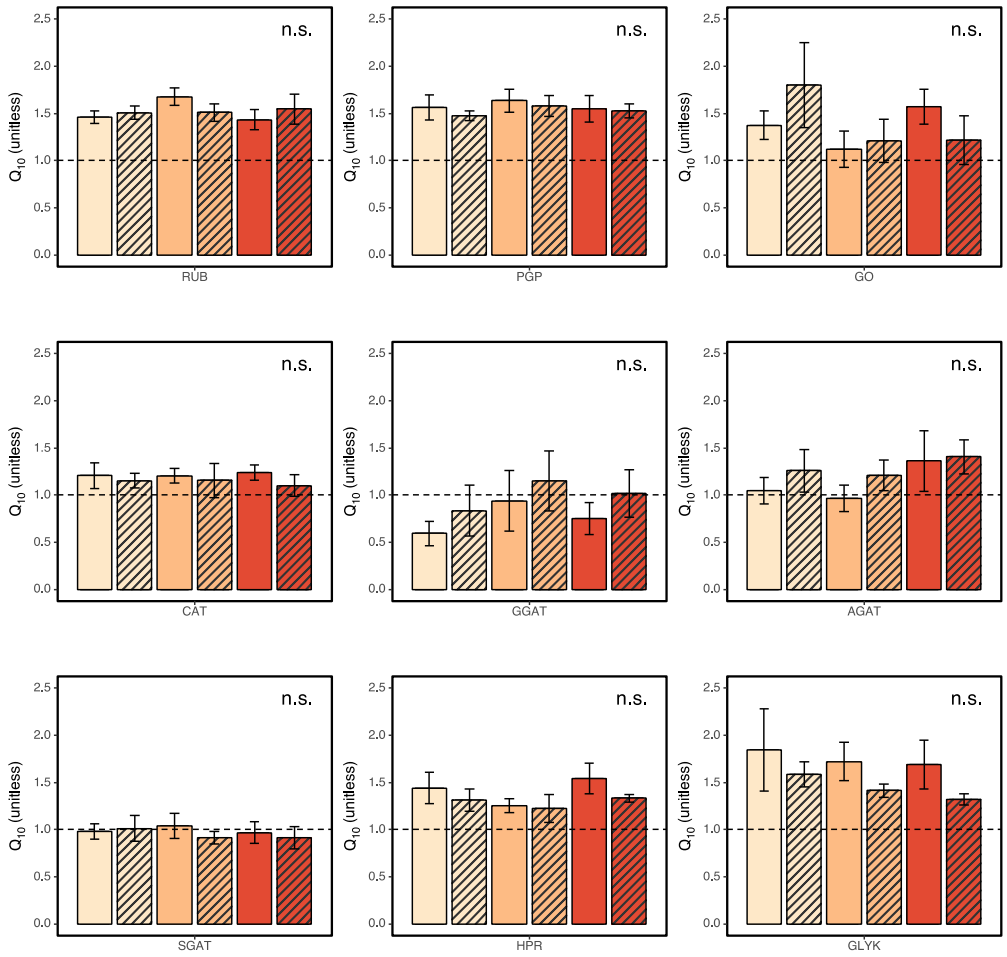

Figure 3.9. Q_{10} ratio of the photorespiratory enzyme activities in *B. papyrifera*. The Q_{10} ratio of the specific activities per m^2 leaf area were calculated by dividing the activity at 35◦C by the activity at 25◦C for each enzyme in *B. papyrifera*. Shown are the means of 6 biological replicates with ± SE bars. Colors represent temperature treatments, with ambient temperature in yellow, ambient temperature +4◦C in orange, and ambient temperature +8◦C in red. No hatching pattern denotes ambient CO_2 concentration, while hatching pattern represents elevated CO_2. Significant difference between treatment types is indicated by letters as determined by Two-way ANOVA with $p < 0.05$.

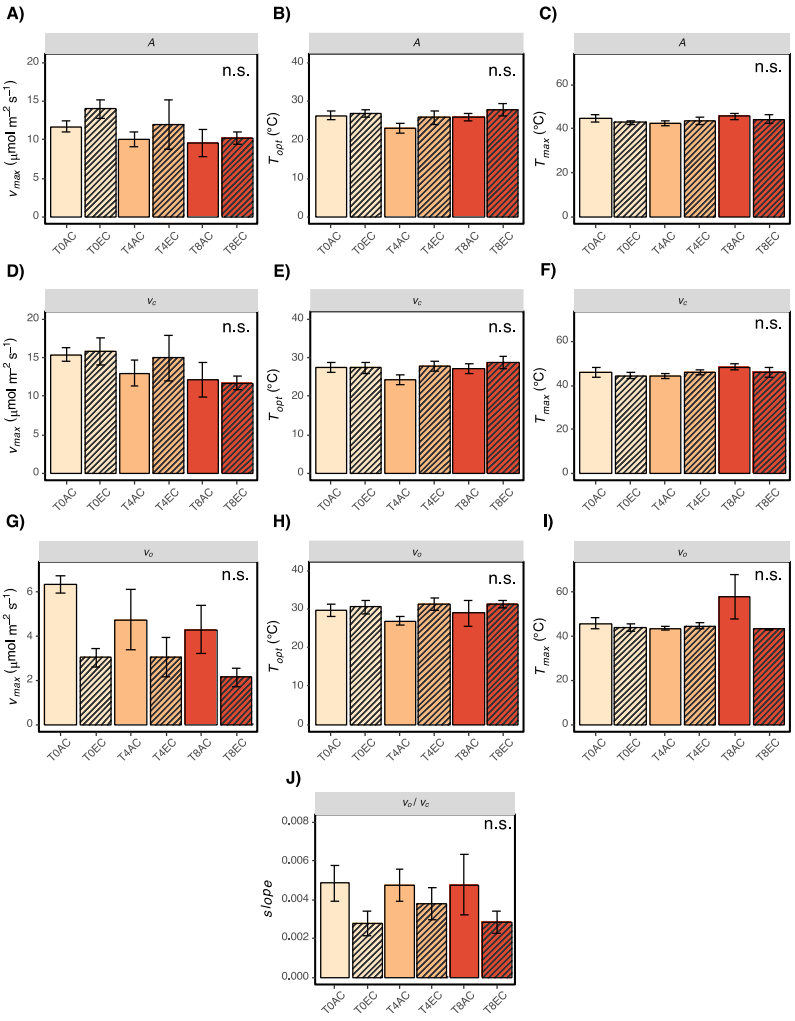

Figure 3.10. Output Parameters in the Temperature Response Non-Linear Model and Linear Regression in *B. papyrifera*. The output parameters of the non-linear temperature response model in *A*, v_c, and v_o in *B. papyrifera* (V_{max}, T_{opt}, T_{max}; A-I), and the linear regression in v_o/v_c (slope; J). Shown are the means of 3-5 biological replicates with ± SE bars. Colors represent temperature treatments, with ambient temperature in yellow, ambient temperature +4◦C in orange, and ambient temperature +8◦C in red. No hatching pattern denotes ambient CO_2 concentration, while hatching pattern represents elevated CO_2. Significant difference between treatment types is indicated by letters as determined by Two-way ANOVA with $p < 0.05$.

Tables

Table 3.1. Chloroplastic photorespiratory enzyme activities in *B. papyrifera* at 25°C and 35°C under leaf area, leaf mass, protein, chlorophyll normalization. Specific activities per m^2 leaf area, per g leaf mass, per mg protein, and per mg chlorophyll were measured in *B. papyrifera* using crude protein extracts for the enzymes rubisco (RUB), phosphoglycolate phosphatase (PGP), and glycerate kinase (GLYK). Shown are the means of 5-6 biological replicates with ± SD.

Species	Enzyme	Treatment	Temperature	Leaf Area	Leaf Mass	Protein	Chlorophyll
unitless	unitless	unitless	C	µmol m-2 s-1	µmol g-1 s-1	nmol mg-1 s-1	µmol mg-1 s-1
B. papyrifera	GLYK	T0AC	25	12.54±5.55	0.08±0.04	4.23±1.94	0.72±0.34
B. papyrifera	GLYK	T0AC	35	29.91±22.61	0.19±0.15	9.24±6.89	1.56±1.08
B. papyrifera	GLYK	T0EC	25	12.15±5.41	0.08±0.03	4.29±2.05	0.7±0.39
B. papyrifera	GLYK	T0EC	35	21.74±4.97	0.14±0.03	7.79±3.58	1.26±0.6
B. papyrifera	GLYK	T4AC	25	10.25±5.04	0.07±0.03	4.24±1.8	0.66±0.33
B. papyrifera	GLYK	T4AC	35	19.91±9.71	0.13±0.07	8.29±3.95	1.27±0.68
B. papyrifera	GLYK	T4EC	25	14.58±6.36	0.07±0.03	4.33±1.73	1.05±0.48
B. papyrifera	GLYK	T4EC	35	23.58±4.73	0.11±0.02	6.96±1.42	1.64±0.44
B. papyrifera	GLYK	T8AC	25	11.85±7.09	0.08±0.04	4.07±1.63	0.93±0.53
B. papyrifera	GLYK	T8AC	35	22.4±9.03	0.15±0.04	7.92±2.66	1.7±0.67
B. papyrifera	GLYK	T8EC	25	15.1±10.75	0.08±0.06	5.5±2.97	1±0.62
B. papyrifera	GLYK	T8EC	35	23.01±11.82	0.13±0.06	8.07±2.7	1.45±0.61
B. papyrifera	PGP	T0AC	25	5.93±2.47	0.04±0.02	1.86±0.71	0.32±0.12
B. papyrifera	PGP	T0AC	35	8.82±2.5	0.05±0.02	2.79±0.74	0.47±0.11
B. papyrifera	PGP	T0EC	25	6.17±1.57	0.04±0.01	2.26±1.12	0.34±0.13
B. papyrifera	PGP	T0EC	35	9.05±2.27	0.06±0.01	3.26±1.46	0.5±0.2
B. papyrifera	PGP	T4AC	25	4.86±1.39	0.03±0.01	2.09±0.77	0.31±0.1
B. papyrifera	PGP	T4AC	35	7.84±2.33	0.05±0.02	3.45±1.59	0.5±0.19
B. papyrifera	PGP	T4EC	25	5.58±1.78	0.03±0.01	1.66±0.39	0.39±0.12
B. papyrifera	PGP	T4EC	35	8.66±2.66	0.04±0.01	2.62±0.74	0.6±0.17
B. papyrifera	PGP	T8AC	25	4.99±0.34	0.03±0	1.88±0.6	0.38±0.12
B. papyrifera	PGP	T8AC	35	7.71±1.8	0.05±0.01	2.84±0.99	0.59±0.2
B. papyrifera	PGP	T8EC	25	5.79±2.81	0.03±0.02	2.18±0.98	0.36±0.14
B. papyrifera	PGP	T8EC	35	8.71±3.94	0.05±0.02	3.22±1.23	0.53±0.18
B. papyrifera	RUB	T0AC	25	20.94±11.58	0.13±0.08	6.02±1.6	1.06±0.34
B. papyrifera	RUB	T0AC	35	30.13±16.2	0.19±0.11	8.73±2.42	1.51±0.48
B. papyrifera	RUB	T0EC	25	16.24±6.04	0.1±0.04	5.21±1.03	0.88±0.3
B. papyrifera	RUB	T0EC	35	24.69±9.89	0.15±0.06	8.11±2.23	1.3±0.47
B. papyrifera	RUB	T4AC	25	10.96±3.33	0.07±0.02	4.56±0.94	0.69±0.2
B. papyrifera	RUB	T4AC	35	19.32±6.91	0.13±0.05	7.61±1.58	1.21±0.42
B. papyrifera	RUB	T4EC	25	15.57±4.69	0.08±0.03	4.65±1.02	1.09±0.32
B. papyrifera	RUB	T4EC	35	25.03±10.44	0.12±0.05	7.03±1.79	1.67±0.56
B. papyrifera	RUB	T8AC	25	12.17±4.56	0.08±0.02	4.43±1.23	0.93±0.39
B. papyrifera	RUB	T8AC	35	18.32±8.87	0.12±0.04	6.2±1.41	1.39±0.64
B. papyrifera	RUB	T8EC	25	12.71±4.42	0.07±0.02	4.47±1.06	0.78±0.32
B. papyrifera	RUB	T8EC	35	18.68±4.84	0.1±0.03	6.93±2.4	1.26±0.55

Table 3.2. Peroxisomal photorespiratory enzyme activities in *B. papyrifera* at 25°C and 35°C under leaf area, leaf mass, protein, chlorophyll normalization. Specific activities per m^2 leaf area, per g leaf mass, per mg protein, and per mg chlorophyll were measured in *B. papyrifera* using crude protein extracts for the enzymes glycolate oxidase (GO), catalase (CAT), glutamate glyoxylate aminotransferase (GGAT), alanine glyoxylate aminotransferase (AGAT), serine glyoxylate aminotransferase (SGAT), and hydroxypyruvate reductase (HPR). Shown are the means of 5-6 biological replicates with ± SD.

Species	Enzyme	Treatment	Temperature	Leaf Area	Leaf Mass	Protein	Chlorophyll
unitless	unitless	unitless	C	µmol m-2 s-1	µmol g-1 s-1	nmol mg-1 s-1	µmol mg-1 s-1
B. papyrifera	AGAT	T0AC	25	16.63±4	0.1±0.03	5.78±2.57	1.01±0.53
B. papyrifera	AGAT	T0AC	35	16.53±2.89	0.1±0.02	5.34±1.28	0.92±0.27
B. papyrifera	AGAT	T0EC	25	16.35±6.32	0.1±0.04	5.87±3.07	0.91±0.45
B. papyrifera	AGAT	T0EC	35	18.72±4.8	0.12±0.03	6.52±2.41	1.05±0.4
B. papyrifera	AGAT	T4AC	25	18.68±19.08	0.12±0.13	8.42±9.53	1.21±1.35
B. papyrifera	AGAT	T4AC	35	15.33±5.54	0.1±0.04	6.67±3.4	0.97±0.38
B. papyrifera	AGAT	T4EC	25	17.63±6.96	0.08±0.03	5.43±2.42	1.28±0.67
B. papyrifera	AGAT	T4EC	35	19.68±5.4	0.09±0.02	6.21±2.7	1.42±0.54
B. papyrifera	AGAT	T8AC	25	17±8	0.11±0.04	5.8±1.69	1.26±0.57
B. papyrifera	AGAT	T8AC	35	21.7±21.93	0.15±0.16	8.06±9.64	1.66±1.88
B. papyrifera	AGAT	T8EC	25	15.07±8.43	0.08±0.04	5.67±4.09	0.96±0.52
B. papyrifera	AGAT	T8EC	35	19.57±4.44	0.11±0.03	7.28±2.49	1.23±0.38
B. papyrifera	CAT	T0AC	25	708.37±322.13	4.33±2.11	209.73±60.12	35.75±9.63
B. papyrifera	CAT	T0AC	35	838.98±338.88	5.13±2.19	255.73±95.68	42.47±13.55
B. papyrifera	CAT	T0EC	25	575.48±214.89	3.59±1.31	186.95±41.43	31.68±14.21
B. papyrifera	CAT	T0EC	35	679.91±286.46	4.23±1.76	212.33±67.61	38.39±19.16
B. papyrifera	CAT	T4AC	25	492.93±193.04	3.28±1.3	196.02±43.76	30.93±12.43
B. papyrifera	CAT	T4AC	35	599.11±278.53	3.99±1.89	249.23±105.43	38.12±18.62
B. papyrifera	CAT	T4EC	25	435.64±167.41	2.1±0.89	135.66±61.48	30.58±12.88
B. papyrifera	CAT	T4EC	35	490.86±190.95	2.37±0.93	146.73±57.09	33.3±10.4
B. papyrifera	CAT	T8AC	25	498.1±107.32	3.47±0.9	189.91±70.62	37.26±10.52
B. papyrifera	CAT	T8AC	35	633.53±227.96	4.45±1.77	255.72±142.27	48.16±20.71
B. papyrifera	CAT	T8EC	25	481.93±179.49	2.63±0.99	173.21±49.98	30.29±10
B. papyrifera	CAT	T8EC	35	507.81±134.82	2.78±0.79	185.48±52.91	33.97±15.4
B. papyrifera	GGAT	T0AC	25	7.12±7.8	0.04±0.05	2.04±1.32	0.37±0.28
B. papyrifera	GGAT	T0AC	35	2.77±1.35	0.02±0.01	0.93±0.35	0.16±0.08
B. papyrifera	GGAT	T0EC	25	5.59±4.62	0.03±0.03	1.54±1	0.3±0.19
B. papyrifera	GGAT	T0EC	35	3.42±1.16	0.02±0.01	1.11±0.63	0.2±0.08
B. papyrifera	GGAT	T4AC	25	4.46±2.14	0.03±0.01	1.93±0.71	0.27±0.1
B. papyrifera	GGAT	T4AC	35	3.79±1.76	0.03±0.01	1.78±1.14	0.24±0.12
B. papyrifera	GGAT	T4EC	25	4.52±2.15	0.02±0.01	1.44±0.58	0.33±0.12
B. papyrifera	GGAT	T4EC	35	4.29±1.65	0.02±0.01	1.47±0.67	0.33±0.12
B. papyrifera	GGAT	T8AC	25	4.77±2.36	0.03±0.02	1.6±0.67	0.34±0.13
B. papyrifera	GGAT	T8AC	35	3.33±1.03	0.02±0.01	1.16±0.4	0.24±0.07
B. papyrifera	GGAT	T8EC	25	4.76±2.67	0.03±0.01	1.67±0.94	0.28±0.13
B. papyrifera	GGAT	T8EC	35	4.32±1.65	0.02±0.01	1.42±0.49	0.27±0.12
B. papyrifera	GO	T0AC	25	4.93±1.84	0.03±0.01	1.54±0.51	0.26±0.09
B. papyrifera	GO	T0AC	35	6.94±3.28	0.04±0.02	2.09±0.84	0.35±0.12
B. papyrifera	GO	T0EC	25	5.46±1.96	0.03±0.01	1.66±0.42	0.31±0.1
B. papyrifera	GO	T0EC	35	8.24±5.07	0.05±0.03	2.46±1.29	0.44±0.22
B. papyrifera	GO	T4AC	25	4.48±1.39	0.03±0.01	1.9±0.76	0.28±0.08
B. papyrifera	GO	T4AC	35	4.79±1.75	0.03±0.01	2.05±1.11	0.31±0.13
B. papyrifera	GO	T4EC	25	5.16±3.04	0.02±0.02	1.53±0.89	0.35±0.21
B. papyrifera	GO	T4EC	35	5.55±2.27	0.03±0.01	1.74±0.9	0.4±0.21
B. papyrifera	GO	T8AC	25	3.1±1.68	0.02±0.01	1.06±0.37	0.24±0.13
B. papyrifera	GO	T8AC	35	4.56±2.28	0.03±0.01	1.59±0.7	0.34±0.15
B. papyrifera	GO	T8EC	25	4.46±3.5	0.02±0.02	1.51±0.95	0.29±0.24
B. papyrifera	GO	T8EC	35	4.34±2.28	0.02±0.01	1.56±0.62	0.27±0.12
B. papyrifera	HPR	T0AC	25	118.44±32.88	0.73±0.24	36.72±6.58	6.26±1.04
B. papyrifera	HPR	T0AC	35	168.59±59.67	1.03±0.37	51.24±13.47	8.71±1.99
B. papyrifera	HPR	T0EC	25	122.35±46.84	0.76±0.29	39.72±8.95	6.83±2.85
B. papyrifera	HPR	T0EC	35	155.45±55.27	0.97±0.34	50.05±7.24	8.59±3.46
B. papyrifera	HPR	T4AC	25	107.82±54.86	0.72±0.37	43.37±18.59	6.87±3.75
B. papyrifera	HPR	T4AC	35	134.17±47.68	0.89±0.32	53.53±12.95	8.47±3.18
B. papyrifera	HPR	T4EC	25	116.06±36.17	0.56±0.18	34.85±10.13	8.16±2.86
B. papyrifera	HPR	T4EC	35	137.29±46.19	0.66±0.23	41.18±19.04	9.5±3.65
B. papyrifera	HPR	T8AC	25	95.22±33.21	0.64±0.15	33.07±6.49	7.01±2.27
B. papyrifera	HPR	T8AC	35	144.28±64.83	0.97±0.38	49.25±15.26	10.28±3.08
B. papyrifera	HPR	T8EC	25	94.46±28.96	0.52±0.16	33.97±8.03	6.13±2.51
B. papyrifera	HPR	T8EC	35	123.52±41.39	0.67±0.24	44.14±11.15	8.09±3.44
B. papyrifera	SGAT	T0AC	25	12.08±3.72	0.07±0.02	3.9±0.91	0.67±0.2
B. papyrifera	SGAT	T0AC	35	11.63±2.37	0.07±0.02	3.83±0.76	0.64±0.16
B. papyrifera	SGAT	T0EC	25	12.55±3.91	0.08±0.02	4.46±1.8	0.68±0.2
B. papyrifera	SGAT	T0EC	35	12.06±3.49	0.08±0.02	4.3±0.89	0.69±0.25
B. papyrifera	SGAT	T4AC	25	11.36±4.29	0.08±0.03	4.78±1.74	0.72±0.3
B. papyrifera	SGAT	T4AC	35	11.74±2.56	0.08±0.02	5.12±1.73	0.75±0.17
B. papyrifera	SGAT	T4EC	25	12.84±4.41	0.06±0.02	3.89±1.29	0.9±0.29
B. papyrifera	SGAT	T4EC	35	11.34±2.8	0.05±0.01	3.43±0.65	0.8±0.18
B. papyrifera	SGAT	T8AC	25	10.96±3.08	0.08±0.02	4.03±1.35	0.83±0.22
B. papyrifera	SGAT	T8AC	35	10.6±3.07	0.07±0.01	3.71±0.66	0.8±0.26
B. papyrifera	SGAT	T8EC	25	11.77±4.86	0.06±0.03	4.35±1.43	0.73±0.21
B. papyrifera	SGAT	T8EC	35	10.25±2.93	0.06±0.02	3.88±1.16	0.68±0.2

Table 3.3. Summary of the Two-Way ANOVA in *B. papyrifera* showing *F*-values and *p*-values for enzyme activities. Bold numbers represent $p < 0.05$.

	F-value		*p*-value	
Enzyme Activity	25°C	35°C	25°C	35°C
Rubisco				
CO_2	0.013	0.011	0.908	0.918
Temperature	8.217	6.606	**0.001**	**0.002**
CO_2:Temperature	4.018	2.563	**0.022**	0.082
Phosphoglycolate Phosphatase				
CO_2	0.86	0.588	0.361	0.449
Temperature	0.639	0.28	0.535	0.758
CO_2:Temperature	0.075	0.069	0.927	0.933
Glycolate Oxidase				
CO_2	2.852	0.714	0.095	0.400
Temperature	3.227	9.972	**0.044**	**< 0.001**
CO_2:Temperature	0.293	0.569	0.747	0.568
Catalase				
CO_2	1.973	5.208	0.165	**0.026**
Temperature	5.125	5.286	**0.009**	**0.007**
CO_2:Temperature	0.487	0.063	0.617	0.939
Glutamate:Glyoxylate Aminotransferase				
CO_2	0.22	4.105	0.641	**0.046**
Temperature	1.48	3.017	0.235	0.055
CO_2:Temperature	0.298	0.202	0.743	0.818
Alanine:Glyoxylate Aminotransferase				
CO_2	0.306	0.565	0.581	0.454
Temperature	0.443	1.156	0.644	0.319
CO_2:Temperature	0.063	0.954	0.939	0.389
Serine:Glyoxylate Aminotransferase				
CO_2	1.281	0.030	0.260	0.864
Temperature	0.508	1.992	0.604	0.143
CO_2:Temperature	0.136	0.194	0.873	0.824
Hydroxypyruvate Reductase				
CO_2	0.245	0.952	0.622	0.332
Temperature	3.839	2.981	**0.025**	0.055
CO_2:Temperature	0.115	0.448	0.892	0.64
Glycerate Kinase				
CO_2	3.017	0.293	0.086	0.59
Temperature	0.278	1.061	0.758	0.35
CO_2:Temperature	1.07	2.203	0.347	0.116

Table 3.4. Summary of the Two-Way ANOVA in *B. papyrifera* showing *F*-values and *p*-values for rubisco activation state with CO_2 and temperature as the main effects. Bold numbers represent $p < 0.05$.

Leaf Trait	*F*-value	*p*-value
Rubisco Activation State		
CO_2	22.052	**< 0.000**
Temperature	4.369	**0.024**
CO_2:Temperature	0.182	0.834

Table 3.5. Summary of the Two-Way ANOVA in *B. papyrifera* showing *F*-values and *p*-values for gas exchange parameters estimated at leaf harvest. Bold numbers represent p < 0.05.

Gas Exchange Parameters	*F*-value	*p*-value
Net Carbon Assimilation (*A*) at harvest		
CO_2	1.168	0.293
Temperature	0.311	0.736
CO_2:Temperature	0.059	0.943
Rubisco carboxylation (v_c) at harvest		
CO_2	0.066	0.801
Temperature	0.292	0.750
CO_2:Temperature	0.092	0.913
Rubisco oxygenation (v_o) at harvest		
CO_2	11.907	**0.003**
Temperature	0.144	0.867
CO_2:Temperature	0.096	0.909
v_c / v_o at harvest		
CO_2	82.541	**< 0.000**
Temperature	0.010	0.990
CO_2:Temperature	1.899	0.171

Table 3.6. Summary of the Two-Way ANOVA in *B. papyrifera* showing *F*-values and *p*-values for safety factors of downstream photorespiratory enzymes. Bold numbers represent p < 0.05.

Safety Factor	*F*-value	*p*-value
Phosphoglycolate Phosphatase		
CO_2	33.056	**< 0.001**
Temperature	2.794	0.077
CO_2:Temperature	1.149	0.330
Glycolate Oxidase		
CO_2	43.736	**< 0.001**
Temperature	0.469	0.627
CO_2:Temperature	1.116	0.332
Catalase		
CO_2	43.366	**< 0.001**
Temperature	5.395	**0.007**
CO_2:Temperature	2.555	0.085
Glutamate:Glyoxylate Aminotransferase		
CO_2	16.056	**< 0.001**
Temperature	1.658	0.198
CO_2:Temperature	0.677	0.511
Alanine:Glyoxylate Aminotransferase		
CO_2	32.55	**< 0.001**
Temperature	3.522	**0.033**
CO_2:Temperature	0.518	0.597
Serine:Glyoxylate Aminotransferase		
CO_2	98.006	**< 0.001**
Temperature	7.033	**0.001**
CO_2:Temperature	2.064	0.133
Hydroxypyruvate Reductase		
CO_2	106.835	**< 0.001**
Temperature	2.134	0.124
CO_2:Temperature	0.886	0.416
Glycerate Kinase		
CO_2	42.704	**< 0.001**
Temperature	6.349	**0.003**
CO_2:Temperature	2.464	0.09

LITERATURE CITED

Aebi, H. E. (1983). Catalase. In: Bergmeyer, H.U., Ed., Methods of Enzymatic Analysis. *Verlag Chemie, Weinheim*, 273-286.

Alexander, R. M. (1981). Factors of safety in the structure of animals. *Sci Prog, 67*(265), 109-130.

Anderson, J. A. (2002). Catalase activity, hydrogen peroxide content and thermotolerance of pepper leaves. *Scientia Horticulturae, 95*(4), 277-284. doi:https://doi.org/10.1016/S0304-4238(02)00076-6

Anderson, L. E. (1971). Chloroplast and cytoplasmic enzymes II. Pea leaf triose phosphate isomerases. *Biochimica et Biophysica Acta (BBA) - Enzymology, 235*(1), 237-244. doi:https://doi.org/10.1016/0005-2744(71)90051-9

Badger, M. R., & Andrews, T. J. (1974). Effects of CO2, O2 and temperature on a high-affinity form of ribulose diphosphate carboxylase-oxygenase from spinach. *Biochemical and Biophysical Research Communications, 60*(1), 204-210. doi:https://doi.org/10.1016/0006-291X(74)90192-2

Bassham, J. A., Benson, A. A., & Calvin, M. (1950). The path of carbon in photosynthesis. *J Biol Chem, 185*(2), 781-787.

Bernacchi, C. J., Portis, A. R., Nakano, H., von Caemmerer, S., & Long, S. P. (2002). Temperature Response of Mesophyll Conductance. Implications for the Determination of Rubisco Enzyme Kinetics and for Limitations to Photosynthesis in Vivo. *Plant Physiology, 130*(4), 1992-1998. doi:10.1104/pp.008250

Bernacchi, C. J., Singsaas, E. L., Pimentel, C., Portis Jr, A. R., & Long, S. P. (2001). Improved temperature response functions for models of Rubisco-limited photosynthesis. *Plant, Cell & Environment, 24*(2), 253-259. doi:https://doi.org/10.1111/j.1365-3040.2001.00668.x

Betsche, T. (1983). Aminotransfer from Alanine and Glutamate to Glycine and Serine during Photorespiration in Oat Leaves. *Plant Physiol, 71*(4), 961-965. doi:10.1104/pp.71.4.961

Bhat, J. Y., Thieulin-Pardo, G., Hartl, F. U., & Hayer-Hartl, M. (2017). Rubisco Activases: AAA+ Chaperones Adapted to Enzyme Repair. *Frontiers in Molecular Biosciences, 4*. doi:10.3389/fmolb.2017.00020

Bowes, G., & Ogren, W. L. (1972). Oxygen inhibition and other properties of soybean ribulose 1,5-diphosphate carboxylase. *J Biol Chem, 247*(7), 2171-2176.

Bowes, G., Ogren, W. L., & Hageman, R. H. (1971). Phosphoglycolate production catalyzed by ribulose diphosphate carboxylase. *Biochemical and Biophysical*

Research Communications, 45(3), 716-722. doi:https://doi.org/10.1016/0006-291X(71)90475-X

Campbell, W. J., & Ogren, W. L. (1990). Glyoxylate inhibition of ribulosebisphosphate carboxylase/oxygenase activation in intact, lysed, and reconstituted chloroplasts. *Photosynth Res, 23*(3), 257-268. doi:10.1007/bf00034856

Carmo-Silva, A. E., & Salvucci, M. E. (2013). The regulatory properties of Rubisco activase differ among species and affect photosynthetic induction during light transitions. *Plant Physiol, 161*(4), 1645-1655. doi:10.1104/pp.112.213348

Cavanagh, A. P., & Ort, D. R. (2023). Transgenic strategies to improve the thermotolerance of photosynthesis. *Photosynthesis Research, 158*(2), 109-120. doi:10.1007/s11120-023-01024-y

Cen, Y.-P., & Sage, R. F. (2005). The regulation of Rubisco activity in response to variation in temperature and atmospheric CO2 partial pressure in sweet potato. *Plant Physiology, 139*(2), 979-990. doi:10.1104/pp.105.066233

Chastain, C. J., & Ogren, W. L. (1989). Glyoxylate Inhibition of Ribulosebisphosphate Carboxylase/Oxygenase Activation State in vivo. *Plant and Cell Physiology, 30*(7), 937-944. doi:10.1093/oxfordjournals.pcp.a077837

Collier, C. J., Ow, Y. X., Langlois, L., Uthicke, S., Johansson, C. L., O'Brien, K. R., . . . Adams, M. P. (2017). Optimum Temperatures for Net Primary Productivity of Three Tropical Seagrass Species. *Frontiers in Plant Science, 8*. doi:10.3389/fpls.2017.01446

Collins, M., Knutti, R., Arblaster, J., Dufresne, J.-L., Fichefet, T., Friedlingstein, P., . . . Krinner, G. (2013). Long-term climate change: projections, commitments and irreversibility.

Cook, C. M., Mulligan, R. M., & Tolbert, N. E. (1985). Inhibition and stimulation of ribulose-1,5-bisphosphate carboxylase/oxygenase by glyoxylate. *Arch Biochem Biophys, 240*(1), 392-401. doi:10.1016/0003-9861(85)90044-x

Crafts-Brandner, S. J., & Salvucci, M. E. (2000). Rubisco activase constrains the photosynthetic potential of leaves at high temperature and CO₂. *Proceedings of the National Academy of Sciences, 97*(24), 13430-13435. doi:doi:10.1073/pnas.230451497

Dat, J. F., Lopez-Delgado, H., Foyer, C. H., & Scott, I. M. (1998). Parallel changes in H2O2 and catalase during thermotolerance induced by salicylic acid or heat acclimation in mustard seedlings. *Plant Physiol, 116*(4), 1351-1357. doi:10.1104/pp.116.4.1351

Dat, J. F., Pellinen, R., Beeckman, T., Van De Cotte, B., Langebartels, C., Kangasjärvi, J., . . . Van Breusegem, F. (2003). Changes in hydrogen peroxide homeostasis

trigger an active cell death process in tobacco. *The Plant Journal, 33*(4), 621-632. doi:https://doi.org/10.1046/j.1365-313X.2003.01655.x

Dellero, Y., Jossier, M., Schmitz, J., Maurino, V. G., & Hodges, M. (2016). Photorespiratory glycolate–glyoxylate metabolism. *Journal of Experimental Botany, 67*(10), 3041-3052. doi:10.1093/jxb/erw090

Diamond, J. (2002). Quantitative evolutionary design. *The Journal of Physiology, 542*(2), 337-345. doi:https://doi.org/10.1113/jphysiol.2002.018366

Drake, B. G., Gonzàlez-Meler, M. A., & Long, S. P. (1997). More efficient plants: a consequence of rising atmospheric CO2? *Annual Review of Plant Biology, 48*(1), 609-639.

Dusenge, M. E., Madhavji, S., & Way, D. A. (2020). Contrasting acclimation responses to elevated CO(2) and warming between an evergreen and a deciduous boreal conifer. *Glob Chang Biol, 26*(6), 3639-3657. doi:10.1111/gcb.15084

Escobar, L., Salvador, C., Contreras, M., & Edgardo Escamilla, J. (1990). On the application of the Clark oxygen electrode to the study of enzyme kinetics in apolar solvents: The catalase reaction. *Analytical Biochemistry, 184*(1), 139-144. doi:https://doi.org/10.1016/0003-2697(90)90026-6

Feierabend, J., Schaan, C., & Hertwig, B. (1992). Photoinactivation of Catalase Occurs under Both High- and Low-Temperature Stress Conditions and Accompanies Photoinhibition of Photosystem II. *Plant Physiol, 100*(3), 1554-1561. doi:10.1104/pp.100.3.1554

Flügel, F., Timm, S., Arrivault, S., Florian, A., Stitt, M., Fernie, A. R., & Bauwe, H. (2017). The Photorespiratory Metabolite 2-Phosphoglycolate Regulates Photosynthesis and Starch Accumulation in Arabidopsis. *The Plant Cell, 29*(10), 2537-2551. doi:10.1105/tpc.17.00256

Friso, G., & van Wijk, K. J. (2015). Posttranslational Protein Modifications in Plant Metabolism. *Plant Physiol, 169*(3), 1469-1487. doi:10.1104/pp.15.01378

Galmés, J., Aranjuelo, I., Medrano, H., & Flexas, J. (2013). Variation in Rubisco content and activity under variable climatic factors. *Photosynthesis Research, 117*(1), 73-90. doi:10.1007/s11120-013-9861-y

Gauthier, S., Bernier, P., Kuuluvainen, T., Shvidenko, A. Z., & Schepaschenko, D. G. (2015). Boreal forest health and global change. *Science, 349*(6250), 819-822. Retrieved from http://www.jstor.org/stable/24749186

Gregory, L. M., McClain, A. M., Kramer, D. M., Pardo, J. D., Smith, K. E., Tessmer, O. L., . . . Sharkey, T. D. (2021). The triose phosphate utilization limitation of photosynthetic rate: Out of global models but important for leaf models. *Plant Cell Environ, 44*(10), 3223-3226. doi:10.1111/pce.14153

Gregory, L. M., Roze, L. V., & Walker, B. J. (2023). Increased activity of core photorespiratory enzymes and CO2 transfer conductances are associated with higher and more optimal photosynthetic rates under elevated temperatures in the extremophile Rhazya stricta. *Plant, Cell & Environment, 46*(12), 3704-3720. doi:https://doi.org/10.1111/pce.14711

Hall, N. P., & Keys, A. J. (1983). Temperature dependence of the enzymic carboxylation and oxygenation of ribulose 1, 5-bisphosphate in relation to effects of temperature on photosynthesis. *Plant Physiology, 72*(4), 945-948.

Hammond, E. T., Andrews, T. J., & Woodrow, I. E. (1998). Regulation of ribulose-1,5-bisphosphate Carboxylase/Oxygenase by carbamylation and 2-carboxyarabinitol 1-phosphate in tobacco: insights from studies of antisense plants containing reduced amounts of rubisco activase. *Plant Physiol, 118*(4), 1463-1471. doi:10.1104/pp.118.4.1463

Heinze, M., & Gerhardt, B. (2002). Plant Catalases. In A. Baker & I. A. Graham (Eds.), *Plant Peroxisomes: Biochemistry, Cell Biology and Biotechnological Applications* (pp. 103-140). Dordrecht: Springer Netherlands.

Hermida-Carrera, C., Kapralov, M. V., & Galmés, J. (2016). Rubisco Catalytic Properties and Temperature Response in Crops. *Plant Physiology, 171*(4), 2549-2561. doi:10.1104/pp.16.01846

Hodges, M. (2022). Photorespiration and Improving Photosynthesis. *Progress in Botany, 84*, 171-220. doi:10.1007/124_2022_64

Hodges, M., Jossier, M., Boex-Fontvieille, E., & Tcherkez, G. (2013). Protein phosphorylation and photorespiration. *Plant Biology, 15*(4), 694-706. doi:https://doi.org/10.1111/j.1438-8677.2012.00719.x

Husic, D. W., Husic, H. D., Tolbert, N. E., & Black Jr, C. C. (1987). The oxidative photosynthetic carbon cycle or C2 cycle. *Critical Reviews in Plant Sciences, 5*(1), 45-100. doi:10.1080/07352688709382234

Jordan, D. B., & Ogren, W. L. (1984). The CO2/O2 specificity of ribulose 1,5-bisphosphate carboxylase/oxygenase. *Planta, 161*(4), 308-313. doi:10.1007/BF00398720

Keech, O., Gardeström, P., Kleczkowski, L. A., & Rouhier, N. (2017). The redox control of photorespiration: from biochemical and physiological aspects to biotechnological considerations. *Plant, Cell & Environment, 40*(4), 553-569. doi:https://doi.org/10.1111/pce.12713

Kendziorek, M., & Paszkowski, A. (2008). Properties of serine:glyoxylate aminotransferase purified from Arabidopsis thaliana leaves. *Acta Biochimica et Biophysica Sinica, 40*(2), 102-110. doi:10.1111/j.1745-7270.2008.00383.x

Kim, K., & Portis, A. R., Jr. (2005). Temperature Dependence of Photosynthesis in Arabidopsis Plants with Modifications in Rubisco Activase and Membrane Fluidity. *Plant and Cell Physiology, 46*(3), 522-530. doi:10.1093/pcp/pci052

Laing, W. A. (1974). Regulation of Soybean Net Photosynthetic CO(2) Fixation by the Interaction of CO(2), O(2), and Ribulose 1,5-Diphosphate Carboxylase. *Plant Physiology, 54*(5), 678-685. doi:10.1104/pp.54.5.678

Laisk, A. K. (1977). Kinetics of photosynthesis and photorespiration of C3 in plants.

Lawson, T., Davey, P. A., Yates, S. A., Bechtold, U., Baeshen, M., Baeshen, N., . . . Mullineaux, P. M. (2014). C3 photosynthesis in the desert plant Rhazya stricta is fully functional at high temperatures and light intensities. *New Phytologist, 201*(3), 862-873. doi:https://doi.org/10.1111/nph.12559

Laxa, M., & Fromm, S. (2018). Co-expression and regulation of photorespiratory genes in Arabidopsis thaliana: A bioinformatic approach. *Current Plant Biology, 14*, 2-18. doi:https://doi.org/10.1016/j.cpb.2018.09.001

Lee, H., Calvin, K., Dasgupta, D., Krinner, G., Mukherji, A., Thorne, P., . . . Barrett, K. (2023). Climate change 2023: synthesis report. Contribution of working groups I, II and III to the sixth assessment report of the intergovernmental panel on climate change. 35-115.

Leegood, R. C., Lea, P. J., Adcock, M. D., & Häusler, R. E. (1995). The regulation and control of photorespiration. *Journal of Experimental Botany, 46*(special_issue), 1397-1414. doi:10.1093/jxb/46.special_issue.1397

Liepman, A. H., & Olsen, L. J. (2003). Alanine Aminotransferase Homologs Catalyze the Glutamate:Glyoxylate Aminotransferase Reaction in Peroxisomes of Arabidopsis. *Plant Physiology, 131*(1), 215-227. doi:10.1104/pp.011460

Liu, L., Zhong, S., Yang, R., Hu, H., Yu, D., Zhu, D., . . . Gong, D. (2008). Expression, purification, and initial characterization of human alanine aminotransferase (ALT) isoenzyme 1 and 2 in High-five insect cells. *Protein Expression and Purification, 60*(2), 225-231. doi:https://doi.org/10.1016/j.pep.2008.04.006

López-Calcagno, P. E., Fisk, S., Brown, K. L., Bull, S. E., South, P. F., & Raines, C. A. (2019). Overexpressing the H-protein of the glycine cleavage system increases biomass yield in glasshouse and field-grown transgenic tobacco plants. *Plant Biotechnology Journal, 17*(1), 141-151. doi:https://doi.org/10.1111/pbi.12953

Lorimer, G. H., & Miziorko, H. M. (1980). Carbamate formation on the epsilon-amino group of a lysyl residue as the basis for the activation of ribulosebisphosphate carboxylase by CO2 and Mg2+. *Biochemistry, 19*(23), 5321-5328. doi:10.1021/bi00564a027

Matters, G. L., & Scandalios, J. G. (1986). Effect of elevated temperature on catalase and superoxide dismutase during maize development. *Differentiation, 30*(3), 190-196. doi:https://doi.org/10.1111/j.1432-0436.1986.tb00780.x

Mulligan, R. M., Wilson, B., & Tolbert, N. E. (1983). Effects of glyoxylate on photosynthesis by intact chloroplasts. *Plant Physiol, 72*(2), 415-419. doi:10.1104/pp.72.2.415

Peisker, M. (1974). model describing the influence of oxygen on photosynthetic carboxylation. *Photosynthetica*.

Porra, R. J. (2002). The chequered history of the development and use of simultaneous equations for the accurate determination of chlorophylls a and b. *Photosynthesis Research, 73*(1), 149-156. doi:10.1023/A:1020470224740

Porra, R. J., Thompson, W. A., & Kriedemann, P. E. (1989). Determination of accurate extinction coefficients and simultaneous equations for assaying chlorophylls a and b extracted with four different solvents: verification of the concentration of chlorophyll standards by atomic absorption spectroscopy. *Biochimica et Biophysica Acta (BBA) - Bioenergetics, 975*(3), 384-394. doi:https://doi.org/10.1016/S0005-2728(89)80347-0

Portis, A. R. (2003). Rubisco activase – Rubisco's catalytic chaperone. *Photosynthesis Research, 75*(1), 11-27. doi:10.1023/A:1022458108678

Price, D. T., Alfaro, R. I., Brown, K. J., Flannigan, M. D., Fleming, R. A., Hogg, E. H., . . . Venier, L. A. (2013). Anticipating the consequences of climate change for Canada's boreal forest ecosystems. *Environmental Reviews, 21*(4), 322-365. doi:10.1139/er-2013-0042

R Core Team. (2021). R: A Language and Environment for Statistical Computing. Vienna, Austria: R Foundation for Statistical Computing. Retrieved from https://www.R-project.org

Ritchie, R. J. (2006). Consistent Sets of Spectrophotometric Chlorophyll Equations for Acetone, Methanol and Ethanol Solvents. *Photosynthesis Research, 89*(1), 27-41. doi:10.1007/s11120-006-9065-9

Ritchie, R. J. (2008). Universal chlorophyll equations for estimating chlorophylls a, b, c, and d and total chlorophylls in natural assemblages of photosynthetic organisms using acetone, methanol, or ethanol solvents. *Photosynthetica, 46*(1), 115-126. doi:10.1007/s11099-008-0019-7

Ruuska, S. A., Andrews, T. J., Badger, M. R., Price, G. D., & von Caemmerer, S. (2000). The role of chloroplast electron transport and metabolites in modulating Rubisco activity in tobacco. Insights from transgenic plants with reduced amounts of cytochrome b/f complex or glyceraldehyde 3-phosphate dehydrogenase. *Plant Physiol, 122*(2), 491-504. doi:10.1104/pp.122.2.491

Sage, R. F., Sharkey, T. D., & Seemann, J. R. (1990). Regulation of Ribulose-1,5-Bisphosphate Carboxylase Activity in Response to Light Intensity and CO(2) in the C(3) Annuals Chenopodium album L. and Phaseolus vulgaris L. *Plant Physiol, 94*(4), 1735-1742. doi:10.1104/pp.94.4.1735

Sales, C. R. G., Degen, G. E., da Silva, A. B., & Carmo-Silva, E. (2018). Spectrophotometric Determination of RuBisCO Activity and Activation State in Leaf Extracts. In S. Covshoff (Ed.), *Photosynthesis: Methods and Protocols* (pp. 239-250). New York, NY: Springer New York.

Salvador, A., & Savageau, M. A. (2003). Quantitative evolutionary design of glucose 6-phosphate dehydrogenase expression in human erythrocytes. *Proceedings of the National Academy of Sciences, 100*(24), 14463-14468. doi:doi:10.1073/pnas.2335687100

Salvucci, M. E., & Crafts-Brandner, S. J. (2004a). Inhibition of photosynthesis by heat stress: the activation state of Rubisco as a limiting factor in photosynthesis. *Physiologia Plantarum, 120*(2), 179-186. doi:https://doi.org/10.1111/j.0031-9317.2004.0173.x

Salvucci, M. E., & Crafts-Brandner, S. J. (2004b). Mechanism for deactivation of Rubisco under moderate heat stress. *Physiologia Plantarum, 122*(4), 513-519. doi:https://doi.org/10.1111/j.1399-3054.2004.00419.x

Salvucci, M. E., & Crafts-Brandner, S. J. (2004c). Relationship between the Heat Tolerance of Photosynthesis and the Thermal Stability of Rubisco Activase in Plants from Contrasting Thermal Environments. *Plant Physiology, 134*(4), 1460-1470. doi:10.1104/pp.103.038323

Salvucci, M. E., DeRidder, B. P., & Portis, A. R., Jr. (2006). Effect of activase level and isoform on the thermotolerance of photosynthesis in Arabidopsis. *Journal of Experimental Botany, 57*(14), 3793-3799. doi:10.1093/jxb/erl140

Scafaro, A. P., Posch, B. C., Evans, J. R., Farquhar, G. D., & Atkin, O. K. (2023). Rubisco deactivation and chloroplast electron transport rates co-limit photosynthesis above optimal leaf temperature in terrestrial plants. *Nature Communications, 14*(1), 2820. doi:10.1038/s41467-023-38496-4

Schmiege, S. C., Sharkey, T. D., Walker, B., Hammer, J., & Way, D. A. (2023). Laisk measurements in the nonsteady state: Tests in plants exposed to warming and variable CO2 concentrations. *Plant Physiology, 193*(2), 1045-1057. doi:10.1093/plphys/kiad305

Shen, J., Zeng, Y., Zhuang, X., Sun, L., Yao, X., Pimpl, P., & Jiang, L. (2013). Organelle pH in the Arabidopsis Endomembrane System. *Molecular Plant, 6*(5), 1419-1437. doi:https://doi.org/10.1093/mp/sst079

Somerville, C. R., & Ogren, W. L. (1980). Photorespiration mutants of Arabidopsis thaliana deficient in serine-glyoxylate aminotransferase activity. *Proceedings of the National Academy of Sciences, 77*(5), 2684-2687.

Spreitzer, R. J., & Salvucci, M. E. (2002). Rubisco: structure, regulatory interactions, and possibilities for a better enzyme. *Annual Review of Plant Biology, 53*(1), 449-475.

Streb, P., & Feierabend, J. (1996). Oxidative Stress Responses Accompanying Photoinactivation of Catalase in NaCI-treated Rye Leaves. *Botanica Acta, 109*(2), 125-132. doi:https://doi.org/10.1111/j.1438-8677.1996.tb00552.x

Streb, P., Michael-Knauf, A., & Feierabend, J. (1993). Preferential photoinactivation of catalase and photoinhibition of photosystem II are common early symptoms under various osmotic and chemical stress conditions. *Physiologia Plantarum, 88*(4), 590-598. doi:https://doi.org/10.1111/j.1399-3054.1993.tb01376.x

Suarez, R. K., Staples, J. F., Lighton, J. R., & West, T. G. (1997). Relationships between enzymatic flux capacities and metabolic flux rates: nonequilibrium reactions in muscle glycolysis. *Proceedings of the National Academy of Sciences of the United States of America, 94*(13), 7065-7069. doi:10.1073/pnas.94.13.7065

Szczepanczyk, M., Paul, L., Ruzgas, T., & Björklund, S. (2023). Comparison of Oxygen Electrode Chronoamperometry and Spectrophotometry for Determination of Catalase Activity. *Oxygen, 3*(1), 77-89. Retrieved from https://www.mdpi.com/2673-9801/3/1/6

Taylor, C. R., & Weibel, E. R. (1981). Design of the mammalian respiratory system. I. Problem and strategy. *Respir Physiol, 44*(1), 1-10.

Timm, S., Florian, A., Arrivault, S., Stitt, M., Fernie, A. R., & Bauwe, H. (2012). Glycine decarboxylase controls photosynthesis and plant growth. *FEBS Letters, 586*(20), 3692-3697. doi:https://doi.org/10.1016/j.febslet.2012.08.027

Timm, S., & Hagemann, M. (2020). Photorespiration-how is it regulated and how does it regulate overall plant metabolism? *Journal of Experimental Botany, 71*(14), 3955-3965. doi:10.1093/jxb/eraa183

Timm, S., Woitschach, F., Heise, C., Hagemann, M., & Bauwe, H. (2019). Faster removal of 2-phosphoglycolate through photorespiration improves abiotic stress tolerance of arabidopsis. *Plants, 8*(12). doi:10.3390/plants8120563

Walker, B. J., Kramer, D. M., Fisher, N., & Fu, X. (2020). Flexibility in the Energy Balancing Network of Photosynthesis Enables Safe Operation under Changing Environmental Conditions. *Plants, 9*(3), 301. Retrieved from https://www.mdpi.com/2223-7747/9/3/301

Walker, B. J., Skabelund, D. C., Busch, F. A., & Ort, D. R. (2016a). An improved approach for measuring the impact of multiple CO2 conductances on the apparent photorespiratory CO2 compensation point through slope–intercept regression. *Plant, Cell & Environment, 39*(6), 1198-1203. doi:https://doi.org/10.1111/pce.12722

Walker, B. J., South, P. F., & Ort, D. R. (2016b). Physiological evidence for plasticity in glycolate/glycerate transport during photorespiration. *Photosynthesis Research, 129*(1), 93-103. doi:10.1007/s11120-016-0277-3

Wei, P. S., Hsieh, Y. C., Chiu, H. H., Yen, D. L., Lee, C., Tsai, Y. C., & Ting, T. C. (2018). Absorption coefficient of carbon dioxide across atmospheric troposphere layer. *Heliyon, 4*(10), e00785. doi:10.1016/j.heliyon.2018.e00785

Weibel, E. R., Taylor, C. R., & Hoppeler, H. (1991). The concept of symmorphosis: a testable hypothesis of structure-function relationship. *Proceedings of the National Academy of Sciences of the United States of America, 88*(22), 10357-10361. doi:10.1073/pnas.88.22.10357

Willekens, H., Inzé, D., Van Montagu, M., & van Camp, W. (1995). Catalases in plants. *Molecular Breeding, 1*(3), 207-228. doi:10.1007/BF02277422

Zelitch, I. (1989). Selection and Characterization of Tobacco Plants with Novel O2-Resistant Photosynthesis. *Plant Physiology, 90*(4), 1457-1464. doi:10.1104/pp.90.4.1457

CHAPTER 4: Transgenic lines expressing *Heliobacter pylori* catalase rescue the *cat2*-KO growth defect with lower catalase activities than wildtype *Arabidopsis thaliana*

This research is in prep:

Gregory, L.M., Scott, K.F., Twinamaani, F., Bao, H., & Walker, B.J. Transgenic lines expressing *Heliobacter pylori* catalase rescue the *cat2*-KO growth defect with lower catalase activities than wildtype *Arabidopsis thaliana*.

Abstract

Efforts to improve crop productivity have focused on improving net carbon fixation by elucidating the sources of photorespiratory CO_2 release. The stoichiometric loss of CO_2 per rubisco oxygenation is primarily accredited to the decarboxylation of glycine; however, in certain cases the accumulation of hydrogen peroxide (H_2O_2) causes additional loss of CO_2. The H_2O_2 scavenging enzyme, catalase, plays a critical role in the photorespiratory pathway by maintain the balance of H_2O_2 in the peroxisome. Here we elucidate probable sources and mechanisms of excess CO_2 release using *cat2*-KO lines. Additionally, we determine whether catalase-mediated degradation of H_2O_2 can be optimized to increase photorespiratory efficiency using transgenic expression lines of *Heliobacter pylori* catalase. These results demonstrate that the impact on plant growth due to H_2O_2 accumulation is linked to excess CO_2 release. The excess CO_2 release is attributed to non-enzymatic decarboxylation reactions and the stimulation of the glucose-6-phosphate shunt as probable mechanisms. Additionally, we determined that transgenic lines expressing *H. pylori* isoform of catalase did not reduce excess CO_2 release beyond WT at ambient temperatures. However, two out of the three transgenic lines maintained a similar photorespiratory efficiency as WT with less catalase activity and were able to rescue the *cat2*-KO growth phenotype. These results provide insight into the importance of peroxisomal catalase in maintaining photosynthetic performance and that transgenic manipulation to optimize catalase-mediated degradation of H_2O_2 may be limited in the benefit conferred to photosynthetic performance once a threshold catalase capacity is reached.

Key Words: H_2O_2, catalase, *Heliobacter pylori*, non-enzymatic decarboxylation (NED), glucose-6-phosphate (G6P) shunt, plant growth

Introduction

Plant productivity is closely linked to net carbon fixation (*A*), which can be accurately modeled based on the reaction kinetics of ribulose-1,5,-bisphosphate carboxylase/oxygenase (rubisco) for either CO_2 or O_2 (Walker *et al.*, 2016). Carboxylation of ribulose-1,5,-bisphosphate (RuBP) by rubisco (v_c) leads to a gain in *A*, while oxygenation (v_o) of RuBP initiates photorespiration resulting in a reduction in *A* (Bowes *et al.*, 1971). The decline in *A* from photorespiration is due to a decrease in rubisco efficiency, the diversion of ATP and NADPH from the Calvin-Benson cycle to the photorespiration, and the releasing of photorespiratory CO_2 (Sharkey, 1988). Since photorespiration represents the second largest metabolic fluxes in illuminated leaves of C_3 plants, it has been a critical area of study for improve photosynthetic performance. This realization has led to the development of photorespiratory knockout mutants that exhibit stunted growth due to enzyme deficiencies (Somerville, 1984; Somerville *et al.*, 1979). The exact mechanisms causing stunted growth for each of these mutants are not fully understood but are certainly related to the accumulation of biologically active intermediates. Previous studies have shown that the accumulation of 2-phosphoglycolate (2-PG) inhibits Calvin-Benson cycle enzymes triose phosphate isomerase, and another study determined that glycolate buildup reduces the activation of rubisco, both of which can limit *A* and plant growth (Anderson, 1971; Flügel *et al.*, 2017; Xu *et al.*, 2009). Additionally, photorespiratory mutants have been shown to affect photosynthetic electron transport, as hydroxypyruvate reductase-, glycolate oxidase-, and catalase- deficient lines exhibiting significant increases in nonphotochemical quenching (NPQ) compared to WT lines (Li *et al.*, 2019a). The present work focuses on elucidating the mechanism behind the decrease in plant growth due to the accumulation of hydrogen peroxide (H_2O_2) from photorespiration.

The peroxisome-localized catalase knockout (*cat2*-KO) mutant has emerged as a valuable model for investigating the role of catalase and the balance between H_2O_2 production and scavenging in photosynthetic tissue (Bao *et al.*, 2021; Kendall *et al.*, 1983; Queval *et al.*, 2007). Catalase is an H_2O_2 scavenging enzyme associated with the photorespiration pathway. This scavenging is required when glycolate, produced in the chloroplast, is converted to glyoxylate and H_2O_2 in the peroxisome by glycolate oxidase.

Glyoxylate continues through the pathway until it is converted to 3-phosphoglycerate and reenters the Calvin-Benson cycle, while H_2O_2 is detoxified by catalase into H_2O and O_2. The participation of catalase in photorespiration suggest that it protects photosynthetic tissue from oxidative stress caused by these photorespiratory reactions (Willekens *et al.*, 1997; Willekens *et al.*, 1995). Early signs of catalase participation were in the identification of chemically mutagenized seeds in *Arabidopsis thaliana*, which failed when grow in air, but had normal growth at high CO_2-enriched air (Somerville et al., 1982). In a related selection study, *Hordeum vulgare L.* mutants that failed to grow in air exhibited 90% loss in catalase activity compared to parents in F2 and F3 generations (Kendall et al., 1983). Later on, O_2-resistant *Nicotiana tabacum* plants were generated and when grown under high photorespiratory conditions (42% O_2 and 160 ppm CO_2) were found to have 40%-50% greater catalase activity than wildtype lines (Zelitch, 1989, 1992). Additionally, these high catalase lines had a corresponding increase in *A*, suggesting that H_2O_2 plays a role in photorespiratory CO_2 release. *Cat2*-KO often exhibit stunted growth, highlighting the importance of the enzyme for efficient photorespiration and H_2O_2 management. The precise mechanism causing the stunted growth in these photorespiratory mutants is not fully understood, but one plausible explanation is an excess release of CO_2.

Research efforts have focused on elucidating the sources of CO_2 release per rubisco oxygenation from the photorespiratory pathway, as it is critical to potentially increase plant productivity. The loss of CO_2 predominately occurs through the decarboxylation of glycine by the glycine decarboxylase complex (Abadie *et al.*, 2016; Somerville, 2001; Somerville *et al.*, 1980). However, there has been evidence suggesting additional CO_2 is released from non-enzymatic decarboxylation (NED) reactions that occur with H_2O_2 and photorespiratory intermediates glyoxylate and hydroxypyruvate under at least some conditions (Bao *et al.*, 2021; Cousins *et al.*, 2008; Grodzinski, 1978; Halliwell *et al.*, 1974; Keech *et al.*, 2012). The stoichiometric loss of CO_2 per oxygenation in *Arabidopsis thaliana cat2*-KO lines is greater than wildtype lines at 25°C, due to the increased frequency of NED reactions (0.64 and 0.5, respectively) (Bao *et al.*, 2021). The lower photorespiratory efficiency in *cat2*-KO, defined here as the carbon recycling efficiency of photorespiration, reduces *A* and plant growth compared to

WT lines. The lower photorespiratory efficiency in *cat2*-KO compared to WT is due to the deficiency in catalase capacity, set by the maximal reaction velocity (V_{max}) for catalase, which is unable to keep pace with the photorespiratory demand (v_o). Although NED reactions likely occur in WT lines, these reactions would occur at a lower frequency than *cat2*-KO due to the increase in catalase capacity.

Excess H_2O_2 in the peroxisome in *cat2*-KO lines may lead to the accumulation of other photorespiratory intermediates, such as 2-PG, which possibly stimulates additional release of CO_2 through the glucose-6-phosphate (G6P) shunt. The G6P shunt is cytosolic bypass of the gluconeogenic reactions in the Calvin-Benson cycle, that convert glyceraldehyde-3-phosphate (GAP) to G6P in the cytosol (Sharkey *et al.*, 2016). G6P reenters the chloroplast and in the process of being converted to ribulose 5-phosphate (Ru5P) releases CO_2. The stimulation of the G6P shunt and NED reactions could lead to the additional CO_2 release that reduces *A* in *cat2*-KO. In this paper we hypothesize that decline in photorespiratory efficiency due to NED and the stimulation of the G6P shunt causes the reduction in plant growth in *A. thaliana cat2*-KO lines.

In addition, we explore whether photorespiratory efficiency can be further improved by optimizing catalase-mediated degradation of H_2O_2 with a foreign catalase isoform. Replacing native *A. thaliana* catalase with a more efficient isoform has the potential to improve photorespiratory efficiency if the isoform can further reduce CO_2 release per oxygenation beyond WT stoichiometry of 0.5. If lower concentrations of H_2O_2 were maintained in the peroxisome, we would expect a decline in NED reactions due to substrate limitation. To investigate this question, three transgenic independent expression lines of *Heliobacter pylori* catalase in *A. thaliana cat2*-KO were generated to determine their *in vivo* and *in vitro* impact to photosynthetic and photorespiratory capacity. To understand why *H. pylori* catalase may be more effective at detoxifying H_2O_2 than native *A. thaliana* catalase, we must consider several key factors which arises from its specific environmental adaptations. Although *A. thaliana* and *H. pylori* have monofunctional, heme-containing small-subunit catalases; each has evolved through different taxonomic kingdoms (Chelikani *et al.*, 2004; Zámocký *et al.*, 2012). *H. pylori* operates at 56°C, and its catalase has a higher isoelectric point (9.0-9.3), and a lower Michalis-Menten constant (K_m; 43-127 mM) compared to *A. thaliana* (138 mM) (Hazell *et*

al., 1991; Switala *et al.*, 2002). In particular, the lower K_m of *H. pylori* catalase suggests a higher affinity for H_2O_2 compared to the native *A. thaliana* catalase. Therefore, *H. pylori* catalase could achieve ½ maximum velocity (V_{max}) at lower H_2O_2 concentrations than *A. thaliana* catalase, thus lowering the steady-state pools size of H_2O_2 in the peroxisome. These differences in *H. pylori* catalase collectively may contribute to a greater detoxification of H_2O_2 in the peroxisome compared to native *A. thaliana* catalase.

Materials and Methods

Rescue catalase deficient lines (*cat2*-KO) with *H. pylori* isoforms

To express the *H. pylori* catalase isoforms coding sequences were obtained from public repositories and published reports. The *H. pylori* coding sequence was made compatible for Golden Gate cloning by removing the internal type II restriction sites, and addition of a type 1 peroxisome targeting signal (SKL) was added at the carboxyl terminus.

H. pylori catalase isoform was transformed into *cat2*-KO lines by floral dipping to prepare for later *in vivo* and *in vitro* functional analysis. *Cat2*-KO were used as the transformation background as these lines do not have the native photorespiratory catalase capacity and any conferred benefit to the plant in the *in vivo* and *in vitro* functional analysis will be from the expression of the foreign isoform. Transformation were reformed according to (van Hoof *et al.*, 1996) with the following modifications. In brief, the binary vector was introduced into the *Agrobacterium tumefaciens* strain GV3101 (C58C1 Rifr) pMP90 by electroporation. The transformation vector for the *H. pylori* isoform was under the rubisco small subunit promoter. Plants of ecotype Columbia were grown under a photoperiod of 16h light /8 h dark at 20°C-22°C until primary bolt was 5-15cm long. A 500 mL culture of YEP medium containing the selection antibiotics was inoculated with *A. tumefaciens* and was resuspended in 1 L of infiltration medium. *Arabidopsis* plants were infiltrated with this suspension under 400 mm Hg vacuum for 5 minutes then return to growth chamber. Plants were grown for seed. *H. pylori* transformants were selected on kanamycin and basta plates. After rounds of generating homozygous lines, the genotypes were confirmed by PCR (Figure 4.6).

Confirm localization in the peroxisome

To confirm that *H. pylori* catalase was targeted to the peroxisome, we determined the localization of the catalase isoforms to peroxisomes using confocal microscopy. Co-localization of the florescent peroxisomal dye BODIPY with *H. pylori* catalase N-terminally tagged with M-Cherry in *Nicotiana benthamiana* protoplasts as imaged using confocal microscopy (Figure 4.7).

Plant material and growth conditions

A. thaliana seeds were cold stratified in for 4-6 days in deionized water in 2mL Eppendorf tubes before sowing. *A. thaliana* plants were sown in 0.7 or 1.5 L pots on Sure-Mix potting soil (Michigan Grower Products, Inc.). Plants were grown in growth chamber at a day/night temperature of 23◦C/18◦C, with light intensity ranging between 80-100 µmol photons m^{-2} s^{-1}. For Chl*a* fluorescence and growth analysis the photoperiod was set to 12/12, but for gas exchange and catalase activity assays the photoperiod was switched to 6/18 to develop larger leaves appropriate for gas exchange analysis. Plants were fertilized weekly with ½ -strength Hoagland solution.

Preparing crude protein extract and catalase enzyme assay

Crude protein extracts were prepared from the youngest, fully expanded leaves of *A. thaliana*. Two leaf punches (52.16 mm^2) were removed from *A. thaliana* using a cork borer, immediately frozen in liquid N_2, and stored at -80◦C. Leaf punches were homogenized on ice with 0.5 mL of the Extraction buffer (50 mM EPPS buffer, pH 8.0, containing 1 mM EDTA, 10 mM DTT, 0.1% Triton X-100 [v/v], 0.5% polyvinylpyrrolidone, and 20 µL 1X SigmaFAST Protease Inhibitor Cocktail, EDTA Free (Sigma, St. Louis, MO, USA)), using a 2 mL glass-to-glass homogenizer (Kontes Glass Co., Vineland, NJ, USA). The homogenate was transferred into a 2 mL plastic Eppendorf tube and clarified by centrifugation for 15 min at 15,000 g and 4◦C (Eppendorf Centrifuge 5424R, Eppendorf, Enfield, CT, USA). The supernatant, containing the clarified crude protein extract, was used for catalase activity assays.

The activity of catalase was determined in *A. thaliana* lines by the production of O_2 (Aebi, 1983; Zelitch, 1989) with the following modifications using a Clark-type electrode. The reaction mix (50 mM K-phosphate buffer, pH 8.1) and crude protein extract were incubated for 30 sec to determine the O_2 baseline. The reaction was initiated with 30 mM H_2O_2 and the increase in O_2 production (nmol/mL) was observed for 1 min with 1 sec interval using a Oxygraph+ Oxygen Monitoring System (Hansatech Instruments Ltd). The initial rate of reaction was determined during the first 10 sec and the specific activity was expressed as µmoles O_2 produced m^{-2} s^{-1} (Escobar *et al.*, 1990; Szczepanczyk *et al.*, 2023).

Quantifying CO_2 release from a post illumination CO_2 burst

Gas exchange was measured on the youngest, fully-expanded leaf using a LI-6800 (LI-COR Biosciences) with a 2cm^2 chamber with 50:50 blue:red LEDs. Plants were measured according to (Gregory *et al*; unpublished). In brief, plants were measured for a total of 30 minutes, under a light (10 minute; 1000 µmol PAR m^{-2} s^{-1}) - dark (20 minutes; 0 µmol PAR m^{-2} s^{-1}) transient at 40 Pa at 25°C. Leaves were stabilized at 40 Pa CO_2 at the measuring temperature before starting. Both steady-state assimilation (A_s) and respiration in the dark (R_D) were estimated from the last 10 points in the light and dark, respectively. A linear regression was fit using a baseline correction as the y-intercept, and a slope of 0. The baseline correction was identified during the last 200 seconds in the dark (Bao *et al.*, 2021). The total amount of CO_2 release during the PIB was estimated as the sum up the differences between the linear regression and the measured assimilation values within the burst.

Estimating rates of v_o

v_o for WT, *cat2*-KO, Hp143, Hp432, and Hp615 were estimated according to

$$v_o = \frac{v_c - A - R_L}{t} \quad (1)$$

Where v_c was determined by

$$v_c = \frac{A + R_L}{1 - \Gamma^*/C_c} \quad (2)$$

(Walker *et al.*, 2020). the partial pressure of CO_2 at the site of rubisco catalysis (C_c) was determined by

$$C_c = C_i - \frac{A}{g_m} \quad (3)$$

A and C_i were measured at saturating light (1000 µmol PAR m^{-2} s^{-1}) during the light phase of the PIB curve. g_m, Γ^*, R_L, and t were previously measured or estimated in WT (2.23 µmol m^{-2} s^{-1} Pa^{-1}, 4.482 Pa, 0.51 µmol m^{-2} s^{-1}, 0.5) and *cat2*-KO mutants (2.01 µmol m^{-2} s^{-1} Pa^{-1}, 5.827 Pa, 0.53 µmol m^{-2} s^{-1}, 0.64) (Bao *et al.*, 2021). Using the CO_2 burst size as a proxy, Hp143 assumed *cat2*-KO diffusional and biochemical parameters, while Hp432 and Hp615 used WT.

Chl*a* fluorescence screening across an oxygen transient

For Chl*a* fluorescence analysis, a Dynamic Environment Photosynthetic Imager (Cruz *et al.*, 2016) was used and coupled to a gas mixing system controlled by mass flow controllers (Alicat Scientific, Inc, USA). Nitrogen (N_2; Peak Scientific, USA), carbon dioxide (CO_2; Airgas Specialty Gases, USA), and O_2 (Airgas Specialty Gases, USA) were mixed and passed into an acrylic chamber (25in x 13in x 7in base with a 20° angle roof to minimize back-reflection of actinic and saturating light) to rapidly change the composition of the atmosphere surrounding plants during the screen.

Chl*a* fluorescence screens during an oxygen transient were measured on the entire rosette of *A. thaliana* WT, *cat2*-KO, Hp143*,* Hp432*,* and Hp615 transformed lines. The oxygen transient screen was designed catch transitions between photorespiratory conditions by capturing *NPQ*, φ_{II}, and F_v/F_m during a 3-hour measurement (Smith, 2024). In brief, *A. thaliana* rosettes were dark-adapted for the first 1 hour to capture F_o, then the actinic lights (300 µmol PAR m^{-2} s^{-1}) were turned on for the last 2 hours. Moreover, *A. thaliana* rosettes were exposed to low photorespiratory pressure, 2% O_2 with CO_2: 400 ppm and N_2: 98%, for the first 1.6 hours, then gases were switched to create a high photorespiratory pressure, 40% O_2 with CO_2: 400 ppm and N_2: 60%, for the last 1.3 hours. Images were captured every 2 minutes to determine NPQ and φ_{II} using a standard saturation pulse chlorophyll fluorescence (Baker, 2008). Raw images were processed in Visual Phenomics (Cruz *et al.*, 2016).

Measuring non steady-state *A* with Dynamics Assimilation Technique

Gas exchange was measured using the Dynamic Assimilation Technique (DAT) on the youngest, fully-expanded leaf using a LI-6800 (LI-COR Biosciences) with a 2cm^2 chamber with 50:50 blue:red LEDs. Range matching and dynamic calculations were performed according to the manufacturer's instructions (Tejera-Nieves *et al.*, 2024a; Tejera-Nieves *et al.*, 2024b). Plants were measured under saturating light (1000 µmol PAR m^{-2} s^{-1}) from 5 Pa CO_2 to 150 Pa CO_2 with a flow rate of 200 µmol s^{-1} at 25°C. Leaves were stabilized at 40 Pa CO_2 at the measuring temperature before starting the monotonic increase in CO_2.

CO_2 response curves were fitted for the maximum rate of rubisco carboxylation ($v_{c,max}$), maximum rate of electron transport (*J*), and triose phosphate utilization (*TPU*).

$v_{c,max}$, *J,* and *TPU* were estimated using R-based ACi fitting tool (Gregory *et al.*, 2021; Saathoff *et al.*, 2021) (see https://github.com/poales/msuRACiFit to access the R script with user-friendly interface).

Leaf Trait Measurements

Relative growth rate (RGR) was calculated in ImageJ from projected leaf area images taken every two days after germination (images were stopped once leaves overlapped and true area could not be obtained) (Schneider *et al.*, 2012). Leaf number was counted a week prior before bolting, subsequently plant biomass was cut above ground and weighted to get fresh mass (g). Plants were desiccated and photographed to measure projected leaf area in ImageJ (m^2). Leaves were placed in an envelope and dried at 60°C for 48 hours and weighted for leaf dry mass (g). Leaf areas and dried weights were used to calculate LMA (g m^{-2}) and SLA (m^{-2} kg). Fresh and dried masses were used to resolve water content in tissue on a percentage basis.

Data processing and statistical analysis

Growth analysis, Chl*a* fluorescence, gas exchange and biochemical data were analyzed and visualized using custom scripts in R (R Core Team, 2021). We used emmeans() in the emmeans package for mean. Growth analysis, Chl*a* fluorescence, gas exchange and biochemical data were analyzed using Two-way analysis of variance (ANOVA), accounting for genotype differences, to measure significance. All ANOVA tests were followed with a Tukey's post hoc test.

Results

Determining catalase capacity, photorespiratory influx, and their metabolic balance

To determine catalase capacity in *A. thaliana* lines, we measured catalase activities under saturating substrate concentration to determine an *in vitro* V_{max} (Figure 4.1A). Catalase activities were measured in leaves of *A. thaliana* at 25◦C using crude protein extract (Table 4.1). WT had greater total catalase activity when compared to *cat2*-KO, Hp143, Hp432, Hp615 lines at 25◦C assay temperatures. *Cat2*-KO had 6% of the total catalase activity as WT lines which aligns with 10% that been measured previously (Mhamdi *et al.*, 2010). When comparing the *H. pylori* lines to *cat2*-KO, which is what *H. pylori* catalase isoform was transformed into, the mean activities increased by 1.62 (Hp143), 1.83 (Hp432), 2.86 (Hp615) fold.

To assess rates of photorespiratory influx, we estimated the velocity of rubisco oxygenation (v_o) and the velocity of rubisco oxygenation per carboxylation (v_o/v_c) using steady-state assimilation data at saturating light (1000 µmol PAR m^{-2} s^{-1}) from PIB curves. *Cat2*-KO had significantly lower v_o and v_o/v_c when compared to Hp615 lines, but had similar rates to WT, Hp143, and Hp432 at 25◦C (Figure 4.1B & Table 4.1).

To evaluate the relationship between photorespiratory influx and downstream catalase capacities, safety factors were calculated at 25◦C to quantify the excess capacity (Figure 4.1C and Table 4.1). To calculate “safety factors”, downstream photorespiratory enzyme activities m^{-2} s^{-1} at 25◦C were divided by v_o estimated at 25◦C. This metric helps reveal the metabolic balance between influx and capacity and can resolve whether enzymes activities fall short of v_o (safety factors < 1), are quantitatively matched with v_o (safety factors = 1) or maintain excess capacity to process v_o (safety factors > 1). In the *A. thaliana* lines measured, safety factors were greater than 1 in WT, *cat2*-KO, Hp143, Hp432 and Hp615 lines, indicating that each line maintains a reserve capacity to process v_o. However, WT had a significantly larger safety factor than *cat2*-KO, Hp143, Hp432, and Hp615. Although there are slight differences in v_o between the lines, the lower safety factors are driven by the low absolute catalase activities of *cat2*-KO (27.5 µmol H_2O_2 m^{-2} s^{-1}), Hp143 (44.7 µmol H_2O_2 m^{-2} s^{-1}), Hp432 (50.4 µmol H_2O_2 m^{-2} s^{-1}), and Hp615 (78.7 µmol H_2O_2 m^{-2} s^{-1}) compared to WT (457.7 µmol H_2O_2 m^{-2} s^{-1}).

Evidence for NED rescue from Post Illumination CO_2 Burst

To determine whether the excess photorespiratory CO_2 release from NED was rescued in Hp143, Hp432, and Hp615, we measured Post Illumination CO_2 Burst (PIB; Figure 4.2). The PIB was quantified for the CO_2 burst (i.e., integrated area under the PIB) and steady-state assimilation (i.e., averaged of the last 10 points in the light) using an R-based fitting tool (Gregory *et al.,* unpublished) (Figure 4.2B & C). Our measurements of the PIB reveal the CO_2 burst was greater in *cat2*-KO when compared to WT lines, which agrees with photorespiratory CO_2 evolution found previously in (Bao *et al.*, 2021; Keech *et al.*, 2012). Hp143 had a CO_2 burst size similar to *cat2*-KO, while Hp432 and Hp615 matched WT. Steady-state *A* decreased in *cat2*-KO and Hp143 compared to WT, Hp432, and Hp615 lines. This decrease in steady-state *A* supports the increase in CO_2 evolution through NED reactions in the photorespiratory pathway in *cat2*-KO and Hp143. Additionally, g_{sw} remained statistically similar in the WT, *cat2*-KO, Hp143, Hp432, and Hp615 lines, indicating that the stomata did not limit CO_2 diffusion. However, C_i was lower in Hp615 compared to *cat2*-KO, Hp143, Hp432, and WT lines, which corresponds to the steady-state *A* being the highest (Table 4.1).

***Chla* fluorescence screening under O_2 transient reveals an NPQ phenotype.**

To evaluate the importance of H_2O_2 degradation to photosynthetic capacity under high photorespiratory pressure, we screened non-photochemical quenching (NPQ) under a 2% to 40% oxygen transient in WT, *cat2*-KO, Hp143, Hp432, and Hp615 lines (Figure 4.3). During 2% O_2, WT, cat2-KO, and the three independent *H. pylori* lines had similar NPQ. However, once the atmosphere switched to 40% O_2, the NPQ diverged in WT and *cat2*-KO after ~20 minutes. WT had a lower NPQ, while *cat2*-KO maintained a higher NPQ for the rest of the screening. With the deviation in NPQ at 40% O_2 in the WT and *cat2*-KO mutant, the H_2O_2 degradation ability of the of the three independent expression lines of *H. pylori* can be evaluated. We see that the Hp143 diverged from WT behavior first, followed by Hp432, then Hp615, which reflected their catalase activities.

To assess the influence of H_2O_2 accumulation on productive photochemistry, the quantum yield of photosystem II (φ_{II}) was also measured during the 2% - 40% O_2

transient. Consistent with the NPQ results, as the atmosphere shifted to 40% O_2 and NPQ adjusted to high (*cat2*-KO) or low (WT, Hp143, Hp432, Hp615) levels, φ_{II} inversely adjusted. In *cat2*-KO, the reduction in φ_{II}, decreased linear electron flow (LEF). In contrast, the increased φ_{II} and raised LEF in WT, Hp143, Hp432, and Hp615 lines at the given light intensity.

Evaluating CO_2 response curves and the biochemical limitations of photosynthesis

To evaluate the effect of H_2O_2 accumulation on the CO_2 response curves and the biochemical limitations of photosynthesis, non-steady state *A* were evaluated across five C_i's ranges, and $v_{c,max}$, *J*, and *TPU* were estimated at 25°C in WT, *cat2*-KO, Hp143, Hp432, and Hp615 (Table 4.2 and Figure 4.4).

$v_{c,max}$, *J*, and *TPU* were similar across the genotypes (Table 4.1). Notably, the mean comparisons of $v_{c,max}$, *J*, and *TPU* reflect the catalase activity in Hp143, Hp432, and Hp615, where the lowest activity has the lowest parameter estimates (i.e., Hp143) and the highest activity has the highest parameter estimates (i.e., Hp615).

C_i were chosen to include parts of the curve that were rubisco-limited (12-15 Pa & 32-34 Pa), J-limited (32-34 Pa, 52-55 Pa, 72-75 Pa, 92-95 Pa) and TPU-limited (92-95 Pa, although not all lines showed a TPU-limited response). Under rubisco-limited conditions WT, *cat2*-KO, Hp143, Hp432 and Hp615 all had similar rates of *A*. Under *J*-limited conditions, WT, Hp432, and Hp615 had greater rates of *A* than *cat2*-KO and Hp143. Under TPU-limited conditions, Hp432 and Hp615 had greater rates of *A* than WT, *cat2*-KO, and Hp143 (Table 4.2).

Assessing Plant Growth

To determine the impact of excess photorespiratory CO_2 release on plant development, we measured various growth rate metrics (Table 4.1). Leaves are a platform for photosynthesis, so the number of leaves can help infer capacity for photosynthetic activity. Relative growth rate (RGR) provides information on the plants' overall growth rate per unit time and indicates efficient resource acquisition and utilization. Dry leaf mass per area (LMA) is a complex variable that provides information on leaf structural properties, mainly leaf thickness and density. Our measurements reveal that WT and Hp615 had greater leaf number than *cat2*-KO, Hp143, and Hp432

(Figure 4.5B). Additionally, WT, Hp432, and Hp615 had greater RGR than *cat2*-KO and Hp143 (Figure 4.5C). Finally, WT, Hp432, and Hp615 had greater LMA than *cat2*-KO and Hp143 (Figure 4.5D). Taken together, the small growth phenotype in *cat2*-KO is saved by the *H. pylori* catalase isoform activities of Hp432 and Hp615, but not Hp143. Moreover, the trend of increased plant growth in *H. pylori* lines correspond with the increased catalase activities.

Discussion

Peroxisomal catalase plays an essential role in maintaining plant growth

This study demonstrates that peroxisomal catalase plays an essential role in plant growth by preventing excess CO_2 loss and reducing the impact of H_2O_2 on the light reactions. The photorespiratory mutant, *cat2*-KO, exhibited a severe growth phenotype linked to greater CO_2 release and higher NPQ due to insufficient degradation of H_2O_2 (Figure 4.1A, Figure 4.2C, Figure 4.3A) . The insufficient conversion rate of H_2O_2 is attributed to the catalase capacity deficit in *cat2*-KO, which has 6% of the total catalase activity compared to WT. Although the safety factor (catalase activity under saturating substrate concentrations / v_o) reveals that both lines are working in excess capacity, the enzymatic rates are different under physiologically-relevant H_2O_2 concentrations *in vivo* (Table 4.1). Enzymatic rates typically operate closer to substrate concentrations near K_m (K_m = ½ V_{max}) (Cornish-Bowden, 1976; Somero, 1978). *In vivo* H_2O_2 concentrations in an *A. thaliana* peroxisome have been estimated to be 10 mM (Foyer *et al.*, 2016). At this concentration, it is predicted that the reduction in catalase activity in *cat2*-KO would lead to insufficient conversion of H_2O_2 compared to WT and will have various independent effects linked to the reduction in plant growth.

Cat2-KO lines exhibit decreased photosynthetic performance due to a greater amount of CO_2 loss from photorespiration compared to WT. C*at2*-KO maintains a lower steady-state and non-steady-state *A* than WT lines measured in both the PIB and CO_2 response curve at 25◦C under ambient CO_2 concentrations, respectively (Figure 4.2B and Table 4.2). The decrease in *A* is not associated with CO_2 diffusion limitation through the stomata, as g_{sw} was similar across WT and *cat2*-KO lines (Table 4.1). However, this loss is reflected in the excess CO_2 release in the CO_2 burst (Figure 4.2B). This CO_2 burst, measured during a light-dark transient, is an indication of the photorespiratory release of CO_2 when *A* in the steady-state under illumination. The additional CO_2 release due to the H_2O_2 accumulation is likely from an increased frequency of NED reactions. NED reactions are a probable mechanism as excess photorespiratory carbon is released from H_2O_2 and hydroxypyruvate reaction (Bao *et al.*, 2021). It's worth noting that the CO_2 burst, while being a proxy for photorespiratory CO_2 release, integrates the CO_2 release from the G6P shunt (Li *et al.*, 2019b; Sharkey *et al.*, 2016). *Cat2*-KO likely

stimulates the G6P shunt if H_2O_2 accumulation causes 2-phosphoglycolate (2-PG) buildup. A recent report shows that accumulation of H_2O_2 promotes the sulfenylation of phosphoglycolate phosphatase and inhibits its activity (Fu *et al.*, 2024). The reduction in activity would promote the accumulation of 2-PG, which would inhibit triose phosphate isomerase, and slow Calvin-Benson cycle. This inhibition of metabolism could be overcome with the activation of the G6P shunt (Li *et al.*, 2019b). Therefore, the excess CO_2 burst in *cat2*-KO lines would fall in line with the contribution of CO_2 release from the G6P shunt as well as NED.

The accumulation of H_2O_2 influences photosynthetic carbon fixation through NED reactions and the G6P shunt, but also has an impact on light reactions. H_2O_2 is suggested to be mobile and has the ability to travel across membranes or organelles through diffusive paths or mediated by aquaporin (Dynowski *et al.*, 2008; Mubarakshina *et al.*, 2010). Additionally, there is evidence that once H_2O_2 accumulates in the chloroplast it can activate cyclic electron flow (CEF) through preexisting CEF machinery (Strand *et al.*, 2015). In our *Chla* fluorescence analysis, NPQ increases in *cat2*-KO after ~20 minutes under high photorespiratory pressure (40% O_2), and it is maintained at greater level compared to WT (Figure 4.3A). *Cat2*-KO maintains a higher NPQ because of the acidification of the lumen through CEF being activated by H_2O_2 (Li *et al.*, 2019a; Strand *et al.*, 2015). Although CEF was not measured in this study, an increase in CEF in *cat2*-KO would support the hypothesis that G6P shunt involvement, as excess ATP would need to be generated to energetically support the shunt (Li *et al.*, 2019b).

Moreover, the increase in NPQ reduces φ_{II}, which decreases linear electron flow (LEF; Figure 4.3B). The decrease in LEF in *cat2*-KO reduces the amount of ATP and NADPH that is being produced at a given light intensity, effectively reducing *A* under high photorespiratory pressure by limiting the energy needed for the C_3 cycle. Consistent with these findings, under *J*-limited conditions on the CO_2 response curve, rates of *A* were statistically lower in *cat2*-KO compared to WT (Figure 4.4 and Table 4.2). This suggest that the processes involved in RuBP-regeneration, such as linear electron transport through cytochrome b_6f, are limiting *A* in *cat2*-KO compared to WT (Busch *et al.*, 2024; Johnson *et al.*, 2021; Sharkey *et al.*, 2007). However, under

rubisco-limited conditions, *cat2*-KO had similar *A* rates as WT, indicating that the limitation in *A* occurs during RuBP regeneration (Figure 4.4 and Table 4.2).

The accumulation of H_2O_2 influence both photosynthetic carbon fixation and the light reactions which significantly decreases plant growth in *cat2*-KO compared to WT (Figure 4.5A). The mean leaf number, RGR, and LMA in *cat2*-KO decreased by 0.61, 0.82, and 0.83 compared to WT, respectively (Figure 4.5B, C, D). Taken altogether, the deficiency in catalase capacity in the *cat2*-KO causes the reduction in plant growth due to the accumulation of H_2O_2.

***H. pylori* catalase isoform confer a benefit to photosynthetic performance, with less activity**

Two out of the three independent expression lines of *H. pylori* catalase rescued the *cat2*-KO growth phenotype back to WT growth, with less catalase activity (Figure 4.1A, and Figure 4.5). The catalase activities for the three independent *H. pylori* catalase isoform expression lines (Hp143, Hp432, Hp615), were not statistically different in their activities compared to the *cat2*-KO line, despite having confirmation of the *H. pylori* catalase isoform (Figure 4.6). Interestingly, *in vivo* estimates of the CO_2 burst from Hp432 and Hp615 were similar to WT while having 9.1 and 5.81 less catalase activity on a fold change basis than WT, respectively (Figure 4.2B). In Hp143, the expression line with the least catalase activity (10.2 less than WT), has a comparable CO_2 burst size as the *cat2*-KO (Figure 4.2C). The reduction in CO_2 burst from Hp432 and Hp615 reflected an increase in their steady-state *A*, which were greater than *cat2*-KO. The gain in *A*, like WT, was due to the reduction in CO_2 loss in the CO_2 burst, rather than CO_2 diffusion limitation differences caused by g_{sw}, which were similar in all lines at steady-state under illumination (Figure 4.2 & 4.4 and Table 4.1).

In addition, Hp432 and Hp615 broadly mirror the NPQ behavior of WT line under high photorespiratory pressure, which effectively increases *A* by increases the amount of ATP and NADPH that is being produced at a given light intensity compared to *cat2*-KO for the Calvin-Benson cycle (Figure 4.3). In agreement with these findings, *A* rates under *J*-limited conditions were greater in Hp432 and Hp615 than *cat2*-KO. Interestingly, Hp432 and Hp615 rates of *A* were similar to WT at ambient conditions, which align with steady-state *A* from the PIB, but larger at moderate (72-75 Pa) and

high (92-95 Pa) CO_2 concentrations. This difference is attributed to WT lines becoming *TPU*-limited at high CO_2 concentrations, while Hp432 and Hp615 remain *J*-limited. In addition, under *rubisco*-limited conditions on the CO_2 response curve, Hp432 and Hp615 had similar *A* rates as *cat2*-KO, Hp143, and WT lines, revealing that the difference in *A* occurs during RuBP regeneration (Figure 4.4 and Table 4.1).

Hp432 and Hp615 increase photorespiratory efficiency and prevent high NPQ which rescued the severe growth phenotype in *cat2*-KO back to WT growth (Figure 4.5A). The mean leaf number, RGR, and LMA in Hp432 and Hp615 increased by 1.43, 1.21, 1.26 and 2.04, 1.22, 1.30 compared to *cat2*-KO, respectively (Figure 4.5B, C, D). Hp432 and Hp615 had statistically similar leaf number, RGR and LMA to WT. The upward trend in these growth metrics between the three independent expression lines of *H. pylori* catalase reflect their catalase activity. The differences in catalase activities in Hp143, Hp432, and Hp615 are likely driven by expression differences through gene stability, or chromosomal positional effects (Bandopadhyay *et al.*, 2010; Betts *et al.*, 2019; Matzke *et al.*, 1998; Strauss *et al.*, 2016). Taken altogether, Hp432 and Hp615 have enough catalase capacity to rescue the *cat2*-KO growth phenotype to WT growth, but Hp143 does not.

Efficient H_2O_2 degradation may not require excess capacity

This work also reveals that the catalase activity in WT plants is in excess of what is needed to prevent excess CO_2 loss from putative NED reactions and NPQ increase (Figure 4.1A). There is no additional reduction in CO_2 loss whether the safety factor for catalase is maintained at 128.6 (WT) 15.8 (Hp432), or 20.7 (Hp615). WT is maintaining an 8.13- and 6.21-fold greater safety factor than is required to prevent deleterious effects of H_2O_2 accumulation on plant growth compared to Hp432 and Hp615, respectively. One benefit of maintaining a high catalase activity in WT may be to handle other oxidative stresses. Unlike other peroxidases, like ascorbate peroxidase and glutathione/thioredoxin peroxidase, catalase does not require other substrates, other than H_2O_2, for activity and is therefore less dependent on other enzymes for increased scavenging of H_2O_2. Additionally, catalase is less costly to the cell as it does not require reducing power to operate (Mhamdi *et al.*, 2010; Willekens *et al.*, 1995). However,

testing incremental oxidative stresses, such as increasing temperatures, to assess WT catalase capacity limitations was outside the scope of this study.

Concluding Remarks

The results suggest that peroxisomal catalase plays an essential role in maintaining plant growth but does not require a large surplus capacity to prevent the deleterious effects of H_2O_2. The impact of H_2O_2 includes excess CO_2 release attributed to photorespiratory NED reactions and stimulation of the G6P shunt as the probable mechanism. Second, independent expression lines of *H. pylori* catalase were generated with various activities of catalase. Two out of the three rescued the *cat2*-KO growth phenotype back to WT growth but had less catalase activity. The benefit of maintaining catalase above what is required to sustain photosynthetic performance may be to handle other oxidase stresses but does not provide an additional benefit to photosynthetic performance under ambient conditions. These results provide insight into the importance of peroxisomal catalase in maintaining photosynthetic performance and that transgenic manipulation to optimize catalase-mediated degradation of H_2O_2 may be limited in the benefit conferred once a threshold capacity is reached.

Acknowledgements

We would like to thank Cody Keilen and Nick Deason (MSU Growth Chamber Facility) for overall greenhouse maintenance and pest management during plant cultivation.

Figures

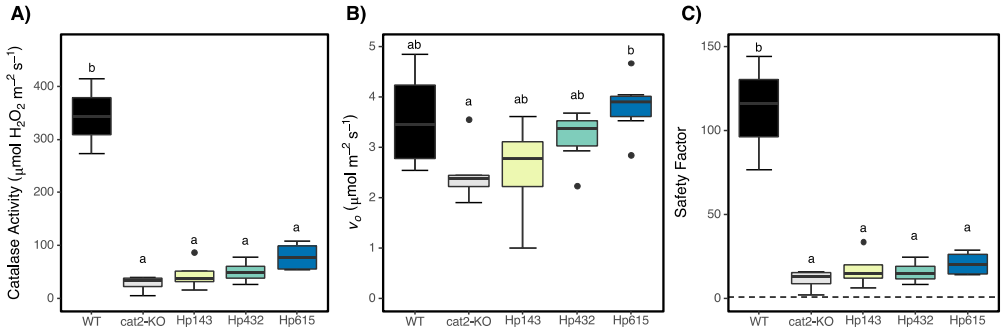

Figure 4.1. Catalase Activity, Photorespiratory Influx, and Safety Factor in *Arabidopsis thaliana*. A) Specific activities per m^2 leaf area were measured in *A. thaliana* at 25◦C using crude protein extract for catalase, B) photorespiratory influx (v_o) were estimated in *A. thaliana* at 1000 µmol PAR m^{-2} s^{-1} and 25◦C using a LI-COR LI-6800 infrared gas analyzer, and C) safety factors were calculated by dividing catalase activity by v_o for each genotype. Colors represent genotype. Shown are the boxplots indicating the biological replicates (n = 4-6). Significant difference between genotypes is indicated by letters as determined by Two-way ANOVA with $p < 0.05$.

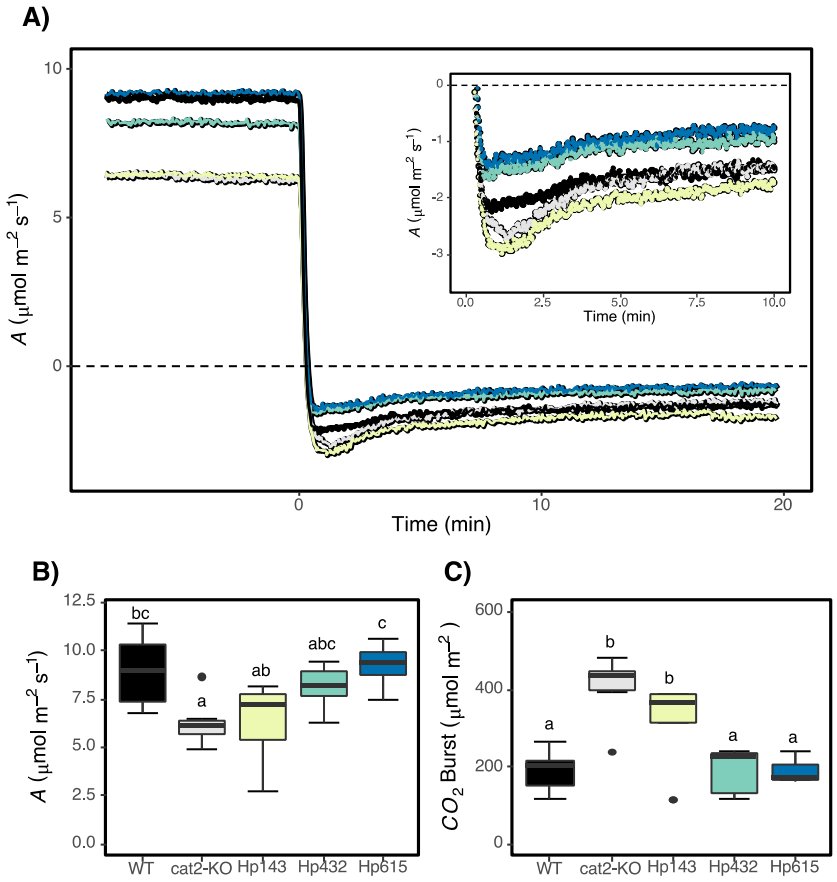

Figure 4.2. Post Illumination CO_2 Burst curves at 25°C in *Arabidopsis thaliana*. A) Net carbon fixation (*A*) was measured in *A. thaliana* during a light (1000 µmol PAR m^{-2} s^{-1}) to dark transient for 30 minutes using a LI-COR LI-6800 infrared gas analyzer, B) Steady-state *A* was averaged across the last 10 seconds in the light, and C) CO_2 burst size was quantified by integration of the peak area of CO_2 release. Colors represent genotype. Shown are the boxplots indicating the biological replicates (n = 6). Significant difference between genotypes is indicated by letters as determined by Two-way ANOVA with $p < 0.05$.

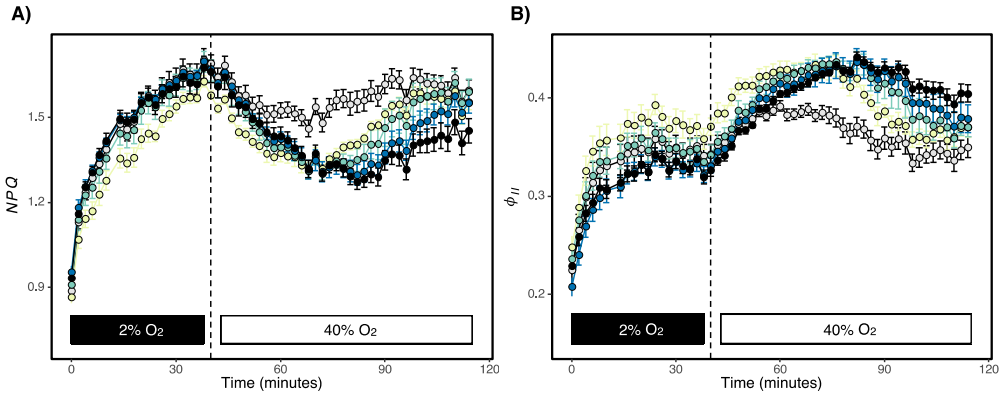

Figure 4.3. Chlorophyll fluorescence screen across an oxygen transient at 25°C in *Arabidopsis thaliana*. A) NPQ and B) ϕ_{II} were screened in *A. thaliana* for 2 hours in the light (300 µmol photons m^{-2} s^{-1}) using Dynamic Environmental Photosynthetic Imager (DEPI). Colors represent genotype. Shown are the mean of the biological replicates (n = 8) with standard error bars.

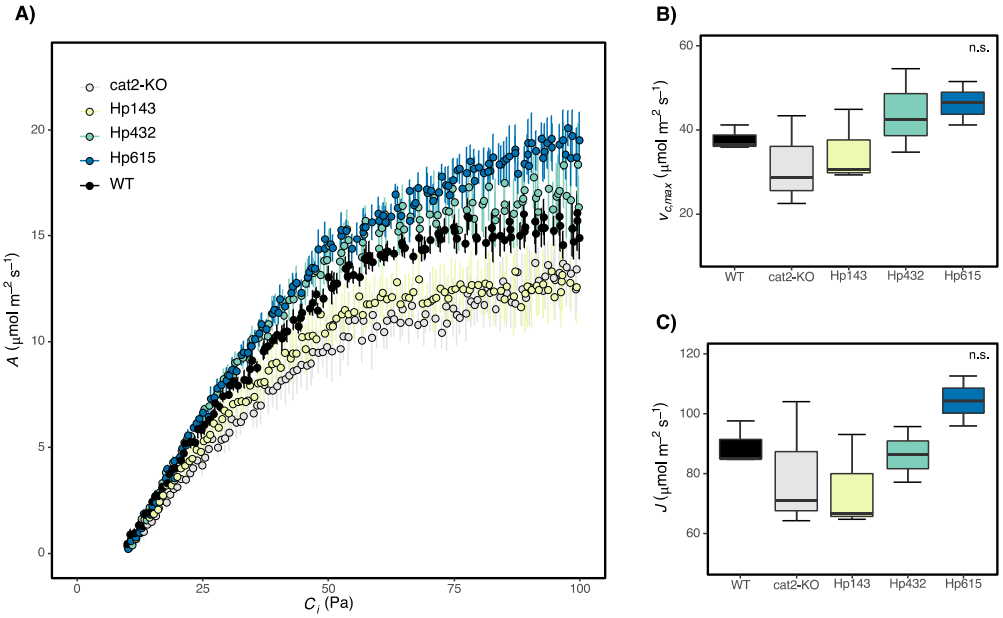

Figure 4.4. CO_2 response curves at 25°C in *Arabidopsis thaliana*. A) Net carbon fixation (*A*) was measured in *A. thaliana* during a monotonic increasing CO_2 response curve at 1000 µmol PAR m^{-2} s^{-1} using a LI-COR LI-6800 infrared gas analyzer, B) $v_{c,max}$ estimation, C) *J* estimation between genotypes. Colors represent genotype. Shown are the boxplots indicating the biological replicates (n = 3).

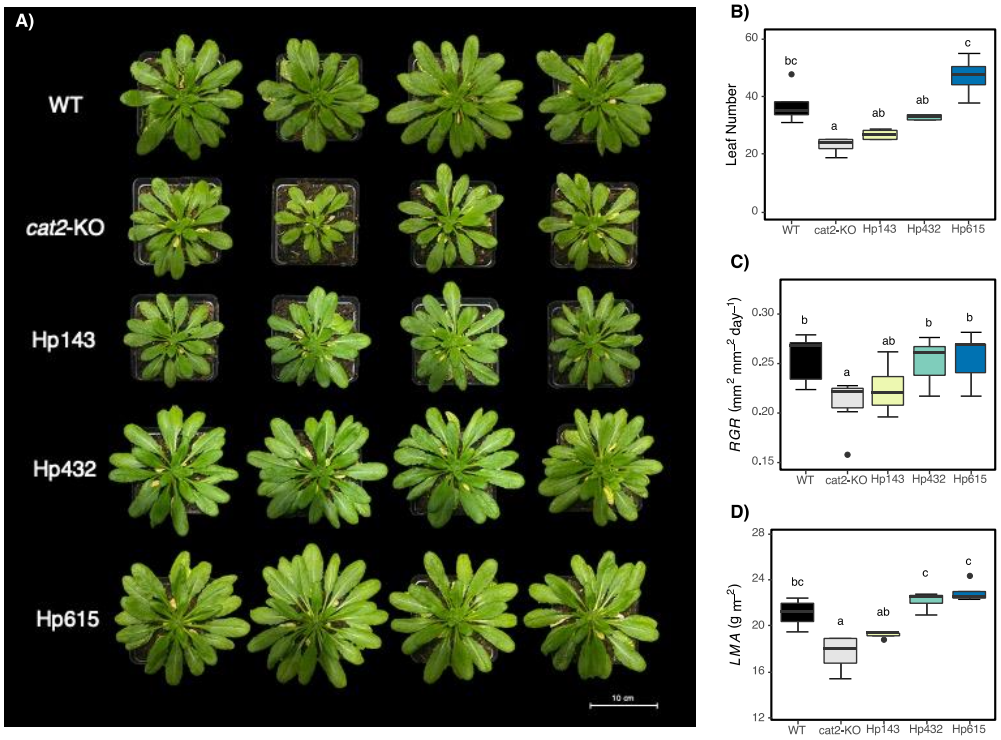

Figure 4.5. Growth Analysis of *Arabidopsis thaliana* genotypes. A) Four replicates of each genotype were grown under 23◦C/18◦C and a 12/12 photoperiod at 80-100 µmol photons m^{-2} s^{-1}, B) Leaf Number was counted a week before bolting, C) relative growth rate (RGR), and D) Leaf Dry Mass per Area was counted a week before bolting. Colors represent genotype. Shown are the boxplots indicating the biological replicates (n = 4-7). Significant difference between treatment types is indicated by letters as determined by Two-way ANOVA with $p < 0.05$.

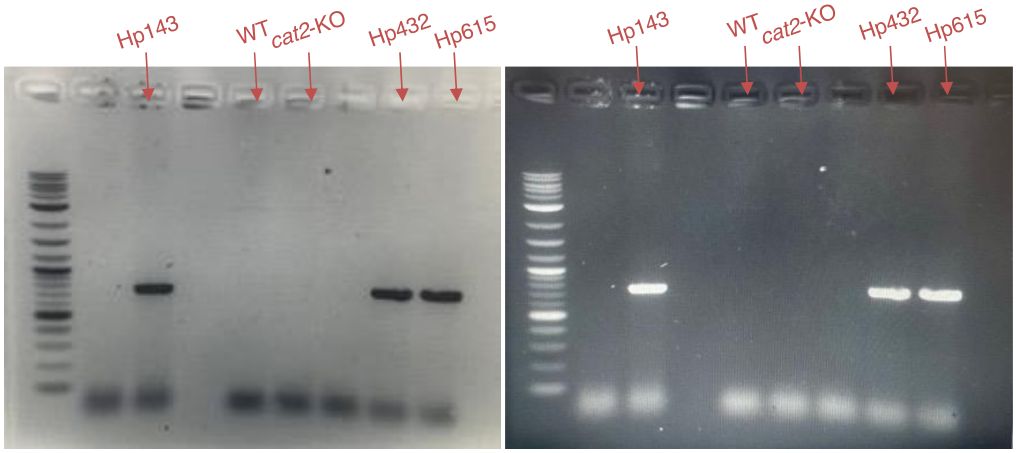

Figure 4.6. PCR genotyping in *Arabidopsis thaliana*.

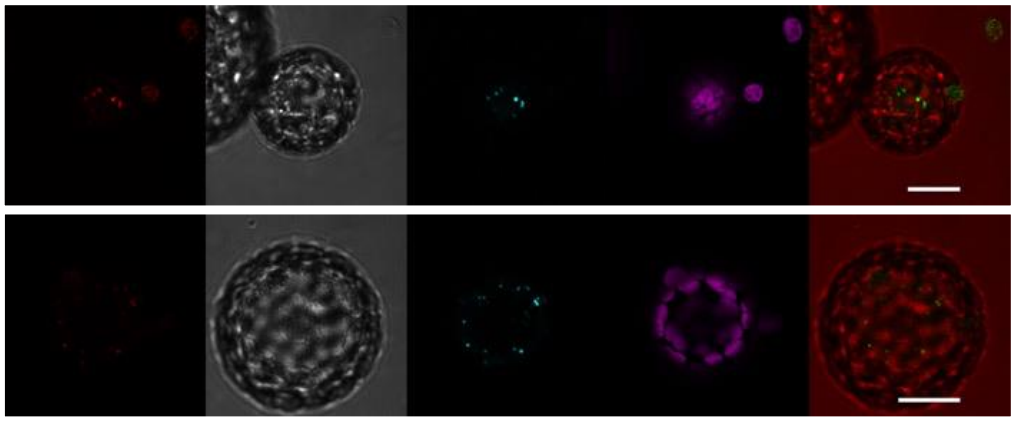

Figure 4.7. Recombinant catalase is located in the peroxisome. Co-localization of the florescent peroxisomal dye BODIPY with *H. pylori* catalase N-terminally tagged with M-Cherry in *N. benthamiana* protoplasts as imaged using confocal microscopy. Shown are M-Cherry (A), BODIPY peroxisomal dye (B), merged (C), chlorophyll fluorescence (D), and light (E) microscope image.

Tables

Table 4.1. Various plant physiological and biochemical metrics were identified in WT, *cat2*-KO, Hp143, Hp432, and Hp615 lines. Leaf traits, photosynthetic metrics, *A*/C_i analysis, PIB analysis, Catalase Activity in WT, *cat2*-KO, Hp143, Hp432, and Hp615 lines. Shown are the means of 3-7 biological replicates with ± SE.

Parameter	Unit	WT	*cat2*-KO	Hp143	Hp432	Hp615
Leaf Traits						
Leaf Number	unitless	$37.3 \pm 3.7_{bc}$	$23 \pm 1.4_{a}$	$26.8 \pm 1.0_{ab}$	$33 \pm 0.6_{ab}$	$47 \pm 3.5_{c}$
Water Content	%	$92.4 \pm 0.16_{a}$	$92.0 \pm 0.37_{a}$	$91.7 \pm 0.19_{a}$	$92.2 \pm 0.06_{a}$	$92.4 \pm 0.04_{a}$
RGR	$mm^2\ mm^{-2}\ day^{-1}$	$0.254 \pm 0.009_{b}$	$0.209 \pm 0.009_{a}$	$0.224 \pm 0.009_{ab}$	$0.252 \pm 0.008_{b}$	$0.256 \pm 0.010_{b}$
LMA	$g\ m^{-2}$	$21.1 \pm 0.65_{bc}$	$17.6 \pm 0.85_{a}$	$19.2 \pm 0.16_{ab}$	$22.2 \pm 0.41_{c}$	$22.9 \pm 0.47_{c}$
SLA	$m^2\ kg^{-1}$	$47.6 \pm 1.5_{bc}$	$57.2 \pm 2.9_{a}$	$52.0 \pm 0.4_{ab}$	$45.1 \pm 0.9_{c}$	$43.7 \pm 0.9_{c}$
Photosynthesis						
F_v / F_m	unitless	$0.751 \pm 0.002_{a}$	$0.753 \pm 0.003_{ab}$	$0.762 \pm 0.001_{abc}$	$0.764 \pm 0.002_{bc}$	$0.764 \pm 0.007_{c}$
A	$\mu mol\ m^{-2}\ s^{-1}$	$8.94 \pm 0.788_{bc}$	$6.29 \pm 510_{a}$	$6.40 \pm 0.832_{ab}$	$8.11 \pm 0.458_{abc}$	$9.26 \pm 0.451_{c}$
g_{sw}	$mol\ m^{-2}\ s^{-1}$	$0.237 \pm 0.0132_{a}$	$0.221 \pm 0.0192_{a}$	$0.180 \pm 0.0171_{a}$	$0.217 \pm 0.0188_{a}$	$0.217\pm 0.0106_{a}$
g_m (literature)	$\mu mol\ m^{-2}\ s^{-1}$ Pa	2.23	2.01	2.01	2.23	2.23
C_i	Pa	$32.6 \pm 0.350_{ab}$	$34.3 \pm 0.252_{b}$	$34.3 \pm 0.973_{b}$	$32.5 \pm 0.603a_{b}$	$31.8 \pm 0.379_{a}$
R_L (literature)	$\mu mol\ m^{-2}\ s^{-1}$	0.51	0.53	0.53	0.51	0.51
R_D	$\mu mol\ m^{-2}\ s^{-1}$	$1.36 \pm 0.373_{a}$	$1.20 \pm 0.324_{a}$	$1.59 \pm 0.684_{a}$	$0.867 \pm 0.364_{a}$	$0.626 \pm 0.355_{a}$
Γ^* (literature)	Pa	4.482	5.827	5.827	4.482	4.482
v_o	$\mu mol\ m^{-2}\ s^{-1}$	$3.56 \pm 0.394_{ab}$	$2.47 \pm 0.231_{a}$	$2.57 \pm 0.376_{ab}$	$3.19 \pm 0.218_{ab}$	$3.81 \pm 0.246_{b}$
v_o / v_c	unitless	$0.314 \pm 0.007_{ab}$	$0.293 \pm 0.004_{a}$	$0.295 \pm 0.011_{ab}$	$0.311 \pm 0.007_{ab}$	$0.325 \pm 0.006_{b}$
***A*/C_i analysis**						
$v_{c,max}$	$\mu mol\ m^{-2}\ s^{-1}$	$37.8 \pm 1.70_{a}$	$31.4 \pm 6.19_{a}$	$34.8 \pm 5.04_{a}$	$44.0 \pm 5.79_{a}$	$46.3 \pm 3.02_{a}$
J	$\mu mol\ m^{-2}\ s^{-1}$	$89.2 \pm 4.25_{a}$	$79.8 \pm 12.3_{a}$	$74.9 \pm 9.1_{a}$	$99.6 \pm 14.2_{a}$	$110.0 \pm 7.6_{a}$
TPU	$\mu mol\ m^{-2}\ s^{-1}$	$4.91 \pm 0.434_{a}$	$4.54 \pm 0.652_{a}$	$4.86 \pm 0.653_{a}$	$5.81 \pm 0.674_{a}$	$6.34 \pm 0.356_{a}$
PIB analysis						
CO_2 Burst	$\mu mol\ m^{-2}$	$191 \pm 22_{a}$	$404 \pm 35.4_{b}$	$322 \pm 43.2_{b}$	$196 \pm 23.2_{a}$	$186 \pm 12.5_{a}$
Enzyme Activity						
Catalase 25°C	$\mu mol\ H_2O_2\ m^{-2}\ s^{-1}$	$457.7 \pm 75.9_{b}$	$27.5 \pm 7.81_{a}$	$44.7 \pm 14.9_{a}$	$50.4 \pm 11.0_{a}$	$78.7 \pm 14.0_{a}$

Table 4.2. Net carbon fixation at various intercellular CO_2 concentrations on the Dynamic Assimilation Technique (DAT) curve. Rates of net carbon fixation (*A*) were identified at 5 different intercellular CO_2 concentrations in WT, *cat2*-KO, Hp143, Hp432, and Hp615 lines. Shown are the means of 3 biological replicates with ± SE.

Parameter	Limitation	WT	*cat2*-KO	Hp143	Hp432	Hp615
Assimilation (µmol m^{-2} s^{-1})						
12 – 15 (Pa)	rubisco	$1.74 \pm 0.226_{a}$	$1.05 \pm 0.413_{a}$	$1.41 \pm 0.647_{a}$	$1.54 \pm 0.363_{a}$	$1.61 \pm 0.261_{a}$
32 – 34 (Pa)	rubisco / J	$8.35 \pm 0.114_{bc}$	$6.58 \pm 0.222_{a}$	$7.10 \pm 0.167_{ab}$	$9.23 \pm 0.164_{c}$	$9.40 \pm 0.183_{c}$
52 – 55 (Pa)	J	$13.2 \pm 0.202_{b}$	$10.3 \pm 0.585_{a}$	$11.3 \pm 0.491_{a}$	$14.7 \pm 0.564_{b}$	$14.9 \pm 0.305_{b}$
72 – 75 (Pa)	J	$15.0 \pm 0.226_{b}$	$11.3 \pm 0.595_{a}$	$12.2 \pm 0.550_{a}$	$16.9 \pm 0.636_{bc}$	$17.5 \pm 0.304_{c}$
92 – 95 (Pa)	J / TPU	$15.4 \pm 0.427_{b}$	$12.7 \pm 0.534_{a}$	$13.0 \pm 0.618_{a}$	$18.4 \pm 0.406_{c}$	$19.4 \pm 0.427_{c}$

LITERATURE CITED

Abadie, C., Boex-Fontvieille, E. R., Carroll, A. J., & Tcherkez, G. (2016). In vivo stoichiometry of photorespiratory metabolism. *Nature Plants, 2*(2), 1-4.

Aebi, H. E. (1983). Catalase. In: Bergmeyer, H.U., Ed., Methods of Enzymatic Analysis. *Verlag Chemie, Weinheim*, 273-286.

Anderson, L. E. (1971). Chloroplast and cytoplasmic enzymes II. Pea leaf triose phosphate isomerases. *Biochimica et Biophysica Acta (BBA) - Enzymology, 235*(1), 237-244. doi:https://doi.org/10.1016/0005-2744(71)90051-9

Baker, N. R. (2008). Chlorophyll Fluorescence: A Probe of Photosynthesis In Vivo. *Annual Review of Plant Biology, 59*(1), 89-113. doi:10.1146/annurev.arplant.59.032607.092759

Bandopadhyay, R., Haque, I., Singh, D., & Mukhopadhyay, K. (2010). Levels and Stability of Expression of Transgenes. In C. Kole, C. H. Michler, A. G. Abbott, & T. C. Hall (Eds.), *Transgenic Crop Plants: Principles and Development* (pp. 145-186). Berlin, Heidelberg: Springer Berlin Heidelberg.

Bao, H., Morency, M., Rianti, W., Saeheng, S., Roje, S., Weber, A. P. M., & Walker, B. J. (2021). Catalase protects against nonenzymatic decarboxylations during photorespiration in Arabidopsis thaliana. *Plant Direct, 5*(12), e366. doi:https://doi.org/10.1002/pld3.366

Betts, S. D., Basu, S., Bolar, J., Booth, R., Chang, S., Cigan, A. M., . . . Chilcoat, N. D. (2019). Uniform Expression and Relatively Small Position Effects Characterize Sister Transformants in Maize and Soybean. *Frontiers in Plant Science, 10*. doi:10.3389/fpls.2019.01209

Bowes, G., Ogren, W. L., & Hageman, R. H. (1971). Phosphoglycolate production catalyzed by ribulose diphosphate carboxylase. *Biochemical and Biophysical Research Communications, 45*(3), 716-722. doi:https://doi.org/10.1016/0006-291X(71)90475-X

Busch, F. A., Ainsworth, E. A., Amtmann, A., Cavanagh, A. P., Driever, S. M., Ferguson, J. N., . . . Papanatsiou, M. (2024). A guide to photosynthetic gas exchange measurements: Fundamental principles, best practice and potential pitfalls. *Plant, Cell & Environment, n/a*(n/a). doi:https://doi.org/10.1111/pce.14815

Chelikani, P., Fita, I., & Loewen, P. C. (2004). Diversity of structures and properties among catalases. *Cellular and Molecular Life Sciences CMLS, 61*(2), 192-208. doi:10.1007/s00018-003-3206-5

Cornish-Bowden, A. (1976). The effect of natural selection on enzymic catalysis. *Journal of Molecular Biology, 101*(1), 1-9. doi:https://doi.org/10.1016/0022-2836(76)90062-0

Cousins, A. B., Pracharoenwattana, I., Zhou, W., Smith, S. M., & Badger, M. R. (2008). Peroxisomal malate dehydrogenase is not essential for photorespiration in Arabidopsis but its absence causes an increase in the stoichiometry of photorespiratory CO2 release. *Plant Physiology, 148*(2), 786-795. doi:10.1104/pp.108.122622

Cruz, J. A., Savage, L. J., Zegarac, R., Hall, C. C., Satoh-Cruz, M., Davis, G. A., . . . Kramer, D. M. (2016). Dynamic Environmental Photosynthetic Imaging Reveals Emergent Phenotypes. *Cell Syst, 2*(6), 365-377. doi:10.1016/j.cels.2016.06.001

Dynowski, M., Schaaf, G., Loque, D., Moran, O., & Ludewig, U. (2008). Plant plasma membrane water channels conduct the signalling molecule H2O2. *The Biochemical journal, 414*(1), 53-61. doi:10.1042/bj20080287

Escobar, L., Salvador, C., Contreras, M., & Edgardo Escamilla, J. (1990). On the application of the Clark oxygen electrode to the study of enzyme kinetics in apolar solvents: The catalase reaction. *Analytical Biochemistry, 184*(1), 139-144. doi:https://doi.org/10.1016/0003-2697(90)90026-6

Flügel, F., Timm, S., Arrivault, S., Florian, A., Stitt, M., Fernie, A. R., & Bauwe, H. (2017). The Photorespiratory Metabolite 2-Phosphoglycolate Regulates Photosynthesis and Starch Accumulation in Arabidopsis. *The Plant Cell, 29*(10), 2537-2551. doi:10.1105/tpc.17.00256

Foyer, C. H., & Noctor, G. (2016). Stress-triggered redox signalling: what's in pROSpect? *Plant, Cell & Environment, 39*(5), 951-964. doi:https://doi.org/10.1111/pce.12621

Fu, Z.-W., Ding, F., Zhang, B.-L., Liu, W.-C., Huang, Z.-H., Fan, S.-H., . . . Hua, W. (2024). Hydrogen peroxide sulfenylates and inhibits the photorespiratory enzyme PGLP1 to modulate plant thermotolerance. *Plant Communications*. doi:10.1016/j.xplc.2024.100852

Gregory, L. M., McClain, A. M., Kramer, D. M., Pardo, J. D., Smith, K. E., Tessmer, O. L., . . . Sharkey, T. D. (2021). The triose phosphate utilization limitation of photosynthetic rate: Out of global models but important for leaf models. *Plant Cell Environ, 44*(10), 3223-3226. doi:10.1111/pce.14153

Grodzinski, B. (1978). Glyoxylate decarboxylation during photorespiration. *Planta, 144*(1), 31-37. doi:10.1007/BF00385004

Halliwell, B., & Butt, V. S. (1974). Oxidative decarboxylation of glycollate and glyoxylate by leaf peroxisomes. *The Biochemical journal, 138*(2), 217-224. doi:10.1042/bj1380217

Hazell, S. L., Evans, D. J., Jr., & Graham, D. Y. (1991). Helicobacter pylori catalase. *J Gen Microbiol, 137*(1), 57-61. doi:10.1099/00221287-137-1-57

Johnson, J. E., & Berry, J. A. (2021). The role of Cytochrome b6f in the control of steady-state photosynthesis: a conceptual and quantitative model. *Photosynthesis Research, 148*(3), 101-136. doi:10.1007/s11120-021-00840-4

Keech, O., Zhou, W., Fenske, R., Colas-des-Francs-Small, C., Bussell, J. D., Badger, M. R., & Smith, S. M. (2012). The Genetic Dissection of a Short-Term Response to Low CO₂ Supports the Possibility for Peroxide-Mediated Decarboxylation of Photorespiratory Intermediates in the Peroxisome. *Molecular Plant, 5*(6), 1413-1416. doi:10.1093/mp/sss104

Kendall, A. C., Keys, A. J., Turner, J. C., Lea, P. J., & Miflin, B. J. (1983). The isolation and characterisation of a catalase-deficient mutant of barley (Hordeum vulgare L.). *Planta, 159*(6), 505-511. doi:10.1007/bf00409139

Li, J., Tietz, S., Cruz, J. A., Strand, D. D., Xu, Y., Chen, J., . . . Hu, J. (2019a). Photometric screens identified Arabidopsis peroxisome proteins that impact photosynthesis under dynamic light conditions. *Plant J, 97*(3), 460-474. doi:10.1111/tpj.14134

Li, J., Weraduwage, S. M., Preiser, A. L., Tietz, S., Weise, S. E., Strand, D. D., . . . Sharkey, T. D. (2019b). A Cytosolic Bypass and G6P Shunt in Plants Lacking Peroxisomal Hydroxypyruvate Reductase. *Plant Physiol, 180*(2), 783-792. doi:10.1104/pp.19.00256

Matzke, A. J. M., & Matzke, M. A. (1998). Position effects and epigenetic silencing of plant transgenes. *Current Opinion in Plant Biology, 1*(2), 142-148. doi:https://doi.org/10.1016/S1369-5266(98)80016-2

Mhamdi, A., Queval, G., Chaouch, S., Vanderauwera, S., Van Breusegem, F., & Noctor, G. (2010). Catalase function in plants: a focus on Arabidopsis mutants as stress-mimic models. *Journal of Experimental Botany, 61*(15), 4197-4220. doi:10.1093/jxb/erq282

Mubarakshina, M. M., Ivanov, B. N., Naydov, I. A., Hillier, W., Badger, M. R., & Krieger-Liszkay, A. (2010). Production and diffusion of chloroplastic H2O2 and its implication to signalling. *Journal of Experimental Botany, 61*(13), 3577-3587.

Queval, G., Issakidis-Bourguet, E., Hoeberichts, F. A., Vandorpe, M., Gakière, B., Vanacker, H., . . . Noctor, G. (2007). Conditional oxidative stress responses in the Arabidopsis photorespiratory mutant cat2 demonstrate that redox state is a key modulator of daylength-dependent gene expression, and define photoperiod as a crucial factor in the regulation of H2O2-induced cell death. *The Plant Journal, 52*(4), 640-657. doi:https://doi.org/10.1111/j.1365-313X.2007.03263.x

R Core Team. (2021). R: A Language and Environment for Statistical Computing. Vienna, Austria: R Foundation for Statistical Computing. Retrieved from https://www.R-project.org

Saathoff, A. J., & Welles, J. (2021). Gas exchange measurements in the unsteady state. *Plant, Cell & Environment, 44*(11), 3509-3523. doi:https://doi.org/10.1111/pce.14178

Schneider, C. A., Rasband, W. S., & Eliceiri, K. W. (2012). NIH Image to ImageJ: 25 years of image analysis. *Nature Methods, 9*(7), 671-675. doi:10.1038/nmeth.2089

Sharkey, T. D. (1988). Estimating the rate of photorespiration in leaves. *Physiologia Plantarum, 73*(1), 147-152. doi:https://doi.org/10.1111/j.1399-3054.1988.tb09205.x

Sharkey, T. D., Bernacchi, C. J., Farquhar, G. D., & Singsaas, E. L. (2007). Fitting photosynthetic carbon dioxide response curves for C(3) leaves. *Plant Cell Environ, 30*(9), 1035-1040. doi:10.1111/j.1365-3040.2007.01710.x

Sharkey, T. D., & Weise, S. E. (2016). The glucose 6-phosphate shunt around the Calvin–Benson cycle. *Journal of Experimental Botany, 67*(14), 4067-4077. doi:10.1093/jxb/erv484

Smith, K. E. (2024). *Elucidating the Role of the Energy Demands of Photorespiration in Achieving Energy Balance.* (Ph.D.). Michigan State University, United States -- Michigan. Retrieved from https://ezproxy.msu.edu/login?url=https://www.proquest.com/dissertations-theses/elucidating-role-energy-demands-photorespiration/docview/3047725397/se-2?accountid=12598
https://ezproxy.msu.edu/login?url=https://resolver.ebscohost.com/openurl?sid=&genre=dissertations&issn=&ISBN=9798382315003&volume=&issue=&date=2024&spage=&pages=&title=&atitle=Elucidating+the+Role+of+the+Energy+Demands+of+Photorespiration+in+Achieving+Energy+Balance&aulast=Smith%2C+Kaila+Ellis&id=DOI: Dissertations & Theses @ Big Ten Academic Alliance; ProQuest Dissertations & Theses Global database. (31235439)

Somero, G. N. (1978). Temperature Adaptation of Enzymes: Biological Optimization Through Structure-Function Compromises. *Annual Review of Ecology and Systematics, 9*, 1-29. Retrieved from http://www.jstor.org/stable/2096741

Somerville, C. (1984). analysis of photosynthetic carbon dioxide fixation and photorespiration by mutant selection. *Oxford surveys of plant molecular and cell biology, 1*.

Somerville, C. R. (2001). An early Arabidopsis demonstration. Resolving a few issues concerning photorespiration. *Plant Physiology, 125*(1), 20-24.

Somerville, C. R., & Ogren, W. L. (1979). A phosphoglycolate phosphatase-deficient mutant of Arabidopsis. *Nature, 280*(5725), 833-836.

Somerville, C. R., & Ogren, W. L. (1980). Photorespiration mutants of Arabidopsis thaliana deficient in serine-glyoxylate aminotransferase activity. *Proceedings of the National Academy of Sciences of the United States of America, 77*(5), 2684-2687. doi:10.1073/pnas.77.5.2684

Somerville, C. R., & Ogren, W. L. (1982). Genetic modification of photorespiration. *Trends in Biochemical Sciences, 7*(5), 171-174. doi:https://doi.org/10.1016/0968-0004(82)90130-X

Strand, D. D., Livingston, A. K., Satoh-Cruz, M., Froehlich, J. E., Maurino, V. G., & Kramer, D. M. (2015). Activation of cyclic electron flow by hydrogen peroxide in vivo. *Proceedings of the National Academy of Sciences of the United States of America, 112*(17), 5539-5544. doi:10.1073/pnas.1418223112

Strauss, S. H., & Sax, J. K. (2016). Ending event-based regulation of GMO crops. *Nature Biotechnology, 34*(5), 474-477. doi:10.1038/nbt.3541

Switala, J., & Loewen, P. C. (2002). Diversity of properties among catalases. *Archives of Biochemistry and Biophysics, 401*(2), 145-154. doi:https://doi.org/10.1016/S0003-9861(02)00049-8

Szczepanczyk, M., Paul, L., Ruzgas, T., & Björklund, S. (2023). Comparison of Oxygen Electrode Chronoamperometry and Spectrophotometry for Determination of Catalase Activity. *Oxygen, 3*(1), 77-89. Retrieved from https://www.mdpi.com/2673-9801/3/1/6

Tejera-Nieves, M., Gregory, L. M., Saathoff, A. J., & Walker, B. J. (2024a). A/Ci method using Dynamic Assimilation Technique. In. protocol.io.

Tejera-Nieves, M., Seong, D. Y., Reist, L., & Walker, B. J. (2024b). The Dynamic Assimilation Technique measures photosynthetic CO2 response curves with similar fidelity as steady-state approaches in half the time. *J Exp Bot*. doi:10.1093/jxb/erae057

van Hoof, A., & Green, P. J. (1996). Premature nonsense codons decrease the stability of phytohemagglutinin mRNA in a position-dependent manner. *Plant J, 10*(3), 415-424. doi:10.1046/j.1365-313x.1996.10030415.x

Walker, B. J., Kramer, D. M., Fisher, N., & Fu, X. (2020). Flexibility in the Energy Balancing Network of Photosynthesis Enables Safe Operation under Changing Environmental Conditions. *Plants, 9*(3), 301. Retrieved from https://www.mdpi.com/2223-7747/9/3/301

Walker, B. J., VanLoocke, A., Bernacchi, C. J., & Ort, D. R. (2016). The Costs of Photorespiration to Food Production Now and in the Future. *Annual Review of Plant Biology, 67*(1), 107-129. doi:10.1146/annurev-arplant-043015-111709

Willekens, H., Chamnongpol, S., Davey, M., Schraudner, M., Langebartels, C., Van Montagu, M., . . . Van Camp, W. (1997). Catalase is a sink for H2O2 and is indispensable for stress defence in C3 plants. *The EMBO Journal, 16*(16), 4806-4816. doi:https://doi.org/10.1093/emboj/16.16.4806

Willekens, H., Inzé, D., Van Montagu, M., & van Camp, W. (1995). Catalases in plants. *Molecular Breeding, 1*(3), 207-228. doi:10.1007/BF02277422

Xu, H., Zhang, J., Zeng, J., Jiang, L., Liu, E., Peng, C., . . . Peng, X. (2009). Inducible antisense suppression of glycolate oxidase reveals its strong regulation over photosynthesis in rice. *Journal of Experimental Botany, 60*(6), 1799-1809. doi:10.1093/jxb/erp056

Zámocký, M., Gasselhuber, B., Furtmüller, P. G., & Obinger, C. (2012). Molecular evolution of hydrogen peroxide degrading enzymes. *Archives of Biochemistry and Biophysics, 525*(2), 131-144. doi:https://doi.org/10.1016/j.abb.2012.01.017

Zelitch, I. (1989). Selection and Characterization of Tobacco Plants with Novel O2-Resistant Photosynthesis. *Plant Physiology, 90*(4), 1457-1464. doi:10.1104/pp.90.4.1457

Zelitch, I. (1992). Factors Affecting Expression of Enhanced Catalase Activity in a Tobacco Mutant with O2-Resistant Photosynthesis. *Plant Physiology, 98*(4), 1330-1335. doi:10.1104/pp.98.4.1330

CHAPTER 5: Conclusions and Synthesis

Adapted from:

Fu, X., Smith, K., Gregory, L., Roze, L., & Walker, B. (2023). Modifying photorespiration to optimize crop performance. In *Understanding and improving crop photosynthesis* (pp. 203-222). Burleigh Dodds Science Publishing.

Conclusions and Synthesis:

The overall objective of this dissertation was to identify key photorespiratory mechanisms that maintain net carbon fixation (*A*) under high-photorespiratory environmental conditions, such as elevated temperatures. This work largely focused on characterizing photorespiratory enzymes downstream of rubisco, which directly manage carbon flux through photorespiration in adapted, acclimated, and engineered plant systems. I found that photorespiratory capacity, determined by the maximal reaction velocity (V_{max}) for each enzyme, can limit *A* if it becomes unbalanced with photorespiratory influx (v_o). Adapted plant systems, that maintain large photorespiratory rates, increase their photorespiratory capacity by increasing key enzyme activities to meet the demand of v_o. However, acclimated systems do not exhibit the same plasticity in their enzyme activities based on v_o; instead, they broadly maintain a reserve capacity. In the last chapter, I applied the knowledge gained from adapted and acclimated systems to enhance photorespiratory capacity in an engineered system. Transgenic expression lines of *Heliobacter pylori* catalase isoform were generated to optimize catalase-mediated degradation of H_2O_2. However, these transgenic lines did not confer a benefit to photosynthetic performance as they had similar amounts of CO_2 loss compared to wildtype *Arabidopsis thaliana* lines.

In the following sections, I synthesize the major themes from this dissertation.

Photorespiration must keep "traffic" moving to prevent inhibition of photosynthetic performance

Throughout the main chapters of this dissertation, we have consistently found that photorespiration must keep "traffic" moving to prevent inhibition on photosynthetic performance. When photorespiratory intermediates accumulate due to insufficient conversion rate, photosynthetic carbon fixation is inhibited, leading to a decrease in *A* and plant growth. In natural plant systems, such as *Betula papyrifera* (Chapter 3), it appears that plants maintain a surplus in photorespiratory capacity to handle variable photorespiratory influxes that might occur due to fluctuations in growth conditions (i.e., temperature differences between morning and solar noon, seasonal variation, or heatwave anomalies). In contrast, if high photorespiratory conditions persist, plants like *Rhazya stricta* (Chapter 2) maintain their metabolic balance by adapt greater enzyme

activities to handle higher rates of v_o. This natural adaptation in metabolic capacity circumvents the buildup of inhibitory intermediates as these substrates (2-phosphoglycolate and H_2O_2) are maintained at lower concentrations due to faster degradation. In both cases, the balance between photorespiratory influx and the metabolic capacity of the photorespiratory enzymes ensure photosynthetic performance is maintained in their specific growth environment.

In an engineered system, like *Arabidopsis thaliana* (Chapter 4), knocking out peroxisomal catalase leads to H_2O_2 accumulates due to insufficient conversion rates. This accumulation of H_2O_2, a bioactive photorespiratory intermediate, increases the release of CO_2 via nonenzymatic decarboxylation (NED) reactions and stimulation of the glucose-6-phosphate (G6P) shunt, both of which effectively decrease *A* and result in a severe growth phenotype compared to the wildtype lines.

Therefore, it is evident from these three independent cases in this dissertation that efficient processing of photorespiratory intermediates is essential to prevent the decline in photosynthetic carbon fixation.

Potential use of the safety factor metric: identify promising enzyme targets

This dissertation introduced a safety factor metric (established in Chapter 3) that can be used to identify promising photorespiratory enzyme targets to improve photosynthetic performance. It is calculated by dividing the enzyme activity at saturating substrate concentrations (V_{max}) by the production of 2-phosphoglycolate (v_o). This metric can be used as a proxy to evaluate the metabolic balance between influx and capacity and can reveal whether photorespiratory enzymes activities fall short of v_o (safety factors < 1; capacity deficit), are quantitatively matched with v_o (safety factors = 1) or maintain excess capacity to process v_o (safety factors > 1; capacity surplus). Identification of enzymes with capacity deficits (or that are accurately matched) can potentially reveal reactions in the photorespiratory pathway that are limited by enzyme bottlenecks. Moreover, if the substrates for these reactions are biologically active, there accumulation may confer control over photosynthetic carbon fixation.

I advocate for the future use of the safety factor calculation, as it allows researchers to effectively address the photorespiratory mechanisms that limit photosynthetic carbon fixation. The Walker lab is well-poised to characterize both v_o

(see appendix 1) and photorespiratory enzymes activities (methods section in chapter 1 & 2) in vascular species because of the gas-exchange, stable carbon isotope, and biochemical approaches established in this dissertation.

Initial Recommendation: Efforts to increase metabolic capacity should focus on the front end of the photorespiratory pathway

One strategy to develop heat-resilient crops for future climate conditions is to optimize the photorespiratory pathway to process higher rates of carbon influx. As climates warm, temperature-dependent shifts in rubisco specificity and gas solubility cause greater rates of v_o, resulting in larger metabolic pools of 2-phospholglycolate that need to be recycled by photorespiration. To ensure the photorespiratory pathway can process this excess carbon influx without limiting photosynthetic performance, key photorespiratory enzymes need to be engineered to improve photorespiratory capacity.

We determined that *R. stricta* supports higher rates of photorespiration by increased activity of two of the initial photorespiratory enzymes (phosphoglycolate phosphatase and catalase) compared to *Nicotiana tabacum*. Whereas low safety factors were calculated in *B. papyrifera* for the first two initial photorespiratory enzymes (phosphoglycolate phosphatase, glycolate oxidase) suggest that these reactions may be rate-limiting and potential enzymatic bottlenecks in the pathway. The pattern of underinvestment in enzyme activity in the initial reactions of photorespiration may apply universally to C_3 species. Increasing the capacity of these initial enzymes may be one strategy to improve photosynthetic resilience to elevated temperature. Past work supports the benefit of increasing the activity of the first three enzymes in the photorespiratory pathway, below I discuss each enzyme.

Phosphoglycolate phosphatase

- Insufficient phosphoglycolate phosphatase activities may restrict flux through photorespiration. Leading to the accumulation of 2-phosphoglycolate and inhibition of the C_3 cycle and *A* (Anderson, 1971; Kelly *et al.*, 1976). Moreover, 2-phosphoglycolate pools are high in phosphate, which could reduce available free phosphate from the sugar-phosphates of the C_3 cycle, further limiting *A* (Harley *et al.*, 1991; Sharkey, 1985; Timm *et al.*, 2019; Yang *et al.*, 2016). *Arabidopsis* lines overexpressing phosphoglycolate phosphatase have

higher rates of *A* at elevated temperatures (high photorespiratory conditions) compared to wild type lines, presumably because of the faster degradation of 2-phophoglycolate (Flügel *et al.*, 2017; Timm *et al.*, 2019). Therefore, maintaining high capacity for 2-phophoglycolate cycling may be important for minimizing inhibitory consequences and sustaining higher rates of *A* under high photorespiratory conditions.

Glycolate oxidase

- Elevated glycolate oxidase activities may improve the photosynthetic efficiency of crops by maintaining carbon flux through photorespiration under high photorespiratory conditions. If a higher level of peroxisomal glycolate oxidase is not available to degrade glycolate, large pools of glycolate can accumulate, which have been linked to the inhibition of rubisco (González-Moro *et al.*, 1997; Wendler *et al.*, 1992). Indeed, glycolate oxidase suppression lines show a photorespiratory phenotype, most likely from a severe reduction in *A* (Cui *et al.*, 2016; Lu *et al.*, 2014; Xu *et al.*, 2009). However, rice lines overexpressing glycolate oxidase maintain a higher photosynthetic rate under high temperatures compared to WT lines (Cui *et al.*, 2016).

Catalase

- Insufficient catalase activity leads to the accumulation of H_2O_2, which can react with the photorespiratory intermediates glyoxylate and/or hydroxypyruvate and release excess CO_2, reducing the carbon recycling efficiency of photorespiration (Bao *et al.*, 2021; Cousins *et al.*, 2008; Cousins *et al.*, 2011; Grodzinski *et al.*, 1976; Keech *et al.*, 2012). Mutant analysis of photorespiratory genes indicates that under laboratory conditions, the enzymatic decarboxylation of photorespiratory intermediates predominates, but it is unclear if the efficiency of photorespiration is maintained under stress conditions. For example, combined measurements of gas exchange and rubisco biochemistry indicate that the stoichiometric amount of CO_2 released from photorespiration may increase under elevated temperatures in many model and crop species, consistent with increases in non-enzymatic

decarboxylation reactions (Walker *et al.*, 2013; Walker *et al.*, 2017). It is therefore possible that catalase activity is insufficient under some conditions to decrease rates of non-enzymatic decarboxylation, offering a potential route for increasing photorespiratory efficiency.

Increasing the activities of phosphoglycolate phosphatase, glycolate oxidase, and catalase in C_3 species will improve photosynthetic carbon fixation under high photorespiratory influx. Additionally, all three of these enzymes degrade bioactive photorespiratory intermediates that directly affect photosynthetic carbon fixation. By increasing the activities of these enzymes, lower concentrations of these substrate will accumulate due to faster degradation. Thus, one strategy to future-proofing C_3 crop is to optimize photorespiration to reducing its control over photosynthetic performance.

Open Questions Remain

Findings from this dissertation increase our overall understanding of the strategies employed by the photorespiratory pathway to maintain photosynthetic performance under high photorespiratory pressure. These findings contribute to the long-range goal of engineering photorespiratory capacity to improve *A* under future climate conditions in C_3 crops. However, as often is the case, these findings also raised many new unanswered questions. I address these emerging questions below.

Could multiple photorespiratory intermediates co-limit photosynthetic performance?

From the work in this dissertation and what is known in the literature, it appears that multiple photorespiratory intermediates are biologically active (i.e., phosphoglycolate, glycolate, H_2O_2). The accumulation of multiple biologically active intermediates is a reasonable consideration that could occur under heatwave anomaly if photorespiratory capacity for certain enzymes were lower than v_o. While photorespiratory influx outpaces capacity, each intermediate could accumulate and influence photosynthetic performance through independent mechanisms. These mechanisms include, but are not limited to, the inhibition C_3 cycle enzyme, reduction in the available free phosphate, increase in the photorespiratory CO_2 release, increase NPQ and/or decrease LEF. Collectively, the accumulation of multiple photorespiratory

intermediates is likely to contribute to the further reduction of *A* compared to if one intermediate accumulated.

This could be tested experimentally by generating a double overexpression line of two photorespiratory enzymes (with bioactive substrates) and comparing it to the single overexpression lines of the same enzymes in *Arabidopsis thaliana*. Once stable and homozygous lines are achieved, *in vivo* (i.e., CO_2 response curve, Laisk curve, Post-Illumination Burst) and *in vitro* (i.e., enzyme activity assays) functional analysis under high photorespiratory conditions could determine whether there is an additional benefit to *A*, photorespiratory efficiency, or plant growth by maintaining a reserve capacity in single overexpression line, or multiple overexpression line compared to wildtype. The results of this experiment would help pinpoint whether multiple bioactive substrates co-limit photosynthetic performance. Additionally, this would determine whether the increase in capacity of numerous enzyme activities is beneficial compared to one.

How do other warm-adapted and extremophile C_3 species optimize their photorespiratory pathways?

In this dissertation I have investigated the hallmarks of a thermotolerant photorespiratory pathway in one C_3 species (*Rhazya stricta*). However, there are multiple C_3 species that thrive under hot-arid conditions, such as *Larrea tridentata*, *Ambrosia Dumosa*, *Lycium andersonii*, *Lycium pallidum*, or *Encelia farinosa* (Newingham *et al.*, 2014). It would be interesting to investigate the photorespiratory capacity for all of these C_3 species that are native to the Mojave Desert. Methods would mirror what was done in Chapter 2, where there would be a focus on estimating v_o and characterizing photorespiratory enzyme activities. Additionally, *Nicotiana tabacum* would be used as a control as it was in Chapter 2.

The results of this study would help 1) identify whether *Larrea tridentata*, *Ambrosia Dumosa*, *Lycium andersonii*, *Lycium pallidum*, or *Encelia farinosa* manage higher rates of *A* and photorespiration, 2) determine if photorespiratory influx is managed with an optimized photorespiratory pathway, and 3) elucidate the enzymes involved in boosting photorespiratory capacity for each species. My hypothesis would be that these species would broadly mirror the photorespiratory pathway identified in *R.*

stricta, where phosphoglycolate phosphatase and catalase activities would increase to process the greater photorespiratory influx.

Investigate photorespiratory plasticity in warm-adapted C_3 crop systems.

In this dissertation I assessed photorespiratory plasticity in one C_3 species (*Betula papyrifera*). *Betula papyrifera* trees inhabit high latitude regions and are frequently found in boreal forests biomes that experience cold-moderate temperatures, with freezing temperatures for over half the year (Gauthier *et al.*, 2015). Under a boreal forest environment, we would expect *B. papyrifera* to be adapted to low photorespiratory pressure, therefore a minimal photorespiratory capacity should be maintained. I would like to explore the photorespiratory plasticity in warm-adapted C_3 crops, like *Triticum aestivum* (wheat), *Arachis hypogaea* (peanut), or *Vigna unguiculata* (cowpea).

In *B. papyrifera*, rubisco deactivates with increasing temperatures, and estimated rates of photorespiration remained constant at 0◦C, 4◦C, and 8◦C. I would expect warm-adapted species could operate at higher temperatures without a decline in their functional rubisco activity. If v_o increased with temperature, then it may be a better system to look at plasticity in photorespiratory biochemistry. Additionally, safety factor calculations would determine the photorespiratory mechanisms that limit photosynthetic carbon fixation, which would be valuable information to improve plant productivity in these three economically-valued C_3 crops.

LITERATURE CITED

Anderson, L. E. (1971). Chloroplast and cytoplasmic enzymes II. Pea leaf triose phosphate isomerases. *Biochimica et Biophysica Acta (BBA) - Enzymology, 235*(1), 237-244. doi:https://doi.org/10.1016/0005-2744(71)90051-9

Bao, H., Morency, M., Rianti, W., Saeheng, S., Roje, S., Weber, A. P. M., & Walker, B. J. (2021). Catalase protects against nonenzymatic decarboxylations during photorespiration in Arabidopsis thaliana. *Plant Direct, 5*(12), e366. doi:https://doi.org/10.1002/pld3.366

Cousins, A. B., Pracharoenwattana, I., Zhou, W., Smith, S. M., & Badger, M. R. (2008). Peroxisomal malate dehydrogenase is not essential for photorespiration in Arabidopsis but its absence causes an increase in the stoichiometry of photorespiratory CO2 release. *Plant Physiology, 148*(2), 786-795. doi:10.1104/pp.108.122622

Cousins, A. B., Walker, B. J., Pracharoenwattana, I., Smith, S. M., & Badger, M. R. (2011). Peroxisomal hydroxypyruvate reductase is not essential for photorespiration in Arabidopsis but its absence causes an increase in the stoichiometry of photorespiratory CO2 release. *Photosynth Res, 108*(2-3), 91-100. doi:10.1007/s11120-011-9651-3

Cui, L.-L., Lu, Y.-s., Li, Y., Yang, C., & Peng, X.-X. (2016). Overexpression of Glycolate Oxidase Confers Improved Photosynthesis under High Light and High Temperature in Rice. *Frontiers in Plant Science, 7*(1165). doi:10.3389/fpls.2016.01165

Flügel, F., Timm, S., Arrivault, S., Florian, A., Stitt, M., Fernie, A. R., & Bauwe, H. (2017). The Photorespiratory Metabolite 2-Phosphoglycolate Regulates Photosynthesis and Starch Accumulation in Arabidopsis. *The Plant Cell, 29*(10), 2537-2551. doi:10.1105/tpc.17.00256

Gauthier, S., Bernier, P., Kuuluvainen, T., Shvidenko, A. Z., & Schepaschenko, D. G. (2015). Boreal forest health and global change. *Science, 349*(6250), 819-822. Retrieved from http://www.jstor.org/stable/24749186

González-Moro, B., Lacuesta, M., Becerril, J. M., Gonzalez-Murua, C., & Muñoz-Rueda, A. (1997). Glycolate accumulation causes a decrease of photosynthesis by inhibiting RUBISCO activity in maize. *Journal of Plant Physiology, 150*(4), 388-394. doi:https://doi.org/10.1016/S0176-1617(97)80087-9

Grodzinski, B., & Butt, V. S. (1976). Hydrogen peroxide production and the release of carbon dioxide during glycollate oxidation in leaf peroxisomes. *Planta, 128*(3), 225-231. doi:10.1007/BF00393233

Harley, P. C., & Sharkey, T. D. (1991). An improved model of C3 photosynthesis at high CO2: Reversed O 2 sensitivity explained by lack of glycerate reentry into the chloroplast. *Photosynth Res, 27*(3), 169-178. doi:10.1007/bf00035838

Keech, O., Zhou, W., Fenske, R., Colas-des-Francs-Small, C., Bussell, J. D., Badger, M. R., & Smith, S. M. (2012). The Genetic Dissection of a Short-Term Response to Low CO₂ Supports the Possibility for Peroxide-Mediated Decarboxylation of Photorespiratory Intermediates in the Peroxisome. *Molecular Plant, 5*(6), 1413-1416. doi:10.1093/mp/sss104

Kelly, G. J., & Latzko, E. (1976). Inhibition of spinach-leaf phosphofructokinase by 2-phosphoglycollate. *FEBS Letters, 68*(1), 55-58. doi:https://doi.org/10.1016/0014-5793(76)80403-6

Lu, Y., Li, Y., Yang, Q., Zhang, Z., Chen, Y., Zhang, S., & Peng, X. X. (2014). Suppression of glycolate oxidase causes glyoxylate accumulation that inhibits photosynthesis through deactivating Rubisco in rice. *Physiol Plant, 150*(3), 463-476. doi:10.1111/ppl.12104

Newingham, B. A., Vanier, C. H., Kelly, L. J., Charlet, T. N., & Smith, S. D. (2014). Does a decade of elevated [CO2] affect a desert perennial plant community? *New Phytologist, 201*(2), 498-504. doi:https://doi.org/10.1111/nph.12546

Sharkey, T. D. (1985). O(2)-insensitive photosynthesis in c(3) plants : its occurrence and a possible explanation. *Plant Physiol, 78*(1), 71-75. doi:10.1104/pp.78.1.71

Timm, S., Woitschach, F., Heise, C., Hagemann, M., & Bauwe, H. (2019). Faster removal of 2-phosphoglycolate through photorespiration improves abiotic stress tolerance of arabidopsis. *Plants, 8*(12). doi:10.3390/plants8120563

Walker, B. J., & Cousins, A. B. (2013). Influence of temperature on measurements of the CO2 compensation point: differences between the Laisk and O2-exchange methods. *J Exp Bot, 64*(7), 1893-1905. doi:10.1093/jxb/ert058

Walker, B. J., Orr, D. J., Carmo-Silva, E., Parry, M. A. J., Bernacchi, C. J., & Ort, D. R. (2017). Uncertainty in measurements of the photorespiratory CO2 compensation point and its impact on models of leaf photosynthesis. *Photosynthesis Research, 132*(3), 245-255. doi:10.1007/s11120-017-0369-8

Wendler, C., Putzer, A., & Wild, A. (1992). Effect of Glufosinate (Phosphinothricin) and Inhibitors of Photorespiration on Photosynthesis and Ribulose-1,5-Bisphosphate Carboxylase Activity. *Journal of Plant Physiology, 139*(6), 666-671. doi:https://doi.org/10.1016/S0176-1617(11)81708-6

Xu, H., Zhang, J., Zeng, J., Jiang, L., Liu, E., Peng, C., . . . Peng, X. (2009). Inducible antisense suppression of glycolate oxidase reveals its strong regulation over photosynthesis in rice. *Journal of Experimental Botany, 60*(6), 1799-1809. doi:10.1093/jxb/erp056

Yang, J. T., Preiser, A. L., Li, Z., Weise, S. E., & Sharkey, T. D. (2016). Triose phosphate use limitation of photosynthesis: short-term and long-term effects. *Planta, 243*(3), 687-698. doi:10.1007/s00425-015-2436-8

APPENDIX 1: A METHOD FOR DETERMINING THE DIFFUSIONAL AND BIOCHEMICAL PARAMETERS FOR ESTIMATING RATES OF RUBISCO OXYGENATION (v_o) AND RUBISOC CARBOYLATION (v_c)

This work was adapted from the supplemental section of:

Fu, X., Gregory, L.M., Weise, S.E., Walker B.J. (2023). Integrated flux and pool size analysis in plant central metabolism reveals unique roles of glycine and serine during photorespiration. Nat. Plants 9, 169–178.

Background:

This appendix provides the *in vivo* gas exchange and stable carbon isotope techniques developed/used in the Walker Lab to determine the diffusional and biochemical parameters (Γ^*, R_L, and g_m) for estimating rates of rubisco oxygenation (v_o) and rubisco carboxylation (v_c).

3.1 Describing the Gas-Exchange and Carbon Isotope Discrimination System

To estimate g_m, which is required to calculate the intercellular CO_2 concentrations needed to estimate v_o and v_c, in vivo gas exchange measurements of steady-state photosynthesis were combined with on-line measurements of carbon isotope discrimination, Δ, as described earlier (Evans *et al.*, 2013; Tazoe *et al.*, 2011; Ubierna *et al.*, 2018) using a LI-6800 (LI-COR Biosciences, USA) coupled to a tunable infrared laser differential absorption spectrometer (TILDAS_CS, Aerodyne Research, USA).

A computer-controlled front-end was provided for the system, as an integrated hardware and software system “Vinland” created by H. Stuart-Williams at the Australian National University (Contact information available upon request). In brief, software running on a PC/Arduino pair reads and displays output from the laser and controls hardware devices including valves (VICI Valco Instruments Co. Inc., USA) and mass flow controllers (Alicat Scientific, Inc., USA) to manage a gas mixing system to make synthetic air and dope it with isotopically characterized reference CO_2 as required, using pneumatic injection valves with capillaries (SGE MOVPT, SGE International, Ringwood, Australia).

The fully expanded leaf was placed across the leaf chamber avoiding the midrib. The CO_2 in the leaf chamber, flow rate, and irradiance were set to 400 μmol mol^{-1}, 300 μmol s^{-1}, 1750 μmol PAR m^{-2} s^{-1}, respectively. The LI-6800 was located inside a heating cabinet (Percival Scientific, USA) to maintain a 25°C leaf temperature and a 1.2 kPa vapor pressure deficit throughout the measurement. One synthetic air line was bubbled through a flask of water and fed into the LI-6800 air inlet port. In contrast, the other line was doped with a specified concentration of CO_2 ($\delta^{13}C$ vs. VPDB: -4.6 ‰, (Airgas Specialty Gases, USA)) to produce a calibration reference line to correct the raw $\delta^{13}C$ signals. To determine Δ, the reference and sample exhaust lines of the LI-6800 were subsampled into the TILDAS-CS on a rotating basis. To accomplish this, two lines

connected the LI-6800 exhaust ports A and B carried sample and reference airstreams through Nafion tubing and a dry-ice ethanol trap to remove all water vapor from the airstream. These lines and the calibration reference line from the mixing system, were connected to separate ports on the VICI multiposition valve to switch airstreams entering the TILDAS-CS. The TILDAS-CS measured molar ratios of the different carbon dioxide isotopologues ($^{16}O^{12}C^{16}O$, $^{16}O^{12}C^{17}O$, $^{16}O^{12}C^{18}O$ & $^{16}O^{13}C^{16}O$). Scripts running in the Vinland software controlled the valves and mixing and calculated/averaged raw $\delta^{13}C$ values for each measurement period.

$\delta^{13}C$ was calculated as:

$$\delta^{13}C = \left(\frac{R_{sample}}{R_{standard}} - 1\right) * 1000 \quad (1)$$

where R_{sample} is the molar ratio of the fractional abundance of the heavy isotope over the fractional abundance of the light isotope from the airstream that is measured by the TILDAS-CS, $\frac{^{16}O^{13}C^{16}O}{^{16}O^{12}C^{16}O + {}^{16}O^{12}C^{17}O + {}^{16}O^{12}C^{18}O}$. While the $R_{standard}$ is the molar ratio of Vienna Pee Dee Belemnite, the international reference standard for $^{13}C/^{12}C$ and is 0.0111797 (Ubierna *et al.*, 2018).

The TILDAS-CS was calibrated using an offset calibration approach as described earlier (Ubierna *et al.*, 2018) to correct the raw $\delta^{13}C$. With the corrected $\delta^{13}C$, the observed ^{13}C photosynthetic discrimination, Δ_{obs}, was calculated from an equation presented in (Evans *et al.*, 1986; Ubierna *et al.*, 2018):

$$\Delta_{obs} = \frac{\zeta\left(\delta^{13}C_{sample} - \delta^{13}C_{reference}\right)}{1 + \delta^{13}C_{sample} - \zeta\left(\delta^{13}C_{sample} - \delta^{13}C_{reference}\right)} \quad (2)$$

$$\zeta = \frac{^{12}CO_{2;\,reference}}{^{12}CO_{2;\,reference} - {}^{12}CO_{2;\,sample}} \quad (3)$$

where $\delta^{13}C_{sample}$ and $\delta^{13}C_{reference}$ are the carbon isotope compositions of the sample and reference airstreams coming from the LI-6800. ζ is the ratio of the $^{12}CO_2$ mole fraction in the dry air coming into the gas-exchange cuvette over the difference in $^{12}CO_2$ mole fractions of air in and out of the cuvette (Ubierna *et al.*, 2018).

3.2 Measurement Cycle

To find accurate Δ_{obs} values, the system needed to cycle the calibration reference line and the LI-6800 sample and reference lines to calibrate the $\delta^{13}C$ of the gases. A Vinland script automated the calibration and sampling analysis. The calibration reference line was measured at two different concentrations (39 and 46.5 Pa) at the beginning and end of the measurement cycle. In-between the calibration measurements were the LI-6800 reference and sample measurements. These lines were subsampled five times to produce five technical replicates within one measurement cycle. An AutoLog program was written on the LI-6800 GUI to match the timing of the Vinland script so that gas-exchange measurements could be taken simultaneously with the carbon isotope discrimination measurements.

Measurements were corrected through the use of an offset calibration. Offsets were calculated from the true (-4.6 ‰) and measured calibration reference $\delta^{13}C$ values at each CO_2 concentration. With these offsets, a linear regression was modeled between the CO_2 concentrations and offsets to create an offset calibration line. This offset calibration line was applied to correct the raw $\delta^{13}C$ measurements (Ubierna *et al.*, 2018).

3.3 Estimation of g_m

Estimation of g_m was performed using the system, and measurement cycle described above with an equation described earlier (Evans *et al.*, 1986; Ubierna *et al.*, 2018):

$$g_m = \frac{1+t}{1-t}\,\frac{b'_3 - a_m - \frac{\alpha_b}{\alpha_e}e\frac{R_L}{A-R_L}}{\frac{\bar{a}}{1-t}+\frac{1}{1-t}[(1+t)*b'_3-\bar{a}]\frac{C_i}{C_a}-\frac{1+t}{1-t}\frac{\alpha_b}{\alpha_e}e\frac{R_L}{A-R_L}\frac{C_i-\Gamma^*}{C_a}-\frac{1+t}{1-t}\frac{\alpha_b}{\alpha_f}f\frac{\Gamma^*}{C_a}-\Delta_{obs}}\,\frac{A}{C_a} \qquad (4)$$

where, $t = \frac{\alpha_{ac}E}{2g_{ac}}$, and $\bar{a} = \frac{a_b(C_a-C_s)+a_s(C_s-C_i)}{C_a-C_i}$. e was calculated with the assumption that the plant used old photosynthate as the substrate for respiration, $e = \delta^{13}C_{tank} - \delta^{13}C_{atmosphere}$, where $\delta^{13}C_{tank}$ was the measured $\delta^{13}C$ of the sample airstream, and the $\delta^{13}C_{atmosphere}$ was assumed to be -8‰. R_L and Γ^* values were used from the common intersection method (described below). Other variables and fractionation factors used in the equation 4 are defined in the table below as described earlier (Ubierna *et al.*, 2018).

3.4 Measurement of C_i^* and R_L

To measure C_i^* and R_L, we used the common intersection method (Laisk, 1977; Walker *et al.*, 2016). As described above, measurements were performed using a LI-6800. The LI-6800 maintain a 25◦C leaf temperature, a 1.5 kPa vapor pressure deficit, and a flow rate of 500 μmol s^{-1} during the measurement. The common intersection method measurements were linear fits of CO_2 response curves measured at 3, 5, 7, 90 11, 40 (Pa) at irradiances of 250, 165, 120, 80, 50 (μmol PAR m^{-2} s^{-1}). C_i^* and R_L values were determined from the linear regression of the slopes and y-intercepts from each irradiance as described earlier (Walker *et al.*, 2016).

3.5 Calculating Γ^* and iterating to accurate solutions

Γ^* was determined from $\Gamma^* = C_i^* + \frac{R_L}{g_m}$, where g_m, C_i^*, and R_L were determined from the gas exchange, and carbon isotope discrimination approaches described earlier (Walker *et al.*, 2015). g_m, and Γ^* were resolved iteratively using previous g_m, Γ^*, and R_L values to improve solutions accuracy; iterations were stopped when unity was reached. Gas exchange and stable carbon isotope data were analyzed using R; scripts will be available upon request (Betti *et al.*, 2016).

3.6 Calculating v_o and v_c

The key equation for estimating v_o and v_c uses measured rates of A is

$$A = v_c - 0.5v_o - R_L \tag{5}$$

Based on the following relationship from previous work (Von Caemmerer, 2000)

$$\Phi = \frac{v_o}{v_c} \tag{6}$$

$$\Phi = \frac{2\Gamma^*}{C_c} \tag{7}$$

where, Γ^* was determined from section 3.5 above, C_c is the partial pressure of CO_2 at the site of rubisco catalysis (C_c) and was determined by

$$C_c = C_i - \frac{A}{g_m} \tag{8}$$

Where A and C_i were determined from gas exchange measurements and g_m was determined from section 3.3 above.

Rearrange equations (5) – (7), we can estimate v_c and v_o as

$$v_c = \frac{A + R_L}{1 - \Gamma^*/C_C} \quad (9)$$

$$v_o = \frac{v_c - A - R_L}{0.5} \quad (10)$$

LITERATURE CITED

Betti, M., Bauwe, H., Busch, F. A., Fernie, A. R., Keech, O., Levey, M., . . . Weber, A. P. M. (2016). Manipulating photorespiration to increase plant productivity: recent advances and perspectives for crop improvement. *Journal of Experimental Botany, 67*(10), 2977-2988. doi:10.1093/jxb/erw076

Evans, J. R., Sharkey, T. D., Berry, J. A., & Farquhar, G. D. (1986). Carbon Isotope Discrimination measured Concurrently with Gas Exchange to Investigate CO2 Diffusion in Leaves of Higher Plants. *Functional Plant Biology, 13*(2), 281-292. doi:https://doi.org/10.1071/PP9860281

Evans, J. R., & von Caemmerer, S. (2013). Temperature response of carbon isotope discrimination and mesophyll conductance in tobacco. *Plant Cell Environ, 36*(4), 745-756. doi:10.1111/j.1365-3040.2012.02591.x

Laisk, A. K. (1977). Kinetics of photosynthesis and photorespiration of C3 in plants.

Tazoe, Y., S, V. O. N. C., Estavillo, G. M., & Evans, J. R. (2011). Using tunable diode laser spectroscopy to measure carbon isotope discrimination and mesophyll conductance to CO_2 diffusion dynamically at different CO_2 concentrations. *Plant Cell Environ, 34*(4), 580-591. doi:10.1111/j.1365-3040.2010.02264.x

Ubierna, N., Holloway-Phillips, M.-M., & Farquhar, G. D. (2018). Using Stable Carbon Isotopes to Study C3 and C4 Photosynthesis: Models and Calculations. In S. Covshoff (Ed.), *Photosynthesis: Methods and Protocols* (pp. 155-196). New York, NY: Springer New York.

Von Caemmerer, S. (2000). *Biochemical models of leaf photosynthesis*: Csiro publishing.

Walker, B. J., & Ort, D. R. (2015). Improved method for measuring the apparent CO2 photocompensation point resolves the impact of multiple internal conductances to CO2 to net gas exchange. *Plant, Cell & Environment, 38*(11), 2462-2474. doi:https://doi.org/10.1111/pce.12562

Walker, B. J., Skabelund, D. C., Busch, F. A., & Ort, D. R. (2016). An improved approach for measuring the impact of multiple CO2 conductances on the apparent photorespiratory CO2 compensation point through slope–intercept regression. *Plant, Cell & Environment, 39*(6), 1198-1203. doi:https://doi.org/10.1111/pce.12722

APPENDIX 2: THE TRIOSE PHOSPHATE UTILIZATION LIMITATION OF PHOTOSYNTHESTIC RATE: OUT OF GLOBAL MODELS BUT IMPORTANT FOR LEAF MODELS

This research was adapted from:

Gregory, L. M., McClain, A. M., Kramer, D. M., Pardo, J. D., Smith, K. E., Tessmer, O. L., Walker, B. J., Ziccardi, L. G., & Sharkey, T. D. (2021). The triose phosphate utilization limitation of photosynthetic rate: Out of global models but important for leaf models. *Plant, Cell & Environment*, 1– 4.

Opinion Paper:

Xiao *et al*., (2021) present a method for estimating the variability of estimated parameters of the Farquhar, von Caemmerer, Berry (FvCB) model of photosynthesis (Farquhar *et al.*, 1980). This model has been very effective at predicting photosynthetic responses to CO_2, light, and temperature but estimating the parameters of the model can be difficult, with the fitted parameters having various degrees of uncertainty as demonstrated by (Xiao *et al.*, 2021). The original model assumed one of two conditions: (1) rubisco is saturated with ribulose 1,5-bisphosphate (RuBP) and so responds to CO_2 with Michalis Menten kinetics (rubisco-limited) or (2) rubisco uses RuBP as fast as it is made (RuBP regeneration-limited). In condition (2), rubisco activity is determined by the rate of RuBP regeneration, typically as a result of being light-limited. But even though photosynthetic CO_2 assimilation (A) is light limited, it responds to increasing CO_2 because of suppression of photorespiration. Carboxylation plus oxygenation stays constant under RuBP regeneration limited conditions so if oxygenation goes down as CO_2 increases, carboxylation will go up. The model was expanded to include a third condition, where RuBP regeneration is limited by how fast phosphorylated intermediates, primarily triose phosphates, are converted to end products, thereby releasing phosphate (Sharkey, 1985). This is usually called “triose phosphate utilization (*TPU*) limitation.”

The FvCB model is most often parameterized by measuring CO_2 assimilation as a function of CO_2 inside the air spaces of the leaf (C_i), called an A/C_i curve. Rubisco-limited data points show a strong response to CO_2 while RuBP-regeneration-limited points show less response but still increase with increasing CO_2. TPU-limited points are characterized by no response to CO_2 and sometimes an inhibition under increasing CO_2 (Laporte *et al.*, 2001). The condition is further diagnosed by a decline in photosynthetic electron transport caused by an increase in CO_2 or decrease in O_2 (measured by chlorophyll fluorescence analysis). The TPU limitation is rarely seen at physiological CO_2 partial pressure and temperature but is very frequently seen when CO_2 is marginally higher than what the plant experienced during growth, especially if the temperature during the measurement is lower than the growth temperature (Sage *et al.*, 1987). Increasing the capacity for sucrose synthesis, reduces the temperature at which

TPU is observed (Laporte *et al.*, 2001). *TPU* limitations are also associated with oscillations in photosynthetic rate (Sharkey *et al.*, 1986), complicating measurements of *TPU*-limited photosynthesis rates.

The parameters that can be estimated by the fitting models are the maximum rate of rubisco carboxylation (V_{cmax}) and the rate of electron transport (J) (since the analysis can be done at limiting light, this need not be J_{max}). Also estimated are respiration in the light (R_L) (previously called day respiration, R_d) and mesophyll conductance (g_m). If *TPU* is considered, it too is estimated. We have used equations proposed by Busch *et al.* (2018) to include carbon flow out of photorespiration as glycine (α_G) or serine (α_S) which can affect estimates of *TPU*.

Some groups have concluded that TPU limitations are likely to be small and thus constitute an unnecessary complication for modeling photosynthesis at global scales (Kumarathunge *et al.*, 2019; Rogers *et al.*, 2021). Moreover, there is evidence that when plants experience *TPU* for a sustained period, both rubisco capacity and electron transport capacity are reduced until *TPU* is no longer evident. (Xiao *et al.*, 2021) recently described Bayesian methods for estimating parameters of the FvCB model and the uncertainties in those estimates but without including *TPU* in their fitting. We have reanalyzed the data of (Xiao *et al.*, 2021) to test the effect of inclusion of *TPU* on estimates of other parameters.

We began by reanalyzing the experimental data provided by (Xiao *et al.*, 2021). Four A/C_i curves measured with rice were provided. In three out of four cases, reverse sensitivity to CO_2 of A was observed and in all four cases, photochemical yield of photosystem II (Φ_{II}, measured by chlorophyll fluorescence analysis) declined at high CO_2 (Figure A2.1). In repetition 2, Φ_{II} increased at low CO_2 as rubisco activity increased, then abruptly began to decline with increasing CO_2 indicating a transition to *TPU* limitation with no points showing clear RuBP regeneration limitation (constant Φ_{II} with changing CO_2).

These behaviors indicate that *TPU* was occurring in all four repetitions. The authors specified in their methods section that they had to wait much longer for stability at the high CO_2 concentrations and the data at high CO_2 was noisy, also an indicator of *TPU*. We tested the effect of adding *TPU* to the analysis.

We converted the most recent version (2.9) of the fitting spreadsheet that has been provided by Plant Cell and Environment (Sharkey, 2016) to an R script with a user-friendly interface (Shiny app), see https://github.com/poales/msuRACiFit. The script iteratively fits data sets to biochemical models using rubisco-limited, RuBP-regeneration-limited, or *TPU*-limited assumptions, then calculates which process is likely to be rate-limiting for each data point, thus eliminating the need to assign specific limiting process to each of the data points.

We then fitted the data supplied by Xiao et al. (2021), first without *TPU* and then with *TPU* (Figure A2.2). For all four curves supplied, including *TPU* in the fitting improved the fit to the data at high CO_2 and this was reflected in a reduction in the sum of the squared residuals (SSR), by 90% in three out of four repetitions (Table 1). The reduction in SSRs was much greater than could be accounted for by the increase in degrees of freedom introduced by fitting additional parameters (i.e. *TPU*).

When data points are treated as *J*-limited but are actually limited by another process such as *TPU*, *J* is likely to be underestimated. The estimate of *J* was higher when *TPU* was included in the analysis (Table A2.1) but if none of the points are definitely *J*-limited (i.e., repetition 2) then the estimate of *J* is an estimate of the minimum *J*, not a true estimate of *J*. Because *J*-limited measurements hold the most information concerning g_m, g_m can be difficult to measure when A/C_i curves are measured at satuating light. Using high but not saturating light can decrease *TPU* and increase the amount of *J*-limited data, which can improve estimates of g_m (Sharkey, 2019)(see box 1 of that paper). We also note that the method of splitting the measurement of the A/C_i, going from ambient down, returning to ambient and going up sometimes introduces noise that is more apparent in the chlorophyll fluorescence data than *A* (see for example repetition 4, Figure A2.1 light green data, Figure A2.2 panels G and H). This noise in the data comes at the part of the curve that provides most information about g_m and so it is best to avoid the split method of measuring A/C_i curves.

We conclude that 1. it is important to include *TPU* when fitting A/C_i curves when there is evidence that *TPU* is occurring; 2. Additional data may be needed depending on how the fittings are to be used, for example it may be necessary to measure curves at saturating and also sub-saturating light to get robust measures of all parameters.

Because there are many parameters being fitted, some of which are complimentary, there is a danger of over fitting. When possible, parameters should be determined by independent measures. For example, g_m and R_L can be estimated independently and then fixed during fitting.

It must be accepted that some parameters can change within minutes and this biological source of variance should be considered. Very rapid, monotonic A/C_i curves are likely to be very helpful in assessing the physiology of photosynthesis just as a high-speed shutter on a camera helps bring things into focus, especially when the subject is dynamic. The latest technology released by LI-COR allows A/C_i curves to be measured in under five minutes.

Reporting the parameters of the FvCB model can be helpful for global modeling, for detecting effects of the environment on photosynthesis, and changes in specific components of photosynthetic capacity. Because *TPU* is normally a temporary condition, it likely will not improve global models of photosynthesis (Kumarathunge *et al.*, 2019; Rogers *et al.*, 2021). However, for laboratory studies or studies of initial effects of environmental changes on photosynthetic capacity, *TPU* is an important parameter to include in fitting routines and significant uncertainties can arise when it is not included in analysis of A/C_i curves.

For large datasets fitting batches of curves using programs like R can be very helpful. We supply a R package used in this work together with a Shiny app for ease of fitting. What is presented expands on part of an earlier R Package (Duursma, 2015). The Shiny app allows users to test specific hypotheses and can be a convenient way to explore how changing conditions such as temperature and light affect predicted rates of photosynthesis. Please see https://github.com/poales/msuRACiFit for how to access and use the R-script and Shiny app used for this work.

Figures

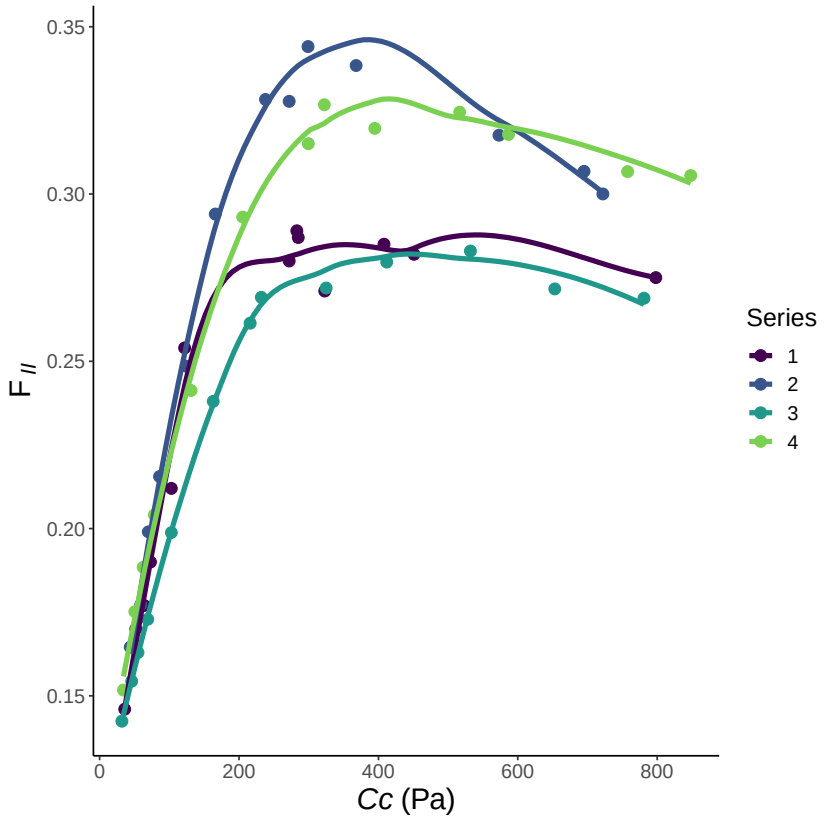

Figure A2.1. Φ_{II} values reported for the four replications of Xiao et al. (2021). Values were determined by chlorophyll fluorescence analysis. Curves 2 and 4 show an abrupt reversal from rubisco-limited (Φ_{II} increasing with increasing CO_2) to triose phosphate utilization(TPU)-limited (Φ_{II} decreasing with increasing CO_2) behavior with no definitive RuBP regeneration limitation (Φ_{II} independent of changes in CO_2).

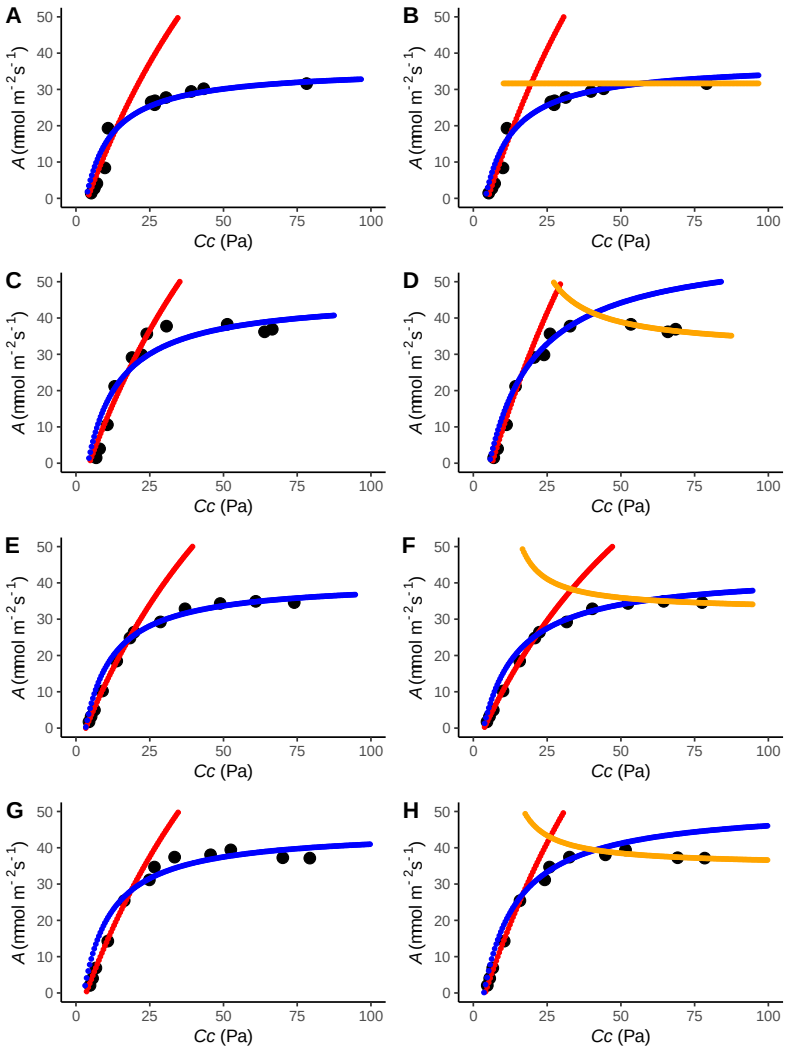

Figure A2.2. Fitting *A*/*C*$_i$ curves. Fits to rice data (replications 1–4 of Xiao et al. 2021) without triosephosphate utilization (TPU) (A, C, E, G), or with TPU (B, D, F, H). Red is the fitted shape for rubisco-limited condition, blue is for the RuBP regeneration–limited condition and gold is for the TPU-limited condition.

Tables

Table A2.1. Comparison of parameter values and sum of squared residuals (SSR).

		Rep 1		Rep 2		Rep 3		Rep 4	
	Units	without TPU	with TPU	without TPU	with TPU	without TPU	with TPU	without TPU	with TPU
V_{cmax}	µmol m^{-2} s^{-1}	183	194	203	232	167	174	179	197
J	µmol m^{-2} s^{-1}	170	178	201	273	177	185	194	222
TPU	µmol m^{-2} s^{-1}	–	10.9	–	12.3	–	12.1	–	12.4
g_m	µmol m^{-2} s^{-1} pa^{-1}	11.4	12.4	6.2	9.5	5.9	7.3	5.5	6.0
R_L	µmol m^{-2} s^{-1}	1.91	1.82	0.72	4.60	0.60	3.55	0.41	1.24
a_G	Unitless	0.33	0.22	0.00	0.01	0.40	0.59	0.38	0.26
a_S	Unitless	0.00	0.00	0.00	0.36	0.00	0.00	0.00	0.00
SSR	(µmol m^{-2} s^{-1})^2	73.3	53.3	174.4	16.9	19.0	1.2	73.8	7.0

Notes: Rice data of Xiao et al. (2021) was analyzed with and without triose phosphate utilization (*TPU*) (fitting of the data in Figure A2.2 (A) – (H)). *J* will always be underestimated when *TPU* limited points are treated as being *J*-limited.

LITERATURE CITED

Busch, F. A., Sage, R. F., & Farquhar, G. D. (2018). Plants increase CO_2 uptake by assimilating nitrogen via the photorespiratory pathway. *Nature Plants, 4*(1), 46-54. doi:10.1038/s41477-017-0065-x

Duursma, R. A. (2015). Plantecophys - An R package for analysing and modelling leaf gas exchange data. *PLOS ONE, 10*(11), e0143346. doi:10.1371/journal.pone.0143346

Farquhar, G. D., von Caemmerer, S., & Berry, J. A. (1980). A biochemical model of photosynthetic CO_2 assimilation in leaves of C_3 species. *Planta, 149*, 78-90.

Kumarathunge, D. P., Medlyn, B. E., Drake, J. E., Rogers, A., & Tjoelker, M. G. (2019). No evidence for triose phosphate limitation of light saturated leaf photosynthesis under current atmospheric CO2 concentration. *Plant, Cell & Environment, 42*(12), 3241-3252. doi:10.1111/pce.13639

Laporte, M. M., Galagan, J. A., Prasch, A. L., Vanderveer, P. J., Hanson, D. T., Shewmaker, C. K., & Sharkey, T. D. (2001). Promoter strength and tissue specificity effects on growth of tomato plants transformed with maize sucrose-phosphate synthase. *Planta, 212*, 817-822.

Rogers, A., Kumarathunge, D. P., Lombardozzi, D. L., Medlyn, B. E., Serbin, S. P., & Walker, A. P. (2021). Triose phosphate utilization limitation: an unnecessary complexity in terrestrial biosphere model representation of photosynthesis. *New Phytologist, in press*(n/a). doi:https://doi.org/10.1111/nph.17092

Sage, R. F., & Sharkey, T. D. (1987). The effect of temperature on the occurrence of O_2 and CO_2 insensitive photosynthesis in field grown plants. *Plant Physiology, 84*, 658-664. Retrieved from http://www.plantphysiol.org/content/plantphysiol/84/3/658.full.pdf

Sharkey, T. D. (1985). O_2-insensitive photosynthesis in C_3 plants: Its occurrence and a possible explanation. *Plant Physiology, 78*, 71-75. Retrieved from http://www.plantphysiol.org/content/78/1/71.full.pdf

Sharkey, T. D. (2016). What gas exchange data can tell us about photosynthesis. *Plant Cell and Environment, 39*(6), 1161-1163. doi:10.1111/pce.12641

Sharkey, T. D. (2019). Is triose phosphate utilization important for understanding photosynthesis? *Journal of Experimental Botany, 70*(20), 5521-5525.

Sharkey, T. D., Stitt, M., Heineke, D., Gerhardt, R., Raschke, K., & Heldt, H. W. (1986). Limitation of photosynthesis by carbon metabolism. II O_2 insensitive CO_2 uptake results from limitation of triose phosphate utilization. *Plant Physiology, 81*, 1123-1129. doi:10.1104/pp.81.4.1123

Xiao, Y., Sloan, J., Hepworth, C., Osborne, C. P., Fleming, A. J., Chen, X., & Zhu, X.-G. (2021). Estimating uncertainty: A Bayesian approach to modelling photosynthesis in C3 leaves. *Plant, Cell & Environment, 44*(5), 1436-1450. doi:https://doi.org/10.1111/pce.13995

APPENDIX 3: MEASURING AND QUANTIFYING CHARACTERISTICS OF THE POST-ILLUMINATION CO_2 BURST

This research was adapted from:

Gregory, L.M., Tejera-Nieves M.D., & Walker, B.J. “Measuring and Quantifying Characteristics of the Post-Illumination CO_2 Burst”. Springer Methods (in press)

Abstract:

Leaf-level gas exchange enables accurate measurements of net CO_2 assimilation in the light, as well as CO_2 respiration in the dark. Net positive CO_2 assimilation in the light indicates that the gain of carbon by photosynthesis offsets the photorespiratory loss of CO_2 and respiration of CO_2 in the light (R_L), while the CO_2 respired in the dark is mainly attributed to respiration in the dark (R_D). Measuring the CO_2 release specifically from photorespiration in the light is challenging since net CO_2 assimilation is composed of three unique processes (the velocity of rubisco carboxylation; v_c, velocity of rubisco oxygenation; v_o, and R_L). However, by employing a rapid light-dark transient, it is possible to transiently measure some of the CO_2 release from photorespiration without the background of v_c-based assimilation in the dark. This method is commonly known as the post-illumination CO_2 burst (PIB) and results in a “burst” of CO_2 immediately after the transition to the dark. This burst can be quantitatively characterized using several approaches. Here, we describe how to set up a PIB measurement and provide some guidelines on how to analyze and interpret the data obtained using a PIB analysis application developed in R.

Key words:

C_3 photosynthesis, net CO_2 assimilation rate, Post-Illumination Burst, PIB, Photorespiration, Light Enhanced Dark Respiration.

1. Introduction:

Since leaf-level gas exchange only measures net CO_2 assimilation (*A*), specialized approaches are needed to estimate the component gross fluxes. The component gross fluxes associated with *A* in C_3 plants are CO_2 assimilation (velocity of rubisco carboxylation; v_c), the photorespiratory loss of CO_2 (usually depicted as $0.5v_o$,where v_o is equal to velocity of rubisco oxygenation) and respiration of CO_2 in the light (R_L) (Farquhar *et al.*, 1980; von Caemmerer, 2013). Accurately measuring the gross CO_2 release from photorespiration in the background of CO_2 uptake can be challenging; however, it is possible to resolve values proportional to photorespiratory CO_2 release using a Post Illumination CO_2 Burst (PIB) (Busch, 2013; Sharkey, 1988).

The PIB method uses leaf-level gas exchange to measure *A* across a light to dark transient. When a leaf is illuminated, net CO_2 assimilation reaches a steady state with $A = v_c - 0.5v_o - R_L$, while in the dark, CO_2 respiration reaches a steady state ($A = R_D$). Consequently, a “burst” of CO_2 commonly occurs during the first few minutes immediately following the light-dark transition presumably since the reactions of the C_3 cycle cease in the darkness much faster than the CO_2 release from the photorespiratory pathway ($0.5v_o$ in the previous equation) (Decker, 1955, 1959).

Many photorespiratory-related metabolites have been hypothesized to contribute to the PIB. Glycine is suggested to be the primary contributor of CO_2 to the burst (Busch, 2013; Parys *et al.*, 2000; Rawsthorne *et al.*, 1991; Sharkey, 1988). Glycine, a photorespiratory intermediate that accumulates in the light, continues its metabolism in the dark longer than CO_2 is assimilated, so the CO_2 released is observed in the burst. In addition to glycine, there is evidence that CO_2 release from non-enzymatic decarboxylation between H_2O_2 and hydroxypyruvate and/or glycolate in the photorespiratory pathway are also captured in the burst (Bao *et al.*, 2021).

Other non-photorespiratory metabolites that accumulate during photosynthesis, such as malate and pyruvate, have also been proposed to contribute to the burst. Since mitochondrial respiration is sensitive to light-dark transients, the decarboxylation of malate and/or pyruvate can stimulate initial rates of respiration in the dark after a period of illumination and has been denoted in the past as light enhanced dark respiration (LEDR) (Atkin *et al.*, 1998; Azcón-Bieto *et al.*, 1983; Sharkey, 1988). Substrate feeding

experiments proved evidence that glycine (200mM) addition increased the burst size by 60% compared to water addition, while malate (200 mM), and pyruvate (200mM) were less effective at increasing the burst size (Parys *et al.*, 2000). While other metabolites have been suggested, it is likely that photorespiratory intermediates play a major role in contributing CO_2 to the PIB.

Although the PIB cannot directly measure the rate of photorespiration, since there are other non-photorespiratory contributors to the PIB and the release depends on pool sizes of photorespiratory intermediates that may or may not decarboxylate at the same rate in the dark as in the light, it is still an effective method for measuring an integrated signal of carbon emptying out of the residual carbon pools in the dark. Since there is a photorespiratory component contributing to the burst, changes in the total burst size are roughly proportional to the amount of photorespiration occurring.
Along with estimates of the absolute burst size, there are additional characteristics of leaf photosynthetic and photorespiratory performance that can be estimated from PIB measurements such as:

Steady-State Net CO_2 Assimilation Rate (A_s): A_s is the steady-state of CO_2 assimilation in the light before the leaf enters the dark and is given in units of µmol/m2/s.

Steady-State Dark Respiration Rate (R_D): R_D is the steady-state CO_2 dark respiration rate and is given in units of µmol/m2/s.

Area of the CO_2 Burst ($Burst_{Area}$): $Burst_{Area}$ is the entire amount of CO_2 released in the burst and is given in units of µmol/m2.

Time of the photorespiratory CO_2 burst ($Burst_{time}$)*:* $Burst_{time}$ is the length of time during the $Burst_{Area}$ and is given in minute units.

Maximum rate of CO_2 loss in the burst (Max_{lost}): Max_{lost} is the greatest rate of CO_2 lost during the $Burst_{Area}$ and is given in µmol/m2/s.

Along with these five unique parameters, it should also be noted that there are differences between species in the PIB response. Some species (i.e., *Arabidopsis thaliana*) give a single burst, where other species (i.e., *Nicotiana tabacum*) give two bursts (Figure A3.1). Sometimes portions of these bursts are referred to as LEDR. It is

outside the scope of this method to explore the cause of these differences, but the protocol outlined below can capture and quantify these different burst types.
Here we describe how to set up a PIB measurement, what to pay attention to while making measurements, and provide some guidelines on how to analyze and interpret the results using some quantitative methods.

2. Materials:

1. Infrared gas exchange analyzer (IRGA) for leaves with power supply or batteries (see Note 1).
2. Light Source (see Note 2)
3. Tripod/Stand to mount the IRGA head.
4. CO_2 cartridges (see Note 3).
5. Soda lime.
6. Desiccant (such as Sorbead® Orange CHAMELEON silica gel beads or Dririte®).
7. Humidifier (If applicable for the IRGA; see Note 4).
8. Computer for data download and processing.
9. Software: ImageJ, Excel R, RStudio (Optional; see Note 5 and Note 6).

3. Methods:

3.1 Machine Setup and Calibration:

We use the LI-6800 portable photosynthetic system for gas-exchange measurements so there may be some differences in setup based on the specific manufacturer used.

1. Before turning the IRGA system on, be sure to refill/replace the CO_2 cartridge. CO_2 scrub, Desiccant, and Humidifier chemicals of needed according to the manufacturer's instructions.
2. If needed, switch the IRGA sensor head to the appropriate leaf chamber (e.g., for the LI-6800 there is the Multiphase Flash Fluorometer, or a Large/Small Light Source that can be used). Additionally, verify that the gaskets of the leaf chamber are fitted to the IRGA sensor head properly and are not damaged. Replace damaged or ill-fitting gaskets.
3. Place the IRGA system on a clear work surface, or in a climate-controlled cabinet set to the desired measuring temperature if measuring under conditions ~±6°C from ambient.

4. Power on the machine and check that the IRGA sensor head is communicating with the IRGA console. Check the temperature control on the IRGA system and set the IRGA system desired temperature. For optimal humidity control, ensure the IRGA temperature closely matches the ambient temperature of the instrument. The IRGA itself will have a limited range of temperatures that can be achieved relative to the ambient temperature. Let the machine equilibrate for at least 45-60 minutes with the chamber closed. This is especially important if you are measuring above or below room temperature.
5. Perform the warm-up test (and/or the start-up checks recommended by the manufacturer). The warm-up test should reveal any warnings or errors that need attention. If there are any warnings or error messages, resolve them before beginning the experiment for the day.
6. Set the desired environmental conditions for the leaf chamber (i.e., flow rate, CO_2 and O_2 concentration, vapor pressure deficit, light intensity, temperature).

3.2 Preparing the Leaf:

1. Place the leaf into the leaf chamber on the IRGA sensor head and close the chamber fully, taking care not to fold or damage the leaf. If the leaf does not cover the entire area of the leaf gasket you will need to measure the area of the leaf after the measurement is taken (refer to *Collect Leaf Area section* below if applicable*).* Ensure that the thermocouple is making firm (but not too firm as to damage the leaf) contact with the bottom of the leaf. Leaf temperature is crucial to obtain accurate transpiration and stomatal conductance measurements. Ensure that the gaskets make a tight seal around the leaf and that there are minimal leaks.
2. Once you are confident with a secure fit onto the leaf, monitor the IRGA console. Verify that the environmental parameters are set correctly and watch the leaf parameters (i.e., A and g_{sw}) until steady state photosynthesis is reached. Visually, steady state photosynthesis will be reached once A and g_{sw} reach a plateau for more than 2-3 minutes.

3.3 Making a PIB Measurement:

PIB is measured during a light to dark transient that can be changed manually or written in an automated program. We recommend measuring *A* rate for 10 minutes in the light and 20 minutes in the dark to ensure good steady-states in the light and dark.

1. To establish a PIB program, create a sequence to control the light intensity of the leaf chamber. Begin the sequence by setting the desired light intensity (i.e., saturating, or sub-saturating) and end the sequence by setting the light intensity to zero (i.e., dark). Set the log interval to 1 second (or the fastest the IRGA system can log measurements). Set the entire program to run over 30 minutes (i.e., 10 minutes in the light, and 20 minutes in the dark) Ensure that there is no additional averaging of data above the log interval.
2. Open an empty log file on the IRGA system where the data can be stored during the measurement according to the manufacturer's directions.
3. Before starting the PIB measurement, it is important to switch the humidity and temperature controls to be constant during the transient, rather than depending on leaf performance (i.e., for the LI-6800 switch VPDleaf to H2O_r and Tleaf to Txchg). It is necessary to switch instrument controls to be constant because it will not result in artifactual changes in *A* or g_{sw} during the transient into the dark while the instrument works to compensate for the reduction in *A* and radiative load.
4. After setting the humidity and temperature controls to remain constant, wait for *A* and g_{sw} to restabilize before starting the measurement.
5. During the measurement one of two behaviors should be present:
    a. *Single Burst Observations*: In the light, the leaf will maintain *A* at a steady state. Immediately following the light-dark transition, a CO_2 burst will appear that will decelerate within minutes in the dark. After 10 minutes in the dark, the leaf will reach a R_D rate at a steady state (Figure A3.1).
    b. *Double Burst Observations*: In the light, the leaf will *A* at a steady state. Once the lights turn off, an initial burst of CO_2 will occur within the first minute, followed by a much longer CO_2 burst. Depending on the species that is measured it is expected to take 15-20 minutes (perhaps longer,

adjust program length accordingly) to reach a R_D rate at a steady state (Figure A3.1).

3.4 Collect Leaf Area (when necessary):

1. Once the PIB measurement is finished, mark the leaf with a marker where the gaskets are clamped on.
2. Release the leaf from the leaf chamber. Place a spare gasket overtop of the leaf and line it up with the marked spots. Place a known scale in the image field, such as a ruler, and take a picture of the leaf with the gasket placed overtop (ideally on a white surface).
3. Using a digital area analyzer, like ImageJ, determine the leaf area inside of the gasket (Schneider *et al.*, 2012).
4. Record the leaf area and correct the gas exchange data accordingly before analyzing the data (column 'S' on LICOR excel file).

3.5 Analyzing and Interpreting the PIB data:

The previous sections were to ensure that the highest quality of data is obtained for the PIB. The following section will provide insight into how to analyze and interpret the PIB data (Figure A3.2).

1. Plot *A* as a function of time and assess the quality of the data.
2. Perform initial quality control on the data. Visually, is there a lot of noise in the measurement? Does *A* rate reach a steady state in the light? Is there a distinct CO_2 burst immediately following the light-dark transition? Does R_D reach a steady state in the dark? If the data is satisfactory, then the PIB parameters can be estimated from the data.
3. To estimate A_s and R_D, average the last few points before the light transition, and the last few points in the dark before the measurement ends, respectively.
4. Add a linear regression overtop of the CO_2 burst, whereby the y-intercept is the solved $R_{D,}$ and the slope is set to zero.
5. To estimate $Burst_{Area}$, sum up the differences between the R_D linear regression and the measured assimilation values within the burst.
6. To estimate $Burst_{Time}$, find the difference between the first and last time point identified as the CO_2 burst.

7. To estimate Max_{Lost}, find the length from the R_D linear regression to the minimum assimilation in the CO_2 burst.

3.6 Using the ShinyApp to Automate Analysis:

The previous sections described how to check PIB data collected for quality, and how to analyze and interpret the PIB parameters manually. The following section introduces a custom-built program (i.e., ShinyApp) that can automate the analysis used to determine the PIB parameters (Figure A3.3).

1. Download the custom-built program from GitHub (https://github.com/L-Gregory/PIB_analyzer).
2. Open the script in RStudio and select Run App, this will open the application in another RStudio window.
3. Upload data by selecting the Browse button, or by "dragging and dropping" the data file into the box. Data must contain net assimilation rate and time columns.
4. Once data is uploaded successfully, select the columns containing time and assimilation. This will plot the data.
5. The data can be visually checked for quality now.
6. If the data are acceptable, click the "Fit" button. This will automatically estimate and display the five parameters of interest (A_s, R_D, $Burst_{Area}$, $Burst_{Time}$, Max_{Lost}) below the plot.
7. If you would like to change the R_D estimate for the linear regression – check the "Change Rd fit" box. Using the slider bar, select the number of points that you want to be included in the linear regression (default = 50).

Notes:

1. This method described here refers to gas exchange measurements made on the LI-6800 portable photosynthetic system (LICOR, Lincoln, NE, USA). The method could be adjusted for instruments from other manufacturers that measure CO_2 and H_2O gas exchange with high temporal resolution, as the general principle of operation, data collection, and analysis/interpretation still applies. However, we have not checked this method performance on other systems.
2. The simplest option is the LED light source made specifically for the leaf chamber in use, designed by the IRGA manufacturer. Depending on experimental requirements other light sources may be required (e.g., when a custom-built or clear top chamber is used, or when a certain light quality is required).
3. CO_2 cartridges should be purchased from the manufacturer if there is not a replaceable pre-filter. Use of generically branded CO_2 cartridges can introduce oil into the system and damage the instrument.
4. If you have a Nafion tube humidifier column, use deionized H_2O sources, instead of non-deionized H_2O as this can cause mineral buildup over time in the instrument.
5. Digital analysis for leaf area can be accomplished using ImageJ. However, this could be adapted to another application quite easily.
6. R code is provided in the supplemental section that automatically analyze and estimate the PIB parameters given PIB dataset.

Figures

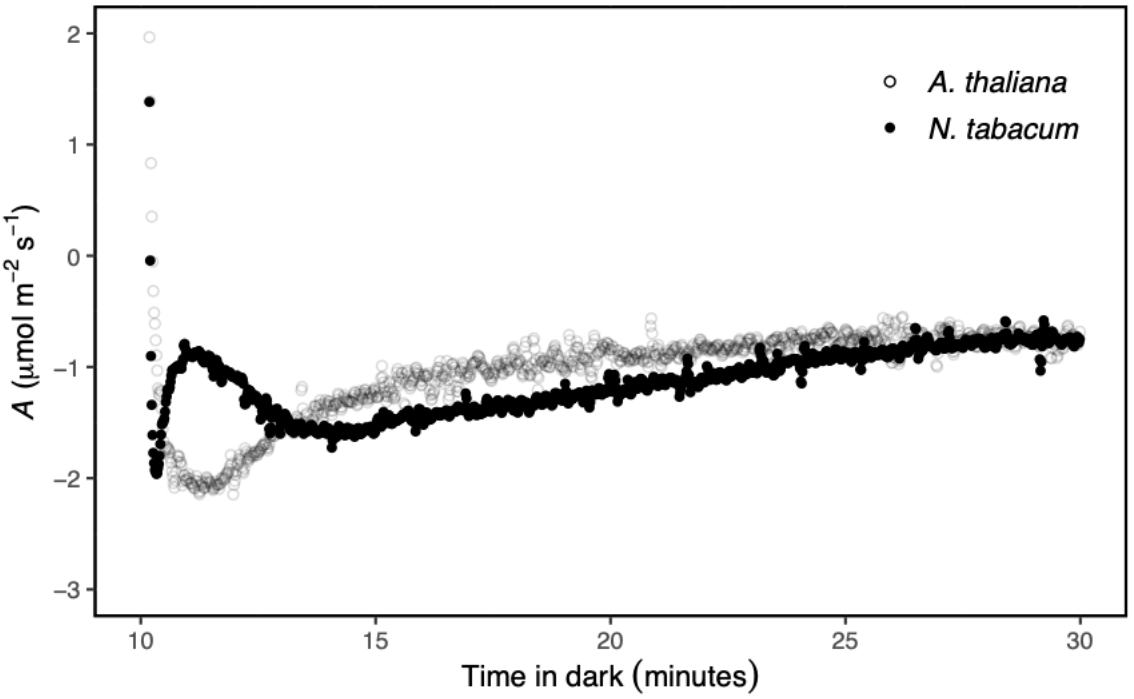

Figure A3.1. Example of a Single and Double Bursts in *Arabidopsis thaliana* and *Nicotiana tabacum*. There are two PIB behaviors that are seen across higher plant species. The first is a single burst (open points) whereby a CO_2 burst will appear immediately after the light-dark transition and will decelerate within minutes in the dark. The second PIB behavior is a double burst (closed points) whereby an initial burst of CO_2 will occur within the first minute, followed by a much longer CO_2 burst.

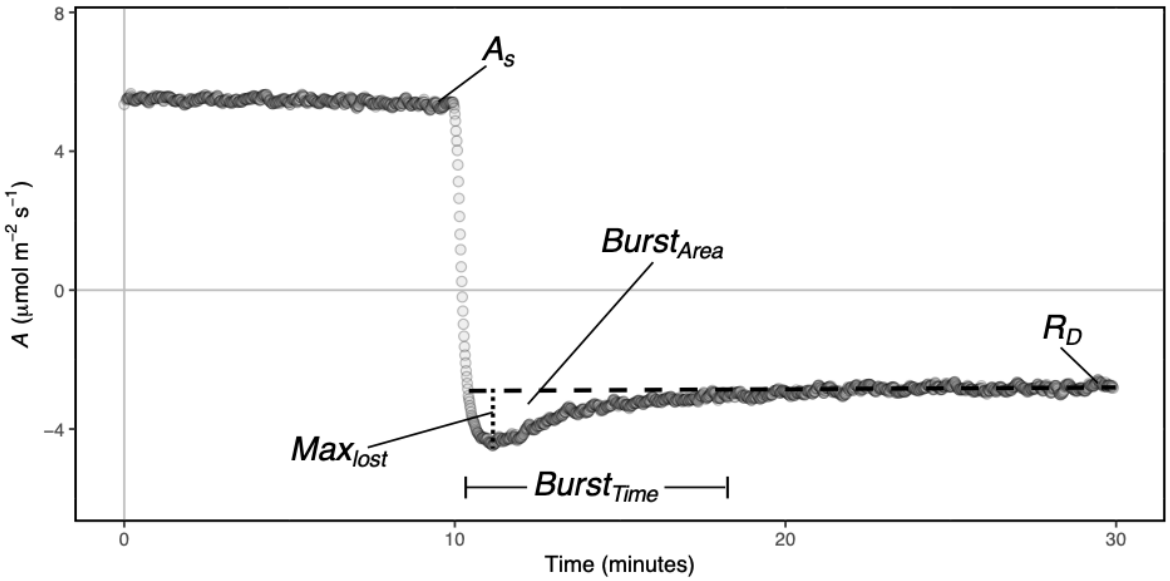

Figure A3.2. Estimated Parameters Overlayed onto Post CO_2 Illumination Burst. There are five unique parameters (A_s, R_D, $Burst_{Area}$, $Burst_{Time}$, Max_{lost}) that provide characteristics of leaf photosynthetic and photorespiratory performance that can be estimated from a PIB. The location of where these parameters are estimated are labeled onto of the PIB.

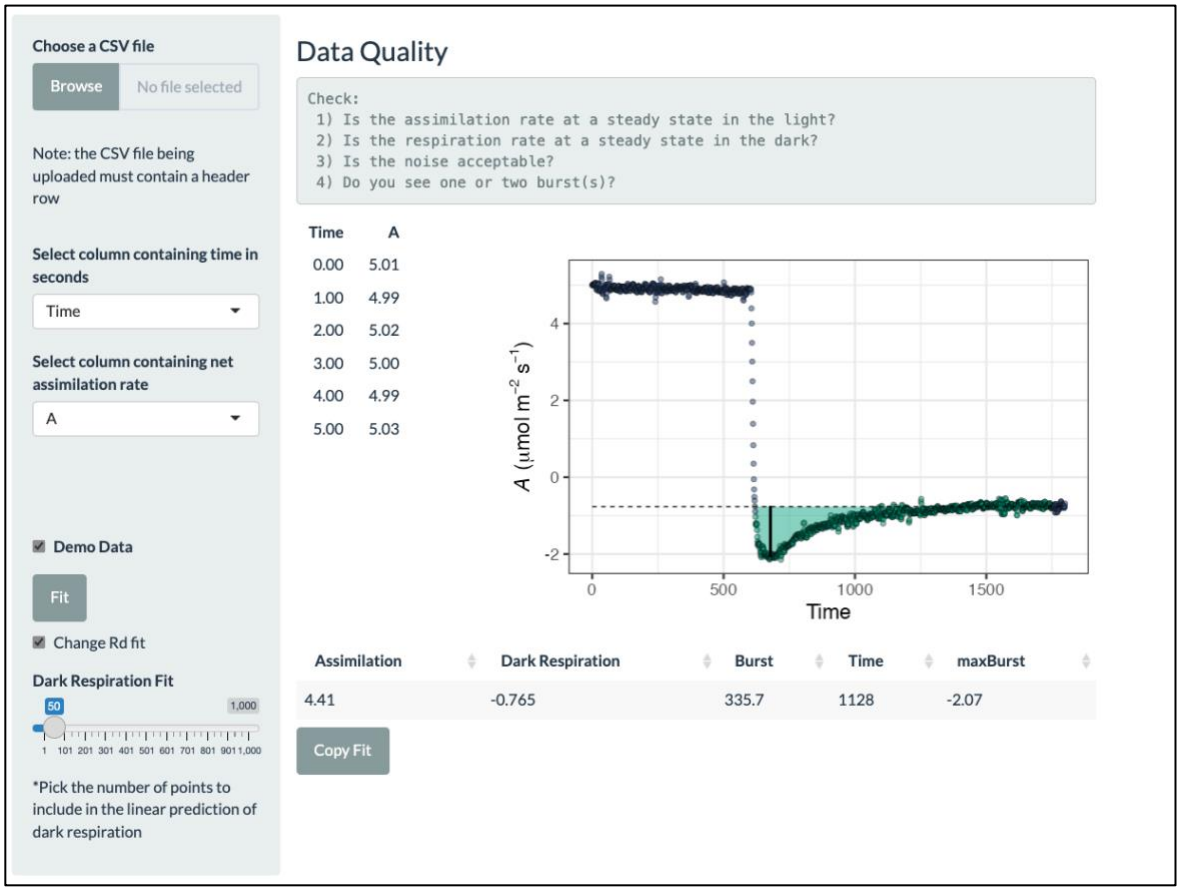

Figure A3.3. Custom-Written Application for Analyzing Post Illumination CO_2 Burst Data. The custom-built program automates the estimation of the five unique parameters (A_s, R_D, $Burst_{Area}$, $Burst_{Time}$, Max_{lost}) from the uploaded PIB data. Upon executing the app, PIB data can be uploaded into the file selection box. After defining the axes, a plot of the data will appear in the main panel. Clicking on the "Fit" button will generate the five parameters of interest. If the linear regression is not fitting properly, the user can adjust the points that are included in it (default = 50).

Tables

Table A3.1. List of parameters, descriptions, and their units.

Parameter	Description	Unit
A	Net CO_2 assimilation rate	µmol/m2/s
A_s	Steady state net CO_2 assimilation rate	µmol/m2/s
g_{sw}	Stomatal conductance to water vapor	mol/m2/s
C_a	The CO_2 partial pressure in the ambient air	Pa
C_i	The CO_2 partial pressure in the intercellular airspace of the leaf	Pa
R_L	Non-photorespiratory release of CO_2 in the light	µmol/m2/s
R_D	Non-photorespiratory release of CO_2 in the dark	µmol/m2/s
T_{leaf}	Leaf Temperature	°C
VPD	Vapor Pressure Deficit	kPa
$Burst_{Area}$	Total Area of the CO_2 burst	µmol/m2
$Burst_{Time}$	Time of the CO_2 burst	minutes
Max_{Lost}	Maximum rate of CO_2 loss in the burst	µmol/m2/s
v_c	Velocity of rubisco carboxylation	µmol/m2/s
v_o	Velocity of rubisco oxygenation	µmol/m2/s

LITERATURE CITED

Atkin, O. K., Evans, J. R., & Siebke, K. (1998). Relationship between the inhibition of leaf respiration by light and enhancement of leaf dark respiration following light treatment. *Functional Plant Biology, 25*(4), 437-443. doi:https://doi.org/10.1071/PP97159

Azcón-Bieto, J., & Osmond, C. B. (1983). Relationship between Photosynthesis and Respiration: The Effect of Carbohydrate Status on the Rate of CO(2) Production by Respiration in Darkened and Illuminated Wheat Leaves. *Plant Physiol, 71*(3), 574-581. doi:10.1104/pp.71.3.574

Bao, H., Morency, M., Rianti, W., Saeheng, S., Roje, S., Weber, A. P. M., & Walker, B. J. (2021). Catalase protects against nonenzymatic decarboxylations during photorespiration in Arabidopsis thaliana. *Plant Direct, 5*(12), e366. doi:https://doi.org/10.1002/pld3.366

Busch, F. A. (2013). Current methods for estimating the rate of photorespiration in leaves. *Plant Biology, 15*(4), 648-655. doi:https://doi.org/10.1111/j.1438-8677.2012.00694.x

Decker, J. P. (1955). A Rapid, Postillumination Deceleration of Respiration in Green Leaves. *Plant Physiol, 30*(1), 82-84. doi:10.1104/pp.30.1.82

Decker, J. P. (1959). Comparative Responses of Carbon Dioxide Outburst and Uptake in Tobacco. *Plant Physiol, 34*(2), 100-102. doi:10.1104/pp.34.2.100

Farquhar, G. D., von Caemmerer, S., & Berry, J. A. (1980). A biochemical model of photosynthetic CO2 assimilation in leaves of C 3 species. *Planta, 149*(1), 78-90. doi:10.1007/bf00386231

Parys, E., & Romanowska, E. (2000). Relationship between postillumination burst of CO2 and enhancement of respiration in tall fescue leaves. *Acta Physiologiae Plantarum, 22*(2), 135-142. doi:10.1007/s11738-000-0068-4

Rawsthorne, S., & Hylton, C. M. (1991). The relationship between the post-illumination CO2 burst and glycine metabolism in leaves of C3 and C3-C4 intermediate species of Moricandia. *Planta, 186*(1), 122-126. doi:10.1007/BF00201507

Schneider, C. A., Rasband, W. S., & Eliceiri, K. W. (2012). NIH Image to ImageJ: 25 years of image analysis. *Nature Methods, 9*(7), 671-675. doi:10.1038/nmeth.2089

Sharkey, T. D. (1988). Estimating the rate of photorespiration in leaves. *Physiologia Plantarum, 73*(1), 147-152. doi:https://doi.org/10.1111/j.1399-3054.1988.tb09205.x

von Caemmerer, S. (2013). Steady-state models of photosynthesis. *Plant, Cell & Environment, 36*(9), 1617-1630. doi:https://doi.org/10.1111/pce.12098